

MOSAIC Digital Environment Feasibility Study

Final Report

November 2020

Report Authors:

Alex Hands, Fraser Baird, Keith Ryden, Clive Dyer, Fan Lei (University of Surrey)

Rafael Rosolem, Sarah Fowler, Daniel Power (University of Bristol)

Jonathan Evans, John Wallbank, Magda Szczykulska (Centre for Ecology and Hydrology)

Table of Contents

1	Executive Summary.....	1
2	Introduction	3
3	COSMOS-UK Network	4
3.1	Description of COMOS-UK	4
3.2	Neutron Monitor Network.....	6
4	Space weather sensitivity in existing COSMOS data.....	9
4.1	Description of Data Sets.....	9
4.2	Space Weather events in COSMOS data.....	11
4.2.1	Forbush Decreases	11
4.2.2	GLEs.....	14
5	Theoretical Sensitivity to historic and future events.....	30
5.1	Atmospheric environment simulations	30
5.1.1	Primary GLE Spectra.....	30
5.1.2	URANOS Simulations.....	35
5.1.3	COSMOS Count Rates.....	40
5.2	Theoretical sensitivity to future events	43
5.2.1	Event Time profile.....	44
5.2.2	Detector time resolution.....	45
5.2.3	Statistical significance	46
5.2.4	Detection Threshold.....	47
5.2.5	Rigidity and Spectral Index.....	48
5.2.6	Terrestrial Gamma-Ray Flashes	50
6	Scope for enhancing the existing network	53
6.1	Time resolution and data transmission	53
6.2	Cybersecurity Considerations	55
6.3	Potential for creating multiple-detector hubs in strategic locations.....	58
6.4	Independent soil moisture adjustment	60
6.5	Use of Artificial Intelligence in data processing.....	64
6.6	Use of complementary data sources to enhance potential alert system.....	64
6.6.1	Neutron Monitor Data	64
6.6.2	Aircraft Monitors.....	66

6.6.3	ICAO Space Weather Thresholds	69
6.6.4	Other atmospheric measurements.....	72
7	Feasibility Assessment Summary	74
8	Conclusions	
	References	79

DRAFT

1 Executive Summary

Key takeaway points from the MOSAIC project:

- A new generalised data acquisition and processing tool has been developed for COSMOS soil moisture sensor data in order to detect space weather events.
- Space weather signals from both ground level enhancements (GLEs) and Forbush decreases have been identified in COSMOS data.
- Monte Carlo simulations of atmospheric radiation propagation have been used to recreate artificial COSMOS data time series during both historic and hypothetical space weather events.
- A single COSMOS detector is sufficient to detect the signal of a medium-strength ground level enhancement (GLE) at high statistical significance, including at fine time-resolution.
- Multiple-detector hubs situated at strategic UK locations could detect a small GLE at high statistical significance and infer crucial information on the nature of the primary spectrum.
- Preliminary analysis shows promising scope to use independent soil moisture data to “correct” for local variations that are not linked to space weather conditions.
- Laboratory-based trials of fine time-resolution data acquisition and rapid data transmission have successfully demonstrated enhanced capability to address space weather impacts.
- Use of fine time-resolution would also provide a capability to detect Terrestrial Gamma Ray Flashes (via secondary neutrons) which are produced by certain lightning discharges and which can provide a hazard to airlights, particularly in tropical regions.
- The COSMOS-UK detector network could be used to provide warnings at the ICAO “Moderate” and “Severe” dose rate thresholds at aviation altitudes, as well providing a capability well beyond the basic ICAO requirements.
- The UK is particularly well situated in having a wide range of geomagnetic latitude (and hence particle cut-off rigidities) and the COSMOS locations could be beneficially extended by siting a monitor in Shetland.
- Additional sources of data, particularly in-flight radiation detectors, could be used in conjunction with COSMOS-UK to provide a UK-centred GLE alert service that makes a major contribution to world coverage.
- It is recommended that modifications to the UK COSMOS network be initiated as soon as possible in order to be prepared for the next GLE as the solar cycle increases towards maximum.

- Management planning issues for this network should be addressed to ensure delivery of vital space weather data under all conditions.

2 Introduction

The aim of the Moisture Sensors for Atmospheric Ionising Radiation Collaboration (MOSAIC) project is to quantify the sensitivity of the UK COSMOS soil moisture network to space weather events and hence explore the feasibility of using the network to provide warnings of radiation events that can provide a hazard to airflight and ground level critical infrastructure. This project brings together an interdisciplinary team comprising expertise in hydrology, radiation detection, transport and effects and space weather.

In 2011 the UK recognised extreme space weather (ESW) events as an example of a high impact natural hazard with a low probability of occurrence in any given year. It was included for the first time as part of the National Risk Assessment, and subsequently added to the National Risk Register. In 2013 the Royal Academy of Engineering produced a report on the impacts of ESW on engineered systems and infrastructure [1]. The scope of this report is broad as it considered all aspects of space weather, including disturbances to the geomagnetic field and ionosphere. However, the report also identified a key risk to infrastructure from another aspect of space weather – relativistic (highly energetic) particles from the Sun. These particles, which are predominantly protons, arrive at Earth without warning as they travel close to the speed of light. In the atmosphere these generate a multiplicity of secondary particles such as neutrons, electrons and muons. This radiation can directly affect several aspects of critical infrastructure, from satellites to ground level electronic systems, by causing so-called single event effects (SEE) in microelectronic components. This can lead to disruption, performance degradation and also complete system failure. In addition, effects in human cells leads to effective dose to astronauts, aircrew and passengers.

The intensity of the atmospheric neutron environment could increase by orders of magnitude during an ESW event [2]. This is a major concern in the field of avionics and is the subject of a technical report from the IEC (International Electro-technical Commission) [3]. SEE in avionics is of critical importance, but the dose received in-flight by passengers and crew is also a major concern. Although the neutron flux at ground level would be much lower than at aviation altitudes, the amount of exposed infrastructure is far greater and thus an increased SEE rate may still cause disruption. A solar energetic particle event (SEP) that is of sufficient intensity at high energies to cause a significant increase to the ground level neutron flux is known as a ground level enhancement (GLE). These have been recorded on average approximately once per year since instruments capable of doing so were developed in the 1940s. GLEs are observed by a worldwide network of neutron monitors (see Section 3.2). However, there is currently no neutron monitor based in the UK. Whilst it may be desirable for a UK to have its own fully operational neutron monitor station, existing UK infrastructure may serve as a reasonable proxy source of space weather data. The UK COsmic-ray Soil Moisture Observing System (COSMOS) network of sensors, which infer soil moisture from observations of low energy neutrons reflected from soil via interactions with cosmic-ray generated neutrons, is operated by the NERC Centre for Ecology and Hydrology (CEH) [4]. The primary objective of the MOSAIC project is to study the feasibility of dual-purposing the COSMOS sensor network for the purpose of providing a new national resource to enhance the resilience of UK critical infrastructure to space weather hazards. We have examined historic data from cosmic ray neutron sensors in the UK and elsewhere and explored the potential for technical capability improvements to the UK COSMOS network. Our assessment of the feasibility of providing a sustainable and cost-effective UK space weather measurement capability, potentially providing real-time alerts via the MET Office space weather operations centre (MOSWOC), is described below.

3 COSMOS-UK Network

3.1 Description of COSMOS-UK

The COSMOS-UK network is the first national Soil Moisture Monitoring Network in the UK and was established in 2013. It is operated by UKCEH as part of their UKSCAPE National Capability programme for environmental monitoring and funded by the Natural Environment Research Council (NERC). There are 49 stations currently operating in England, Scotland, Wales and Northern Ireland, providing research grade hydro-meteorological data (Figure 1 and see Table 4 for site details). Of most relevance to MOSAIC, is the *in situ* ground level measurement of fast or epithermal neutrons at every site by the use of thermal neutron detector proportional counter tubes surrounded by plastic moderator.



Figure 1: Map of COSMOS-UK Sites.

The ground-level neutron count rate (once corrected for pressure etc.) can be related to the soil water content, as the hydrogen atoms in the water are very effective in scattering this neutron energy range, leading to lower energy (thermalised) neutrons, which are largely excluded from detection by the high-density polyethylene (HDPE) moderator around the neutron detector gas tube. Hence, the soil moisture content can be inversely related to the corrected neutron count (of epithermal-fast neutrons). The current application of the network is for soil moisture measurement, with associated weather data, but there is potential that the neutron detectors in the network can provide spatially distributed ground level cosmic ray neutron flux information, in their own right, and the feasibility of this is discussed later in this report.

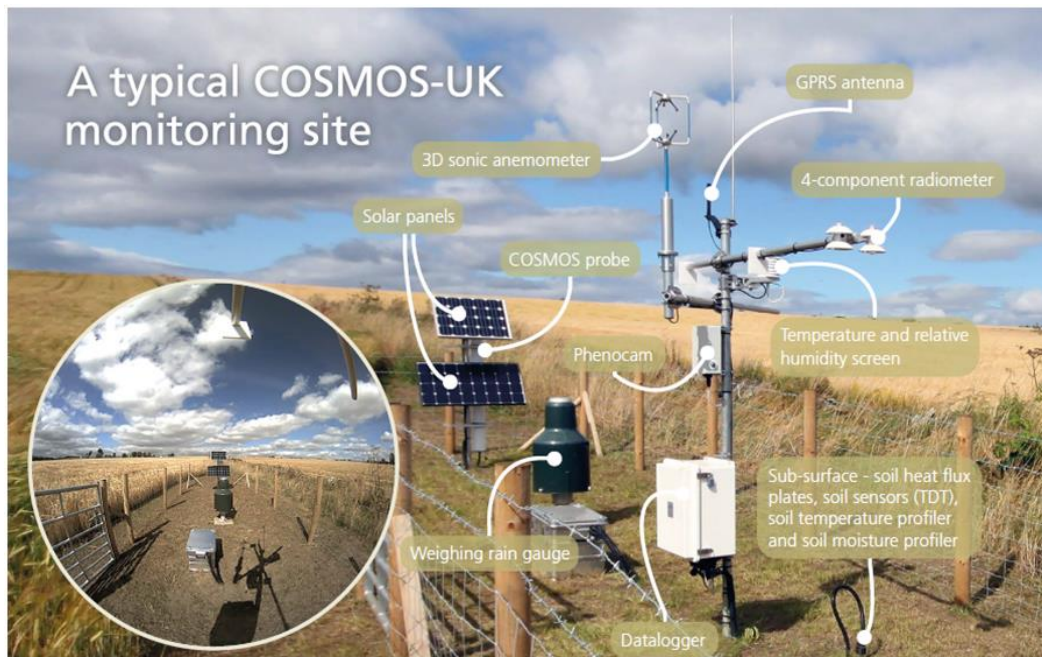


Figure 2: COSMOS-UK Station with Phenocam image (inset)

Full details of the COSMOS-UK network can be found at <https://cosmos.ceh.ac.uk/> and in [4] and [5]. A typical COSMOS-UK station is shown in Figure 2 with the 'COSMOS probe' labelled. The term 'COSMOS' technically refers to a network of such sensors: a COsmic ray Soil Moisture Observing System (COSMOS), but this term has become a convenient shorthand reference for the aforementioned neutron detector or probe, which is also referred to as a Cosmic Ray Neutron Sensor or (CRNS). The sensor counts epithermal-fast neutrons which can be converted to soil moisture after field calibration. Data processing accounts for variations in atmospheric pressure, humidity, and the intensity of incoming cosmic rays.

Zreda et al. [6] describe the detector principle and configuration. These are gas-filled detectors and, for the CRS-2000/B (Figure 3), thermal neutrons (generated by moderation of the epithermal-fast neutrons by the HDPE moderator around the detector), are captured by the boron-10 in the form of boron trifluoride (BF₃). The charged reaction products of neutron capture by B10 and the resulting ionisation are in turn detected by application of a high voltage (~1000 V) across the gas tube (the tube wall acts as the cathode, and the anode is a thin wire running down the central axis of the tube).

A Neutron Pulse Module, model NPM-2000 (Quaesta Instruments, Arizona, USA) provides digital pulse-height discrimination, and cumulative counts of neutrons, as well as a high voltage supply for the gas tube. Both the gas tube and NPM-2000 are contained within the environmentally sealed white metal tube shown on the right, which is connected to a 12 V DC power supply (via battery/solar) and to the station data logger, which transmits data back to UKCEH via mobile phone data networks, or Inmarsat satellite Broadband Global Area Network (BGAN). However, some researchers report that the desired epithermal-fast neutron count may be contaminated by up to 30% of thermal neutrons (which are not sufficiently shielded or blocked by the HDPE moderator) [7].



Figure 3: Model: CRS-2000/B CRNS from Hydroinnova LLC, New Mexico, USA

3.2 Neutron Monitor Network

Ground-level neutron monitors (GLNMs) have been in operation since the late 1940s [8, 9]. They provide continuous monitoring of the space radiation environment by measuring atmospheric neutron flux on the ground. Fluctuations in the galactic cosmic ray (GCR) background and space weather events are the primary causes of variation in the GLNM count rate after corrections for atmospheric pressure and detector efficiency have been applied. The number of active GLNM stations worldwide has decreased in recent years. Figure 4 shows a map of current and former stations, though not all current stations provide data in real time. There are approximately 50 monitors in the network at present [10], with approximately half providing live online data via the NMDB website (<http://www01.nmdb.eu/>).

Neutron monitor data are invaluable for observing and characterising the ground level enhancements (GLEs) that occur during certain types of solar energetic particle events (SEPEs). The distribution of

neutron monitors at different geomagnetic cut-off rigidities (the ratio of momentum-to-charge that a particle must have to be able to penetrate the magnetosphere) enables the network to act as a giant spectrometer and both spectral and spatial information can be inferred from the variations in count rates during a GLE. Typical background count rates during quiescent GCR conditions are of the order of 100 counts per second at sea level for a standard six tube NM64 design [11].

Archive data for the 68 GLEs that have recorded since the first neutron monitors were in operation are available via the NEST interface at nmdb.eu and, in renormalized format, at the GLE database managed by the Oulu neutron monitor station in Finland (<http://gle oulu.fi/>). For example, the measured percentage increases at fifteen neutron monitors during the largest event on record (GLE#5, 23rd February 1956) can be plotted directly from the GLE database and are shown in Figure 5.



Figure 4: Map showing existing (coloured circles) and historical (black circles) neutron monitor station locations [nmdb.eu].

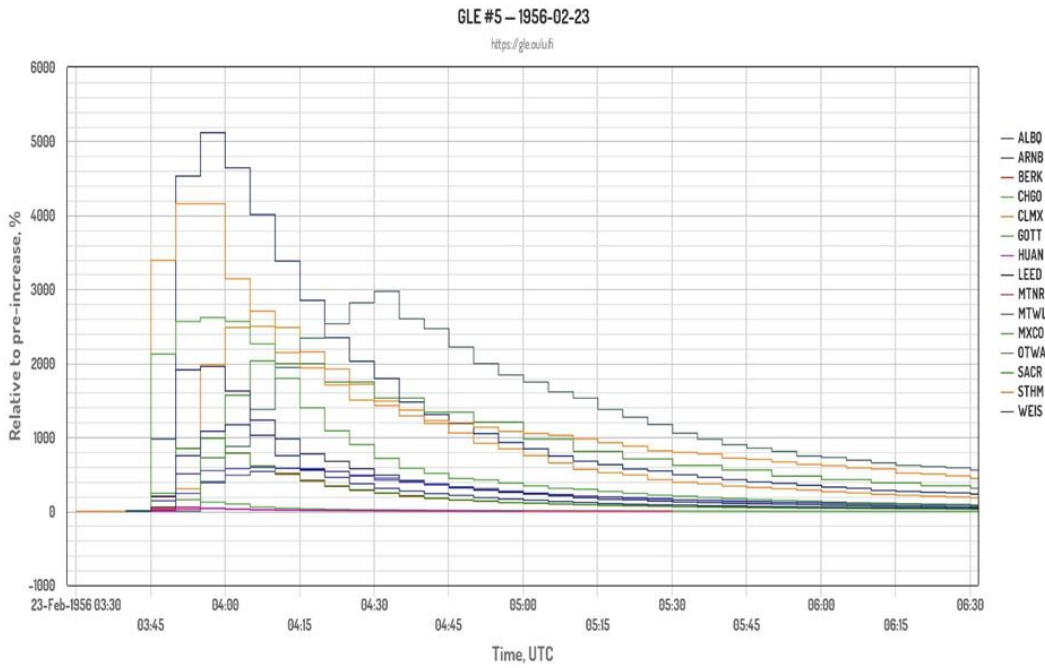


Figure 5: Example output from GLE database at OULU: GLE #5, 23rd February 1956.

The global neutron monitor network is an indispensable resource for responding to space weather effects linked to elevated atmospheric neutron flux, such as increases in effective dose rate to aircraft crew and passengers and single event effect (SEE) rates to both avionics and ground level electronics. However, existing gaps in the spatial coverage of the network, together with a lack of certainty over future maintenance funding at some stations, mean that there is plenty of scope for this resource to be complemented by additional measurements of atmospheric neutron flux. The COSMOS soil moisture sensor network has the potential to be exploited for the dual purposes of hydrology and space weather and potentially therefore to fill some of the gaps within the GLNM system. In the next sections we will examine the practicality of achieving this dual purposing.

4 Space weather sensitivity in existing COSMOS data

4.1 Description of Data Sets

Extensive time-series data from COSMOS-UK are available for up to seven years, depending on the site installation date (see Figure 12). Table 1 shows the publicly available measurements from COSMOS-UK Stations (for the MOSAIC project, raw (uncorrected) neutron counts are also available). This table is taken from the COSMOS-UK User Guide (version 3.0, Sept 2020), and more information is available in this guide.

Table 1: Monitored data available from the COSMOS-UK network

Variables	Units	Recording interval
Precipitation	mm	1 min
Absolute humidity ^[1]		30 min
Relative humidity	%	30 min
Air temperature		30 min
Atmospheric pressure ^[2]	hPa	30 min
Incoming longwave radiation		30 min
Incoming shortwave radiation		30 min
Outgoing longwave radiation		30 min
Outgoing shortwave radiation		30 min
Wind direction		30 min
Wind speed		30 min
3D wind speed data (x3)		30 min
Snow depth	mm	30 min
Volumetric water content at three depths (15cm, 40cm, 65cm) (IMKO Profile)	%	30 min
Soil heat flux (x2)		30 min
Soil temperature at five depths (2cm, 5cm, 10cm, 20cm, 50cm)		30 min
Soil temperature and volumetric water content (10cm, and up to 4 other depths x2) (TDT)	& %	30 min

^[1] There was a small change in the derivation of absolute humidity in November 2019, so that the value is now calculated as part of data processing, rather than on the data logger. The change, which has been applied retrospectively to all data, makes an insignificant difference to the calculated value, but does improve the completeness of the data.

^[2] Reported as recorded at altitude of instrument i.e. not corrected to sea level.

Table 2: Derived data available from the COSMOS-UK network

DERIVED VARIABLES	Units	NOTES
Net radiation		30 min
Volumetric water content (CRNS)	%	Daily/hourly
Typical sensing depth of CRNS (D86)	cm	Daily/hourly
Neutron counts from CRNS (corrected)	Counts per hour (cph)	Hourly
Potential evaporation	mm	Daily
Atmospheric Pressure at sea level	hPa	Daily/30min
Albedo	Dimensionless	Daily
Soil moisture index (SMI)	Dimensionless	Daily
Snow days	Yes/No	Daily
Snow Water Equivalent (CRNS)	mm	Daily
Snow Water Equivalent (SnowFox)	mm	Daily

The processing of cosmic-ray neutron sensors requires several steps to ensure quality control and accurate derived products. The neutron signal needs to be corrected for variation in the atmospheric pressure [6], incoming neutron intensity [12], above ground biomass [13], and atmospheric water vapour [14]. Additionally, for soil moisture readings, site calibration is required that has been improved upon since the first inception of these sensors [15]. Whether the use of cosmic-ray neutron sensors data is for hydrological applications looking at soil moisture dynamics or, alternatively, for monitoring actual neutron counting rates for space weather applications, to date, different national networks employ slightly different data processing and quality control steps. This makes a wider use of cosmic-ray neutrons sensors somewhat limited and is a challenge for space weather applications covering different continents.

As an initial step to harmonize multiple networks of cosmic-ray sensors globally, the University of Bristol team under MOSAIC has developed the Cosmic-Ray Sensor PYthon tool (crspy; [16]). crspy is a comprehensive open-source data processing tool (<https://github.com/danpower101/crspy>) which includes all up-to-date knowledge about the technology and can be used for a wide variety of applications (e.g. hydrology and space weather). crspy is designed to streamline the processing of hundreds of cosmic-ray stations globally relatively quickly (Figure 6). The key purpose of crspy is to increase our ability to compare CRNS sites within different networks, removing the uncertainty surrounding the differing methodologies currently applied, making the technology more accessible to the wider scientific community.

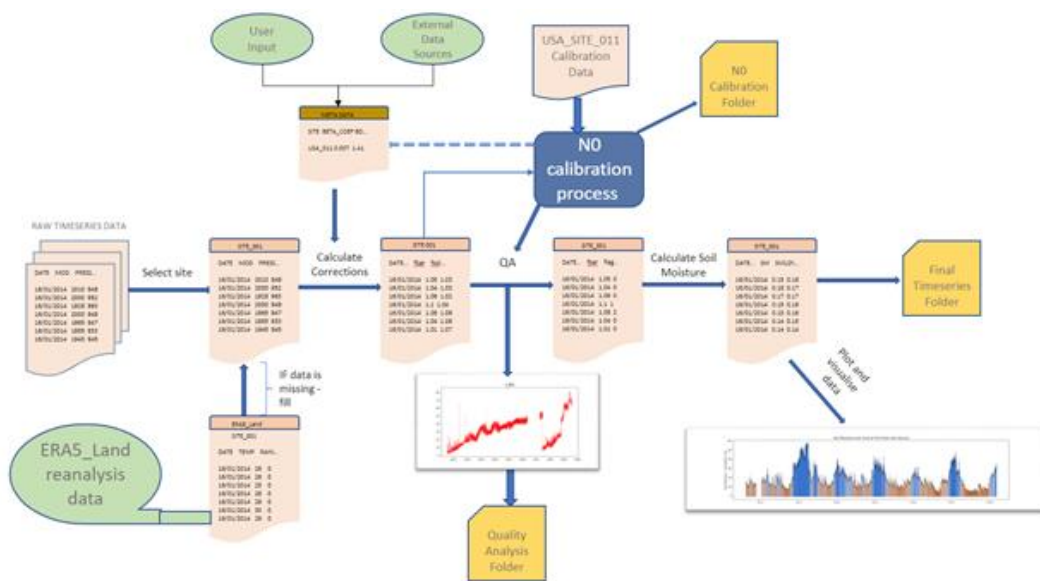


Figure 6: A schematic diagram showing the workflow of the newly developed Cosmic-Ray Sensor PYthon tool (crspy).

Initial use of the crspy tool was done under MOSAIC in order to process a number of high-latitude cosmic-ray stations in the Northern Hemisphere. This ensures that despite coming from different countries and networks, the measured signal by the sensor was processed following the same standard procedure and quality control flags. In total, crspy has harmonized the data processing steps of eight stations available from US COSMOS network (USA and Canada) and an additional three sites located in the UK and maintained by the University of Bristol (see Table 3 for site summary).

Table 3: List of high-latitude cosmic-ray stations processed with the new crspy tool for MOSAIC

Site name	Country	Latitude/Longitude	Data period
Park Falls	USA	45.9459 / -90.2723	19/07/2011- 30/11/2019
UMBS	USA	45.5598 / -84.7138	21/07/2011 – 20/01/2019
Fort Peck	USA	48.3077 / -105.1019	14/08/2011 – 07/03/2018
Saskatoon	Canada	52.1326 / -106.6168	24/10/2013 – 18/10/2015
Trail Valley Upper Plateau	Canada	68.6936 / -133.6974	01/05/2013 – 20/02/2020
Trail Valley Forest	Canada	68.7227 / -133.4955	01/05/2013 – 11/02/2020
Havikpak Main Met	Canada	68.3199 / -133.5198	01/05/2013 – 20/02/2020
Trail Valley Main Met	Canada	68.7455 / -133.5	01/05/2013 – 20/02/2020
Sheepdrove Pounds 2b	UK	51.5153 / -1.4580	01/07/2015 – 10/07/2019
Sheepdrove W2/W3	UK	51.5284 / -1.4675	01/07/2015 – 10/07/2019
Sheepdrove Melville Woods	UK	51.5233 / -1.4861	01/07/2015 – 10/07/2019

4.2 Space Weather events in COSMOS data

4.2.1 Forbush Decreases

Forbush decreases (Fds) are reductions in the counting rate of cosmic ray detectors caused by magnetic disturbances in the heliosphere (such as coronal mass ejections, or fast solar wind streams) modulating primary cosmic rays [17, 18]. Generally, they are characterised by sharp drops in the counting rate of detectors, typically a few percent over 12-24 hours. This is then usually followed by a gradual recovery of the counting rate to the pre-decrease level over a few days [19]. However, these events can be symmetrical in shape, with rapid recoveries, or may not exhibit a return to pre-decrease counting rates for a long period of time (months, in some cases). Fds are more common than GLEs, with some studies estimating that around 300 Fds occurred between 2001 and 2018, with 90 being caused by the passage of a coronal mass ejection [20]. The common occurrence of Fds means that there are many candidates to investigate in the COSMOS-UK data set.

Neutron count data from each COSMOS-UK station were binned into 30-minute intervals and corrected for pressure and humidity variations. Quality control checks were carried out, with data that failed the check removed and interpolated across. For each 30-minute interval, all available corrected neutron count data across the network were averaged, as were the data from point soil moisture probes. Intervals of high variance were identified in the data set, and the neutron count data in the interval was plotted alongside the averaged soil moisture and data from the South Pole Neutron Monitor.

Three examples of positively identified Fds are presented in Figures 7 to 9. These events occur in December 2014, July 2017, and September 2019 respectively, and all show close correlation with the signal from the South Pole neutron monitor and no anti-correlation with soil moisture.

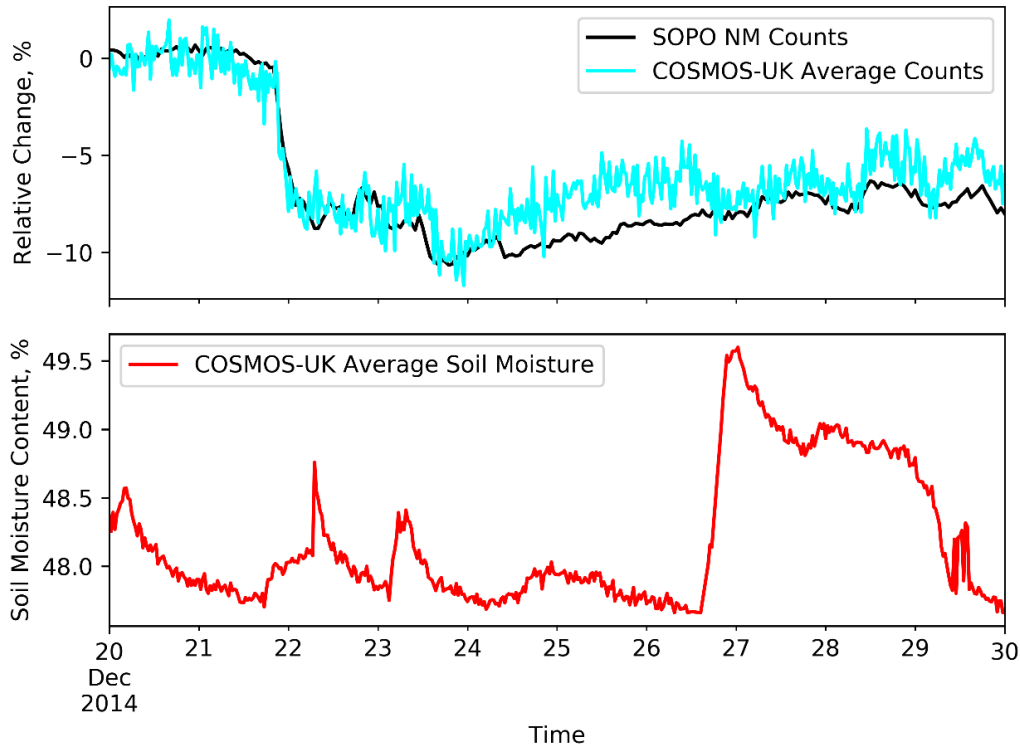


Figure 7: A large Fd identified in both SOPO counts (black) and COSMOS-UK averaged counts (cyan). The average soil moisture content across the COSMOS-UK network as measured by point probes (red) shows no significant increases during the onset of the Fd.

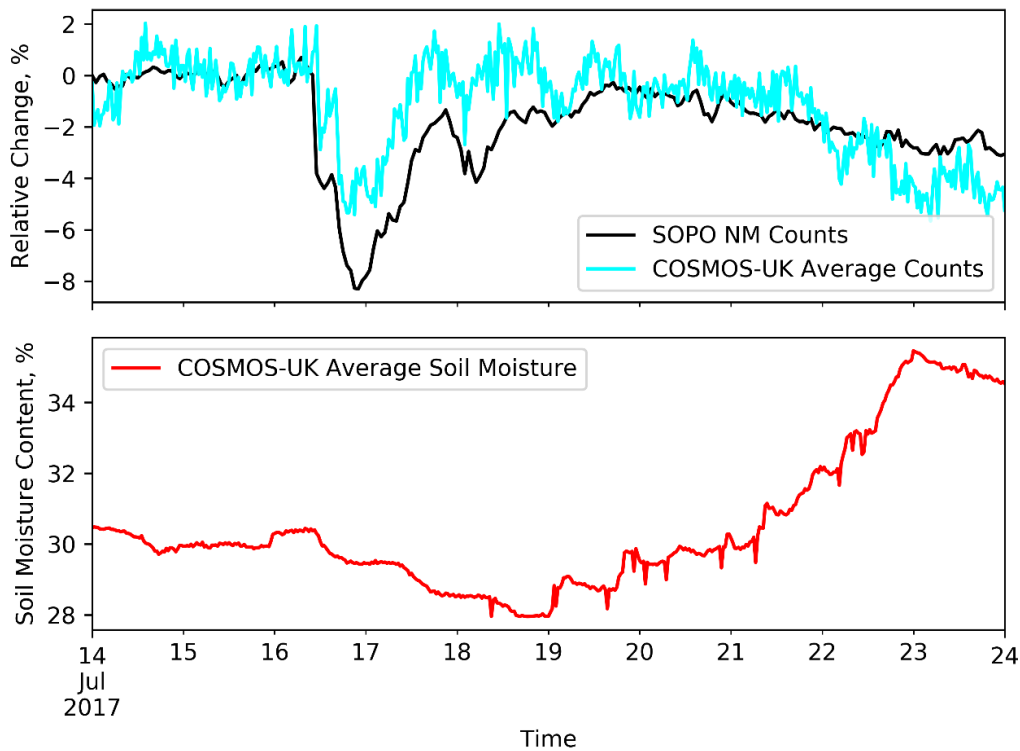


Figure 8: A moderate Fd with a rapid recovery identified in SOPO counts (black) and COSMOS-UK averaged counts (cyan). The averaged soil moisture content across the COSMOS-UK network is in red.

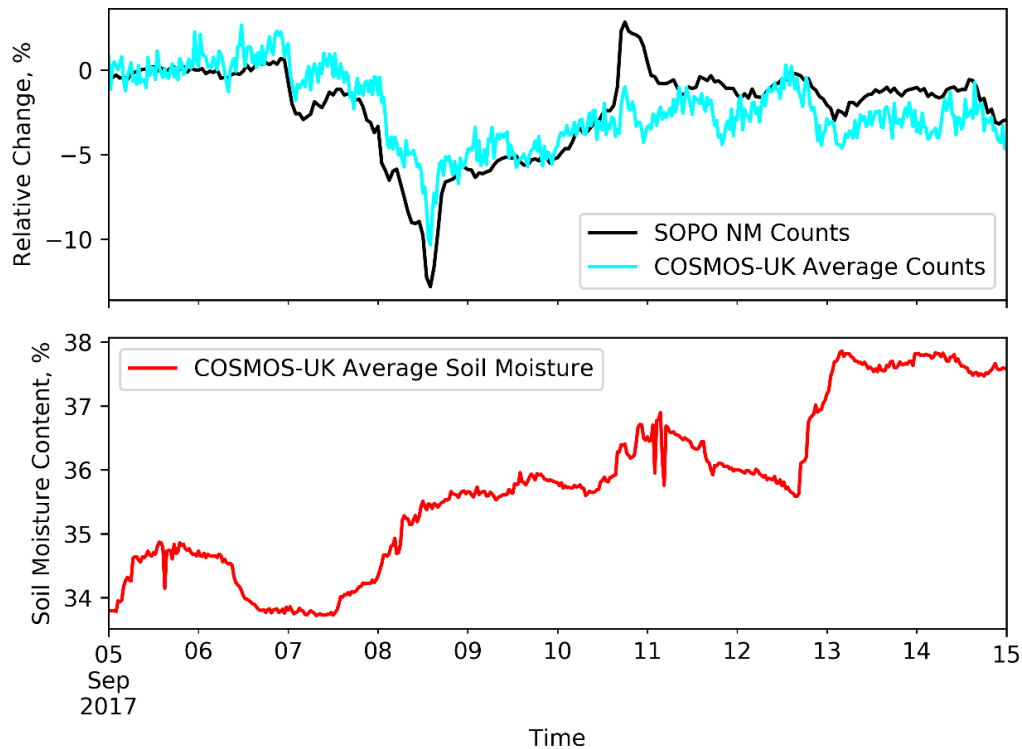


Figure 9: A Fd identified in SOPO NM (black) and average COSMOS-UK counts (cyan). The average of soil moisture across the COSMOS-UK network is displayed as the red trace.

The Fd of December 2014 (Figure 7) occurred when the soil was very wet (~48% soil moisture content). While there was a rapid spike in soil moisture shortly after the decrease, this was on the order of 0.5% and probably had no significant impact on the neutron counts recorded by COSMOS-UK sensors, compared to the effect of the Fd. The sensors record a decrease of 8% in excellent agreement with the change in count rate of the South Pole NM. During the Fd of July 2017 (Figure 8), the average soil moisture content across the COSMOS-UK does not change appreciably. The averaged neutron count trace clearly exhibits the same shape as that of the South Pole NM trace, though it does not have the same depth: the COSMOS-UK average shows a decrease of 5% where the South Pole NM shows a decrease of 8%. The Fd presented in Figure 9 took place in September 2017, immediately preceding GLE 72 (the sharp rise in the SOPO NM counting rate on the 10th of September). Both the South Pole NM and average COSMOS-UK neutron counts exhibit a very deep decrease, 14% and 10% respectively. As with the two previous Fds, the shapes of the traces are both very similar. A small increase of ~2% is observed in the average soil moisture during this Fd. However, due to the small and gradual nature of this variation, it is unlikely to be the cause of the very large decrease in the COSMOS-UK detectors.

While these three Fds have been positively identified, some large decreases with shapes similar to those of a Fd have been identified as being caused by soil moisture variations. One such example, from May 2019, is presented in Figure 10. The average soil moisture content across the UK increases by 4% in one day, before gradually reducing to original levels over several days. This results in a decrease of 6% in the average COSMOS-UK counting rate, followed by a gradual recovery to original counting rates. During this period the South Pole NM does not record any decrease similar to that of the average COSMOS-UK neutron count data. Hence, while it is clear that Fds have been identified in averaged COSMOS-UK neutron count data, it is also clear that in some cases Fds can be hard to identify, or could be incorrectly identified. However, if the response of the sensors to soil moisture

variations can be better understood, then these variations can potentially be corrected for. This could make it possible to consistently identify small Fds in the COSMOS-UK data.

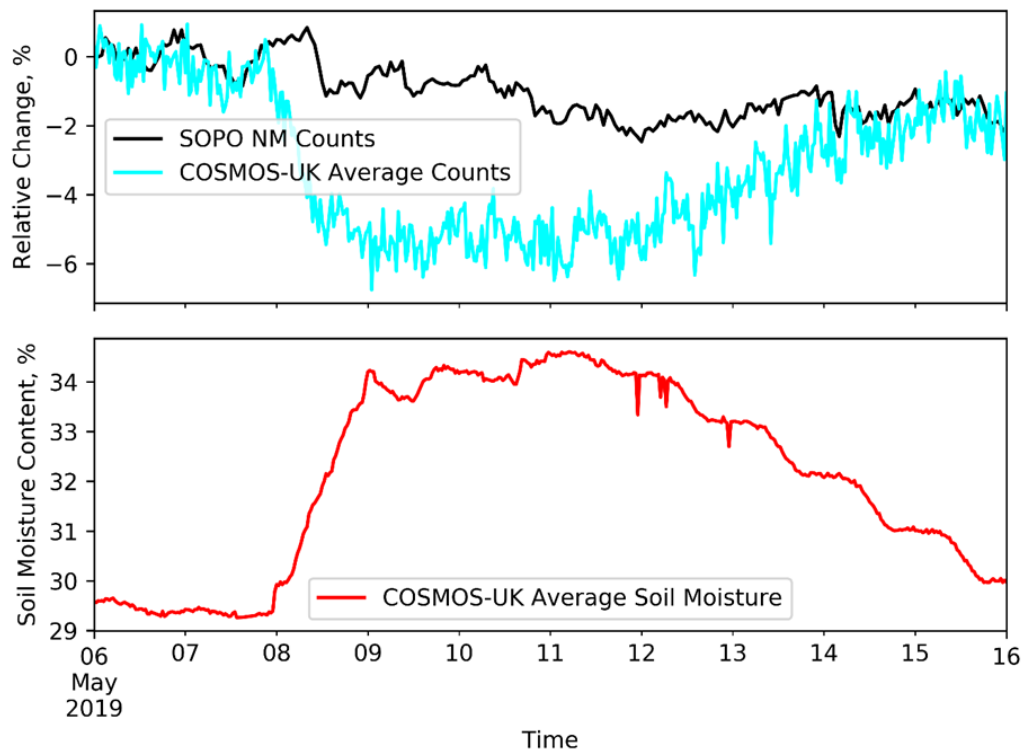


Figure 10: Relative change in count rate from the SOPO NM (black) and average COSMOS-UK counts (cyan). The average of soil moisture across the COSMOS-UK network is displayed in red in the lower plot.

4.2.2 GLEs

COSMOS detectors have been deployed in the UK and North America for approximately one decade. In that timeframe two GLEs were recorded by the GLNM network: GLE #71 on 17th May 2012 [21] and GLE #72 on 10th September 2017 [22, 23]. As can be seen with Oulu neutron monitor data plotted in Figure 11, neither event was large by historical context. GLE71 produced ~15% increases at Oulu in Finland and Apatity in Russia, and at the high-altitude South Pole station. Increases in Canadian low rigidity cut-off neutron monitors were more modest at ~5%. GLE72 was even more moderate with only the high-altitude Antarctic mini neutron monitors DOM-B and DOM-C registering increases in excess of 10%. For both GLEs only neutron monitors at low rigidity cut-off (< 2 GV) observed any significant increase over the GCR background count rate.

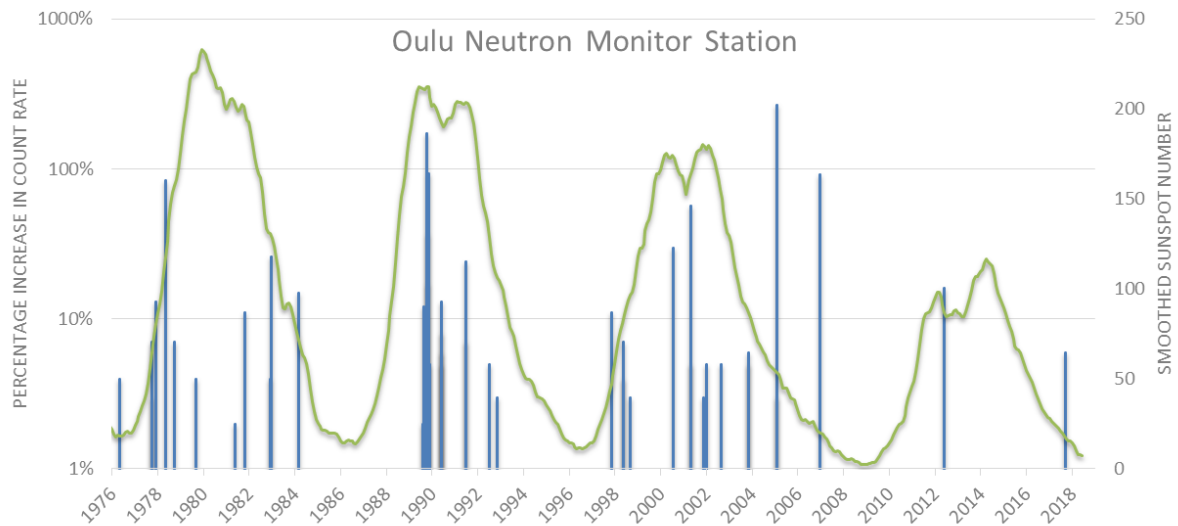


Figure 11: GLE percentage increases since 1976 measured at the OULU neutron monitor in Finland. A smoothed sunspot number is also plotted to show the solar cycle.

This absence of large GLEs in recent years means the scope for discovering GLE signals in COSMOS detector data is extremely limited. This is especially true for the UK COSMOS network because, as shown in Figure 12, processed data are only available since late 2013. A list of station names, coordinates and cut-off rigidities for the UK COSMOS network is given in Table 4, and the rigidity range is further plotted in Figure 13 as a function of geomagnetic index, K_p , as calculated by the MAIRE tool (<https://www.radmod.co.uk/maire>) employing the Tsyganenko geomagnetic field model (note that there is considerable uncertainty in this calculation at high values of K_p [24]).



Figure 12: Temporal coverage of UK COSMOS detectors.

Table 4: List of UK COSMOS Stations and location details.

Ref	Name	Abbr.	Latitude	Longitude	Altitude (m)	R@Kp=0 (GV)
1	Fivemiletown	FIVET	54.2985	-7.29186	174	1.922
2	Heytesbury	HYBRY	51.20289	-2.0796	166	2.755
3	Wimpole	WIMPL	52.13219	-0.04441	30	2.596
4	Writtle	WRITTL	51.734	0.417895	44	2.687
5	Alice Holt	ALIC1	51.15355	-0.85823	80	2.794
6	Balruddery	BALRD	56.4823	-3.11149	130	1.6
7	Bickley Hall	BICKL	53.02635	-2.70053	78	2.325
8	Bunny Park	BUNNY	52.86073	-1.12685	39	2.405
9	Cardington	CARDT	52.1056	-0.42464	29	2.592
10	Cwm Garw	CGARW	51.95136	-4.74658	299	2.52
11	Chimney Meadows	CHIMN	51.70802	-1.47877	65	2.655
12	Chobham Common	CHOBH	51.36795	-0.59748	47	2.752
13	Cockle Park	COCLP	55.21601	-1.69437	87	1.866
14	Crichton	CRICH	55.04312	-3.58337	42	1.838
15	Easter Bush	EASTB	55.86741	-3.20709	208	1.705
16	Elmsett	ELMST	52.09465	0.993065	76	2.608
17	Euston	EUSTN	52.33639	0.795922	18	2.554
18	Gisburn Forest	GISBN	54.02381	-2.38463	246	2.106
19	Glensaugh	GLENS	56.9144	-2.56215	399	1.536
20	Glenwherry	GLENW	54.83809	-6.0046	274	1.82
21	Hadlow	HADLW	51.22856	0.320184	33	2.799
22	Hartwood Home	HARTW	55.81026	-3.82896	225	1.698
23	Harwood Forest	HARWD	55.21594	-2.02355	300	1.856
24	Henfaes Farm	HENFS	53.22541	-4.01244	287	2.243
25	Hillsborough	HILLB	54.447	-6.0684	146	1.91
26	Hollin Hill	HOLLN	54.11068	-0.95952	82	2.129
27	The Lizard	LIZRD	50.03281	-5.19988	85	2.958
28	Loddington	LODTN	52.61016	-0.82642	186	2.469
29	Lullington Heath	LULLN	50.79372	0.18887	119	2.895
30	Moor House	MOORH	54.65942	-2.4678	565	1.959
31	Morley	MORLY	52.54815	1.034231	55	2.507
32	North Wyke	NWYKE	50.77348	-3.90596	181	2.813
33	Plynlimon	PLYNL	52.45338	-3.76259	542	2.428
34	Porton Down	PORTN	51.11988	-1.68125	146	2.783
35	Redmere	RDMER	52.44577	0.42104	3	2.528
36	Redhill	REDHL	51.26287	0.429135	91	2.792
37	Riseholme	RISEH	53.26165	-0.52591	53	2.331
38	Rothamsted	ROTHD	51.81387	-0.37832	131	2.658
39	Sheepdrove	SHEEP	51.53032	-1.48187	170	2.695
40	Sourhope	SOURH	55.47988	-2.22999	487	1.802
41	Stoughton	STGHT	52.60164	-1.04701	130	2.465
42	Stiperstones	STIPS	52.58125	-2.94469	432	2.42
43	Tadham Moor	TADHM	51.2075	-2.82879	7	2.737
44	Waddesdon	WADDN	51.83948	-0.94842	98	2.638
45	Wytham Woods	WYTH1	51.77728	-1.33846	109	2.643
46	Spennymoor	SPENF	53.86886	-1.31886	57	2.172
47	Fincham	FINCH	52.61777	0.510728	15	2.49
48	Moreton Morrell	MOREM	52.19941	-1.56308	53	2.542
49	Sydling	SYDLG	50.82837	-2.52789	249	2.831
50	Cochno	COCHN	55.94142	-4.40354	168	1.66
51	Holme Lacy	HLACY	52.02088	-2.66211	76	2.555

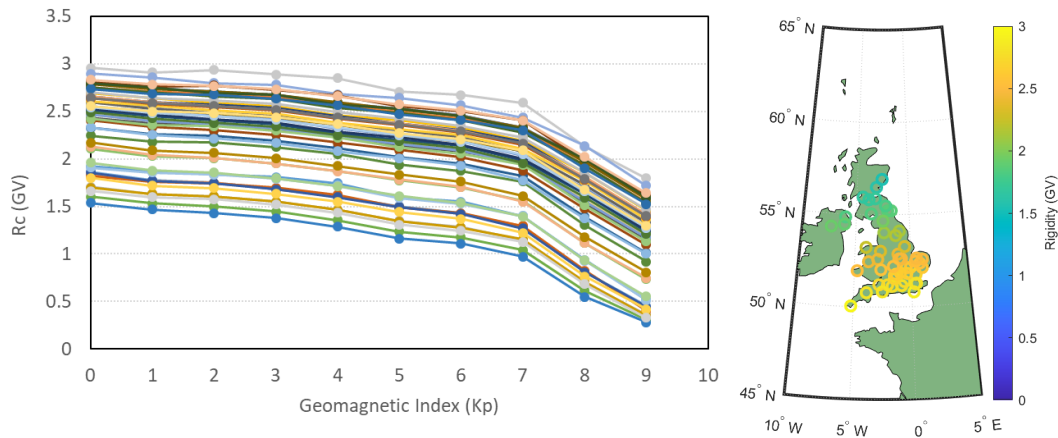


Figure 13: (LHS) UK COSMOS station rigidity cut-off as a function of geomagnetic disturbance index (K_p). (RHS) Map of UK stations with rigidity at $K_p=0$ indicated with a colour scale.

COSMOS-UK counts are collected in 30-minute bins and raw count rates are then corrected for atmospheric pressure and humidity. Figure 14 shows the full range of data available for the Alice Holt station in Hampshire and Figure 15 shows these data for the period around GLE72 only. In both cases uncorrected counts, corrected counts and 24-hr smoothed corrected counts are plotted. Various quality flags are also applied to the corrected count rates. The two dominant influences on the fluctuation of the count rate after pressure and humidity correction are cosmic ray modulation and variation in local soil moisture conditions. In Figure 15 there is also significant statistical fluctuation over short timescales, of the order of 5%, which is consistent with Poisson uncertainty on ~ 600 counts per bin. The planetary K_p index at the time of GLE72 was 2, which corresponds to a rigidity cut-off of 2.7 GV for Alice Holt. This means that we would not expect to see statistically significant evidence of GLE72 in the data, and indeed Figure 15 confirms that this is the case. The same can be said for the higher latitude COSMOS-UK station of Balruddery, which at the time of GLE72 had a cut-off rigidity of 1.5 GV. Figure 16 shows that, although there is a small spike in count rate coincident with the peak of GLE72, it is no larger than other spikes in the same period and thus is fully consistent with statistical fluctuation only.

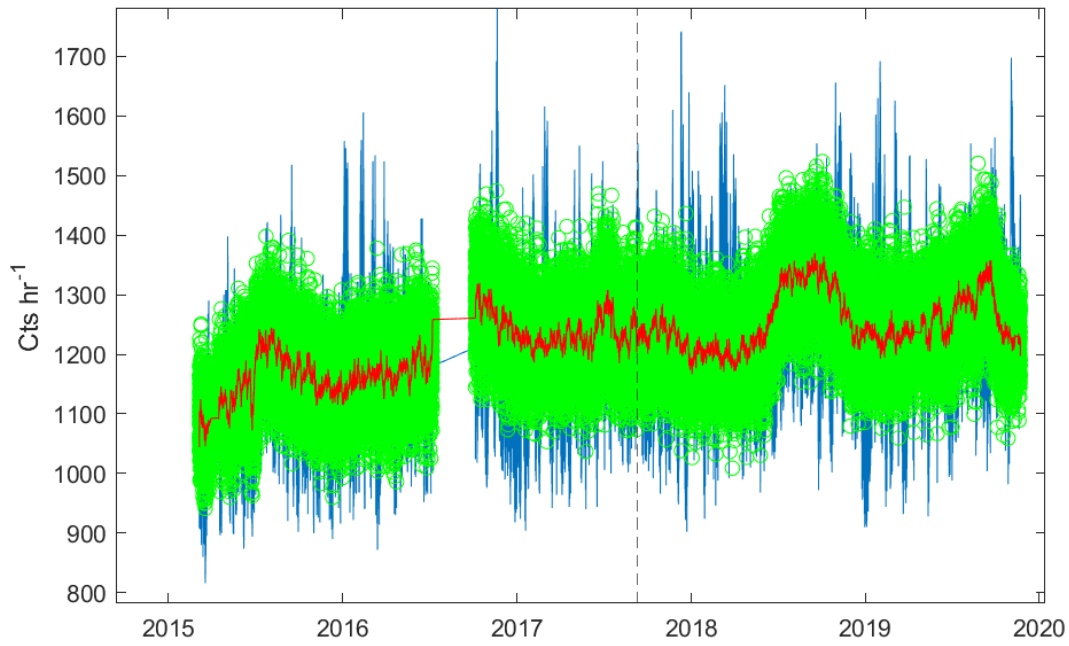


Figure 14: Data from the Alice Holt COSMOS station. The uncorrected count rate, corrected count rate and 24-hr smoothed corrected count rate are represented by the blue line, green circles and red line respectively. GLE72 is represented by a dashed vertical black line.

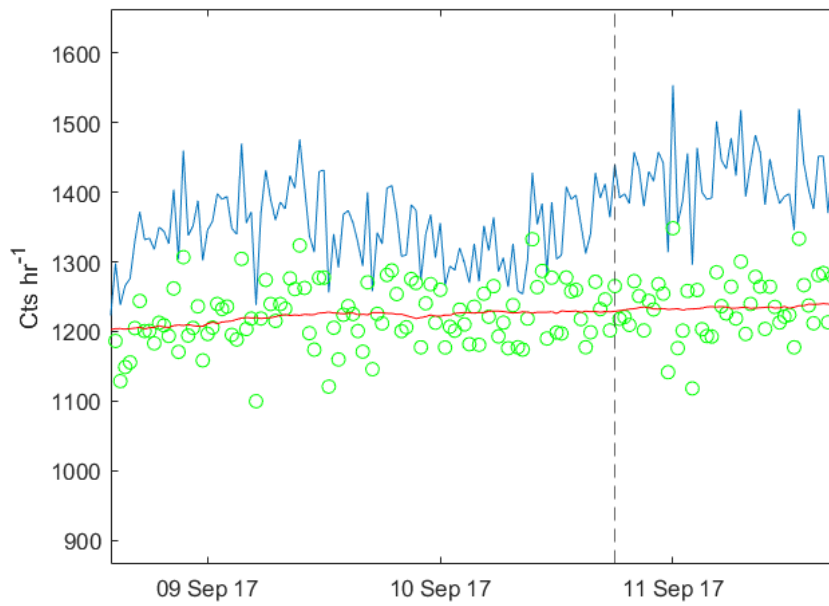


Figure 15: Alice Holt data for the period of time before and after GLE72. The uncorrected count rate, corrected count rate and 24-hr smoothed corrected count rate are represented by the blue line, green circles and red line respectively. GLE72 is represented by a dashed vertical black line.

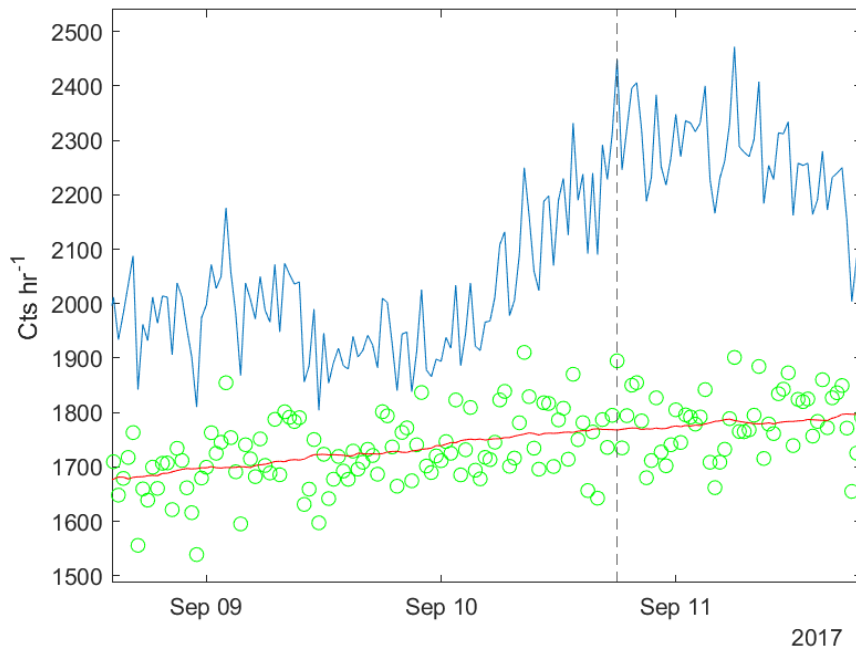


Figure 16: Balruddery COSMOS station data for the period of time before and after GLE72. The uncorrected count rate, corrected count rate and 24-hr smoothed corrected count rate are represented by the blue line, green circles and red line respectively. GLE72 is represented by a dashed vertical black line.

To improve the potential for resolving small increases in the COSMOS-UK count rate, we have aggregated the data for all available stations in the period of GLE72. 43 of the 51 stations recorded data in this period. Figure 17 shows the individual station data and average count rate over two timescales. A small peak (<2% increase) is observed to be coincident with GLE72, however, as with the peak in the Balruddery station data, the magnitude of this peak is consistent with simple statistical fluctuation, so it is inconclusive whether GLE72 is wholly or partly responsible for this peak.

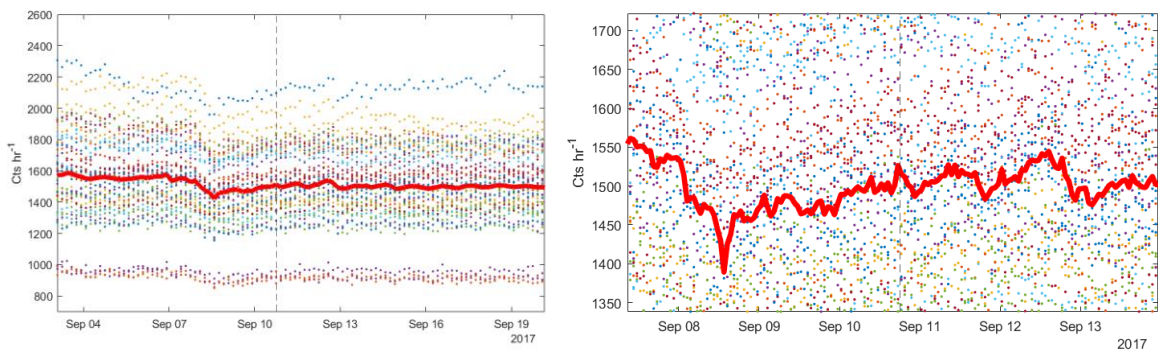


Figure 17: Count rates from 43 UK COSMOS stations (dots) and the average count rate (red line) during the period surrounding GLE72. The spread in individual station count rates is shown in the LHS plot and the fine structure is shown by the hourly-averaged RHS plot. The peak of GLE72 is represented by a dashed vertical black line.

North American COSMOS stations occupy locations with lower cut-off rigidity than COSMOS-UK stations. Table 5 lists the nine stations with the lowest cut-off rigidity (all under 1.5 GV), which we have used in our GLE analysis. Location and rigidity information was sourced from <http://cosmos.hwr.arizona.edu/>, where some raw and processed data are also available for download. Data used in the following analysis were separately obtained and reprocessed by the University of Bristol as part of the MOSAIC project. Three correction factors are applied for

atmospheric pressure, atmospheric water vapour and above ground biomass. The temporal resolution of all raw data is one-hour binning of detector counts. Corrected count rates are shown for all available time periods for each station in Figure 18.

Table 5: North American COSMOS stations with the lowest cut-off rigidity.

Site ID	Site Name	Latitude	Longitude	Altitude (m)	Rigidity (GV)
97	Trail Valley Main Met	68.7455	-133.5	125	0.06
94	Trail Valley Upper Plateau	68.6936	-133.6974	150	0.09
96	Havikpak Main Met	68.3199	-133.5198	125	0.09
95	Trail Valley Forest	68.7227	-133.4955	125	0.1
105	Barrow-ARM	71.3298	-156.6287	4	0.14
88	Saskatoon	52.1326	-106.6168	506	0.86
48	Fort Peck	48.3077	-105.1019	634	1.23
42	Park Falls	45.9459	-90.2723	470	1.25
43	UMBS	45.5598	-84.7138	220	1.31

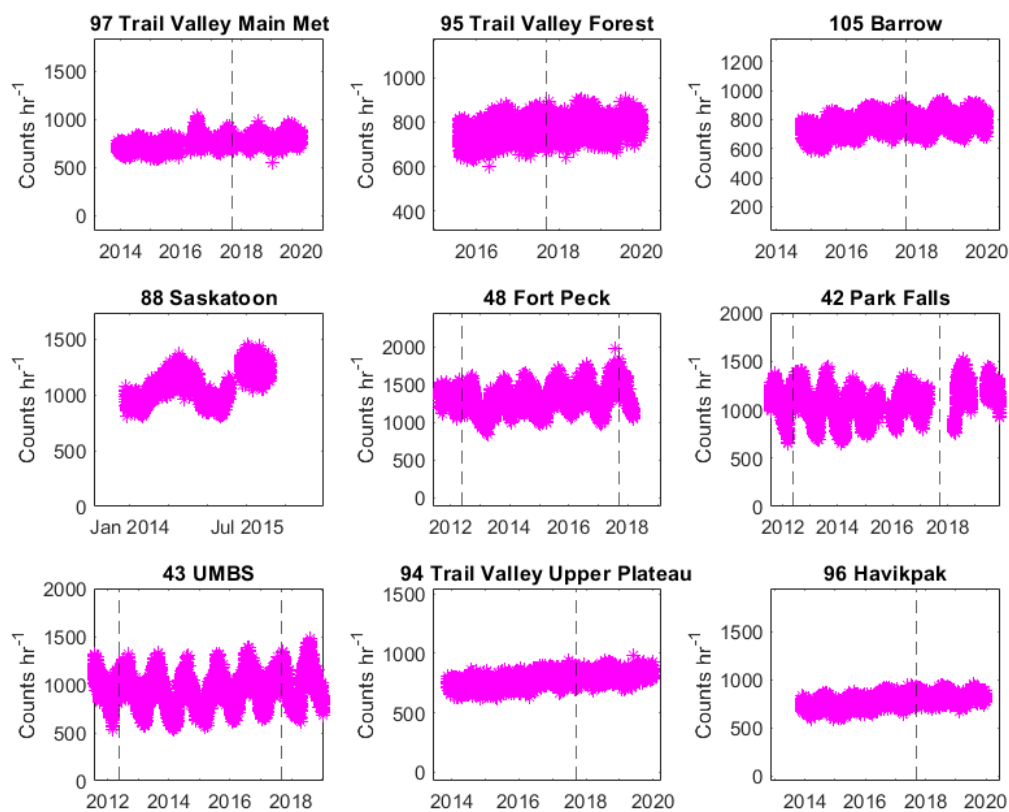


Figure 18: Corrected count rates for nine North American COSMOS stations. GLE71 and GLE72 are represented by dashed vertical black lines.

Seasonal effects in the count rates due to local soil moisture variation are apparent in the data. As is also clear from Figure 18, not all stations have data available for either or both GLEs. Table 6 summarises which stations have data for each GLE – three for GLE71 and seven for GLE72. Although

the Saskatoon station has no data for either GLE, the data set is included in the analysis as it is useful to compare rates of false positive GLE identification.

Table 6: Summary of GLE data coverage for 9 COSMOS stations.

Site ID	Name	GLE71	GLE72
42	Park Falls	✓	x
43	UMBS	✓	✓
48	Fort Peck	✓	✓
88	Saskatoon	x	x
94	TV UP	x	✓
95	TV Forest	x	✓
96	Havikpak	x	✓
97	TV Main Met	x	✓
105	Barrow	x	✓

Figure 19 and Figure 20 show COSMOS data for the periods around GLE71 and GLE72 respectively. In both cases there is a small spike in the averaged count rate data coincident with the GLE. However, in the case of GLE71 the spike is indistinguishable from similar spikes nearby, and hence is consistent with statistical fluctuation. In the case of GLE72 the coincident spike appears more significant, though this appearance is helped substantially by the presence of a significant Forbush decrease in the data immediately before the GLE.

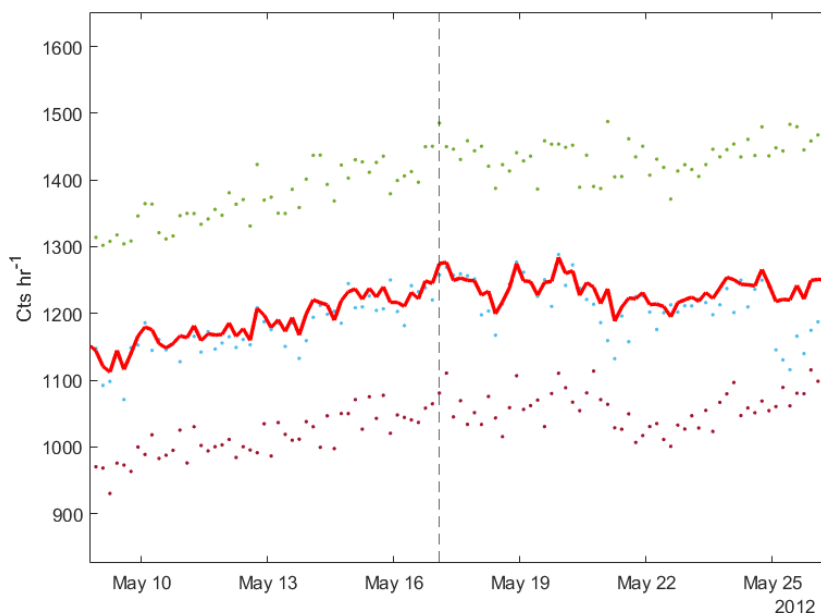


Figure 19: Individual COSMOS station data (dots) and average (red line) for the period surrounding GLE71. All data are binned into 4-hour intervals to further improve the statistics. The GLE is represented by a dashed vertical black line.

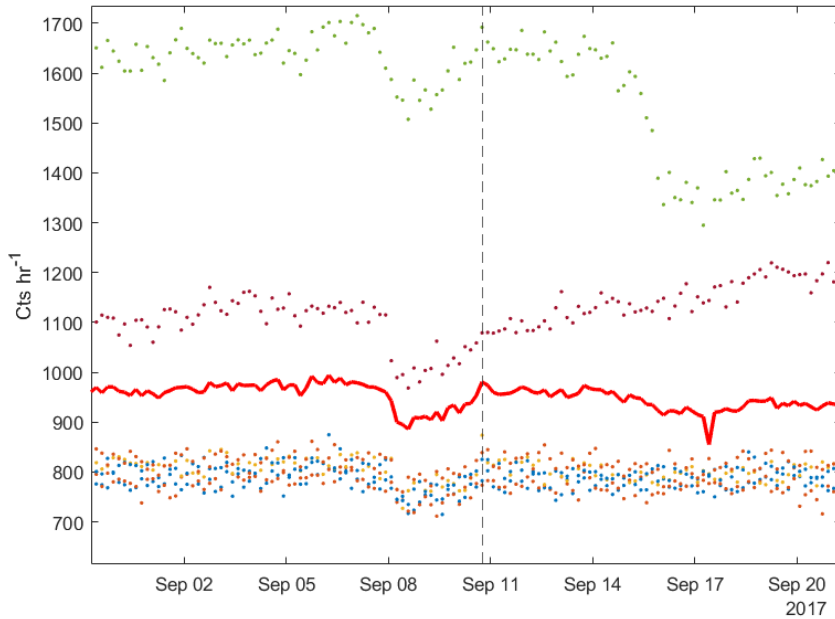


Figure 20: Individual COSMOS station data (dots) and average (red line) for the period surrounding GLE71. All data are binned into 4-hour intervals to further improve the statistics. The GLE is represented by a dashed vertical black line.

To investigate the significance of GLE signals in the individual station data we devised a simple statistical test that can be applied to each entire data series:

$$\text{Sigma} = \frac{\text{Increase in count rate (compared to previous 24 hrs)}}{\text{Average Poisson error of previous 24 hours}} = \frac{\Delta N}{\bar{\sigma}_P}$$

Equation 1

We calculate a value for significance (sigma) for every data point in a 4-hour temporal binning scheme. For example, Figure 20 shows the corrected count rate for the Park Falls COSMOS station in May 2012. The count rate coincident with GLE71 is 1258 cts hr⁻¹, compared to an average count rate in the preceding 24 hours of 1220 cts hr⁻¹. The average Poisson error of the six bins in the preceding 24-hour period is 18.7 cts hr⁻¹, hence using Equation 1 the calculated significance parameter is sigma = 2. It is also possible to use the standard deviation of the count rate over the preceding 24 hours to normalise the increase in count rate, however as the count rate is relatively stable, the Poisson error is a more consistent estimator of the standard deviation of the underlying population.

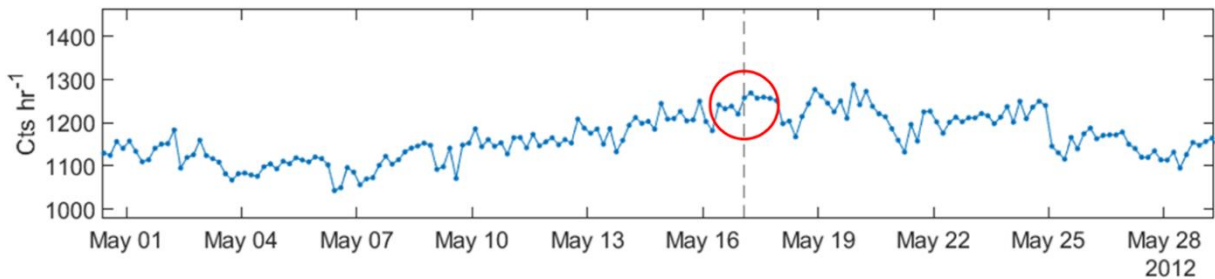


Figure 21: Corrected count rate of Park Falls COSMOS station in May 2012. The data are binned in 4-hour intervals and the data point coincident with GLE71 (counts recorded from 00:00 – 04:00 on 17th May 2012) is highlighted with a red circle.

To put this value for sigma in context, we repeated this calculation for the entire data series. Figure 22 shows Park Falls data for the entire available period, with the corresponding sigma value. The distribution of sigma is plotted as a histogram in Figure 23. It is clear from these plots that the value of sigma at GLE71 (sigma = 2) does not represent an outlier in the Gaussian-like distribution of all sigma values.

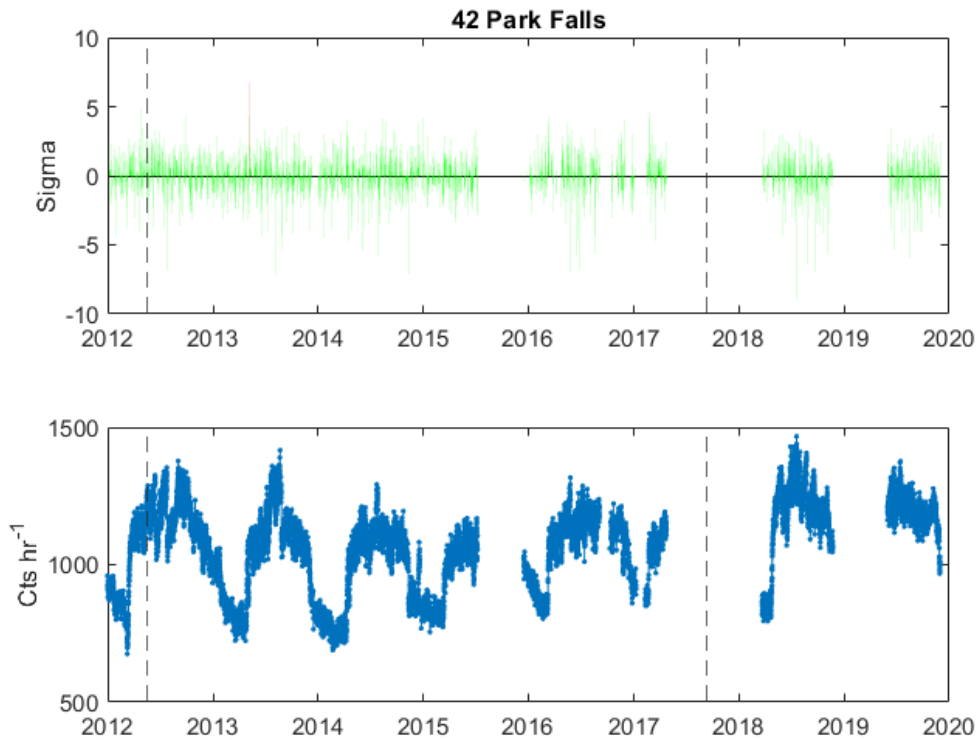


Figure 22: Park Falls COSMOS detector count rates in 4-hr binning scheme (lower panel) with corresponding value for sigma (upper panel). GLE71 and GLE72 are represented by dashed vertical black lines.

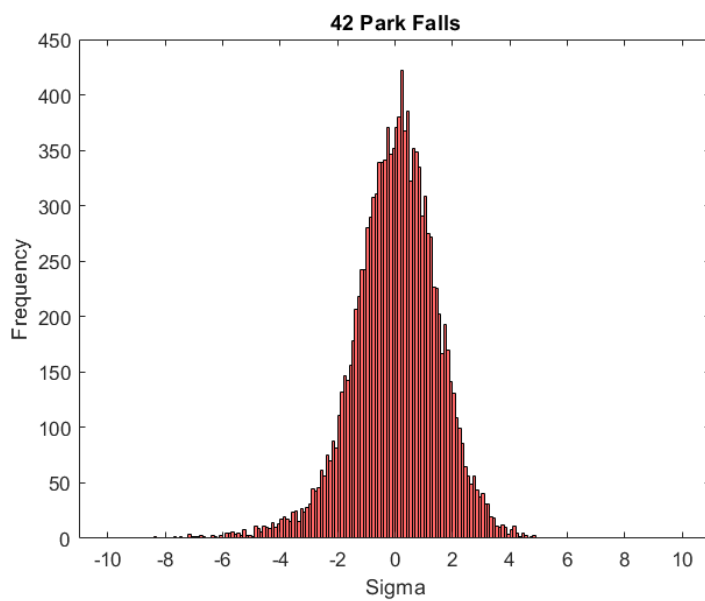


Figure 23: Histogram of calculated sigma values for Park Falls.

We applied this process to all seven of the other low rigidity COSMOS stations with data during one or both GLEs, and to Saskatoon, which has data for neither. The results for stations 43, 48, 88 and 94 are shown in Figure 24, results for stations 95, 96, 97 and 105 are shown in Figure 25. Gaps in the green sigma time series are the result of gaps in data series as we imposed a condition that for a value of sigma to be calculated the data for the previous 24 hours must be complete (see Equation 1). Red lines in the sigma data series are used to highlight instances where $\sigma > 5$.

On this scale the values of sigma at the time of each GLE cannot be read directly of the plots. Table 7 summarises the calculated values for all stations, as well as the number of occasions where a sigma value greater than 5 was recorded (hereafter referred to as “false positives” in the vast majority of cases where these data points are not coincident with a GLE).

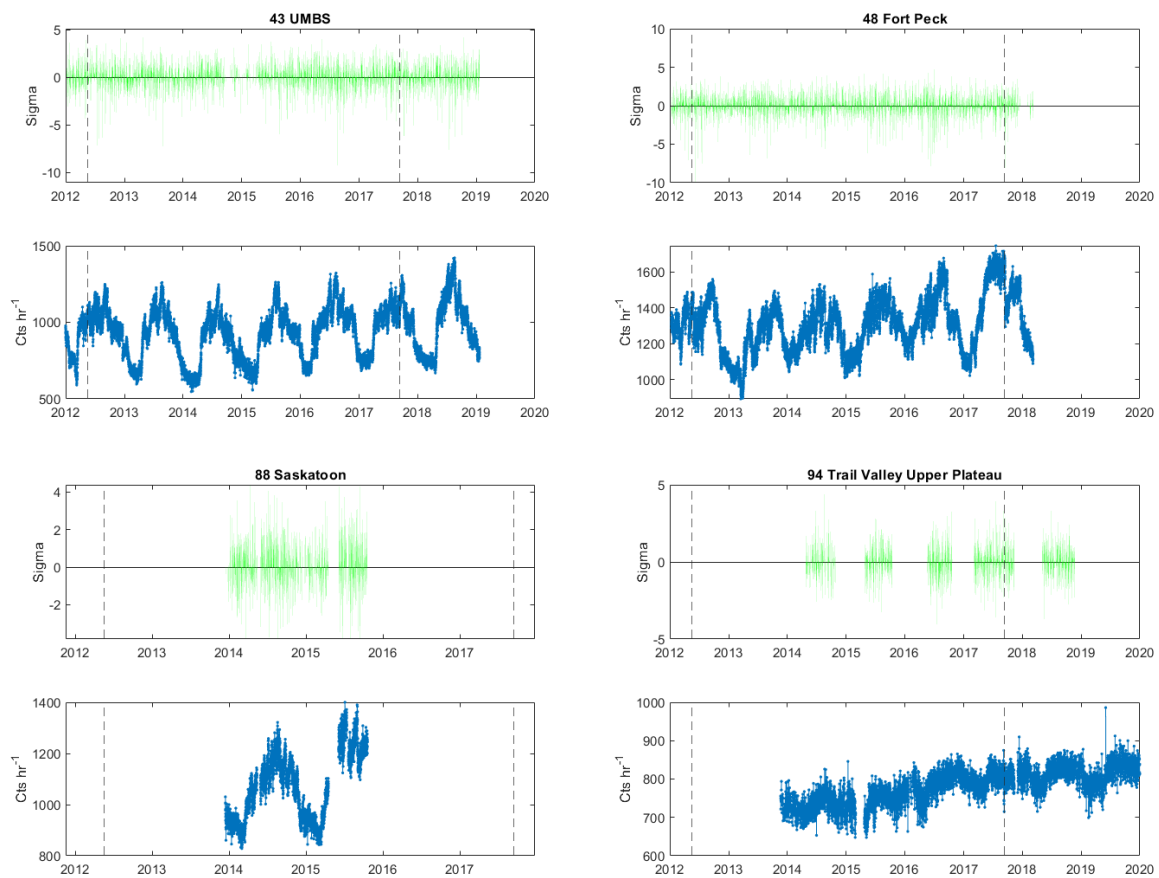


Figure 24: COSMOS detector count rates in 4-hr binning scheme (lower panel) with corresponding value for sigma (upper panel). GLE71 and GLE72 are represented by dashed vertical black lines.

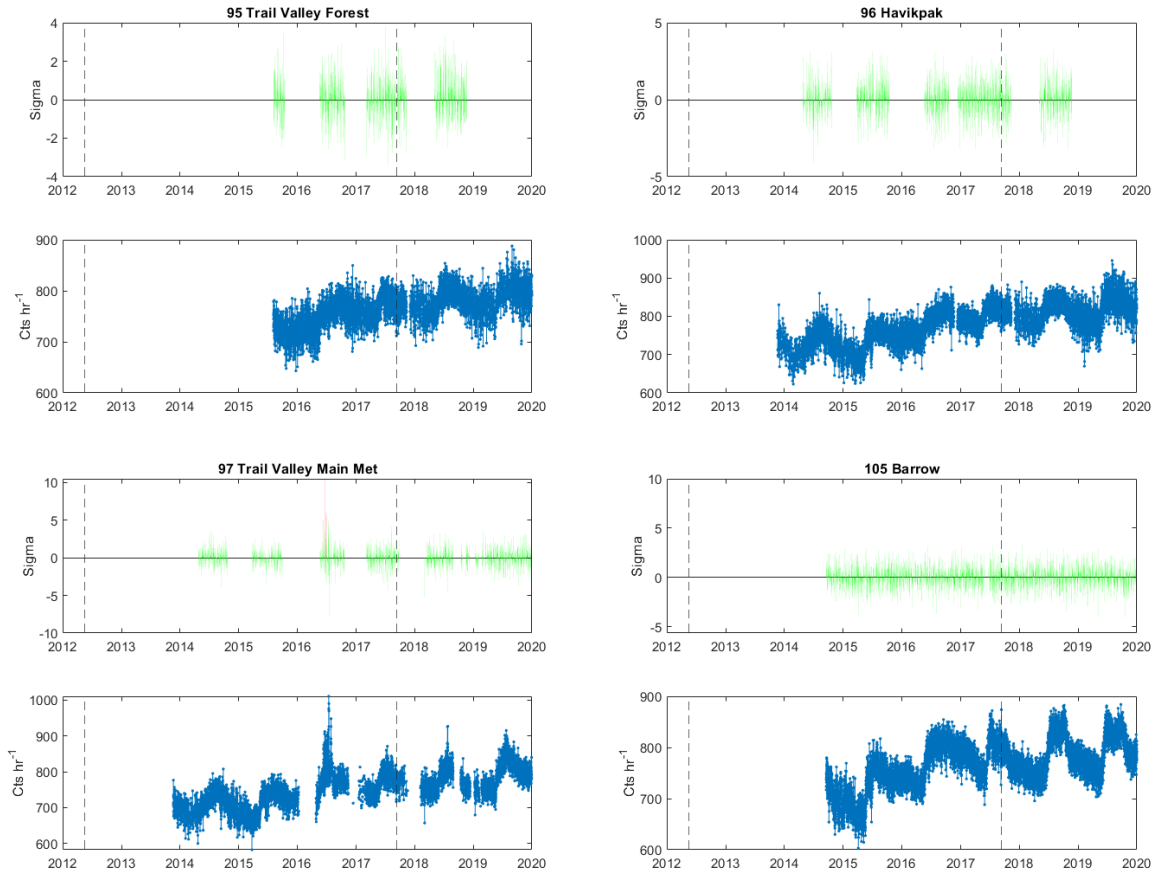


Figure 25: COSMOS detector count rates in 4-hr binning scheme (lower panel) with corresponding value for sigma (upper panel). GLE71 and GLE72 are represented by dashed vertical black lines.

Table 7: Summary of calculated sigma values at each GLE time and the number of occasions where sigma > 5.

Site ID	Name	sigma(GLE71)	sigma(GLE72)	# sigma>5
42	Park Falls	2	-	11
43	UMBS	1.7	2.3	2
48	Fort Peck	3.4	3.5	12
88	Saskatoon	-	-	1
94	TV UP	-	2.8	1
95	TV Forest	-	1.3	0
96	Havikpak	-	2.4	0
97	TV Main Met	-	1.7	13
105	Barrow	-	6.9	1

Table 7 shows that in the entire aggregate data set there is only one occasion where a GLE coincided with a sigma value greater than five. This was for GLE72 in the Barrow data set. Figure 26 shows a zoomed-in version of the binned data series and sigma values for this period. GLE72 coincides with a clear spike in the COSMOS data, however the significance (sigma = 6.9) is enhanced by the Forbush decrease that occurs immediately beforehand. The prominence of the peak relative to the period *after* the GLE is lower. This introduces doubt into the true significance of the peak in the Barrow data. To further illustrate this, Figure 27 shows renormalised count rates for all seven COSMOS stations with

data during GLE72. Plotted on the same relative axis is the count rate for the Inuvik (INVK) neutron monitor station, which is in very close geographical proximity to the three Trail Valley COSMOS stations (#s 94, 95 & 97) and Havikpak (#96), as depicted in Figure 28.

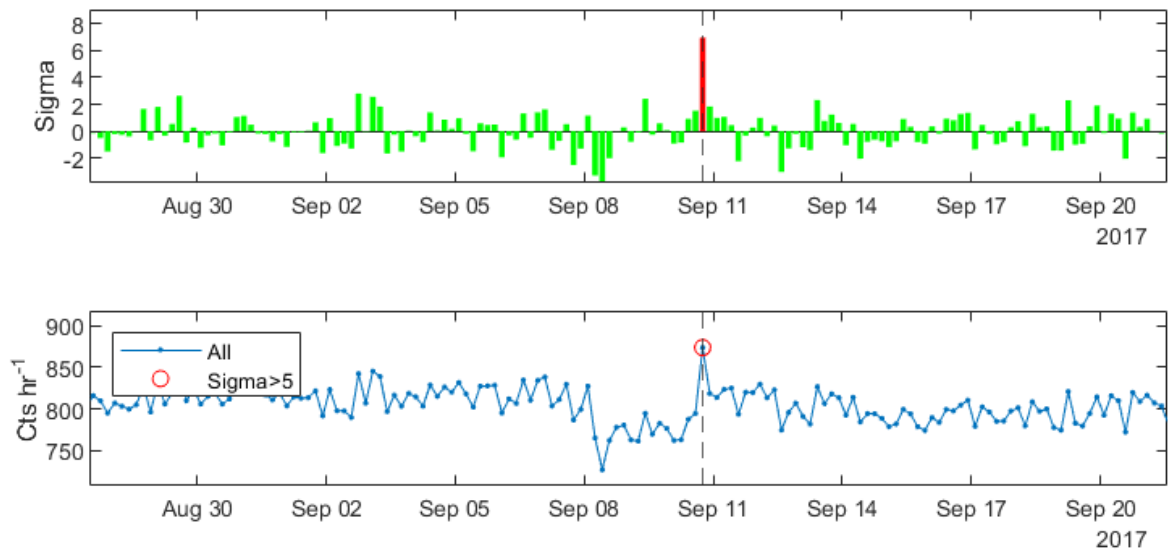


Figure 26: Barrow COSMOS detector count rates in 4-hr binning scheme (lower panel) with corresponding value for sigma (upper panel) in Aug/Sep 2017. GLE72 is represented by a dashed vertical black line.

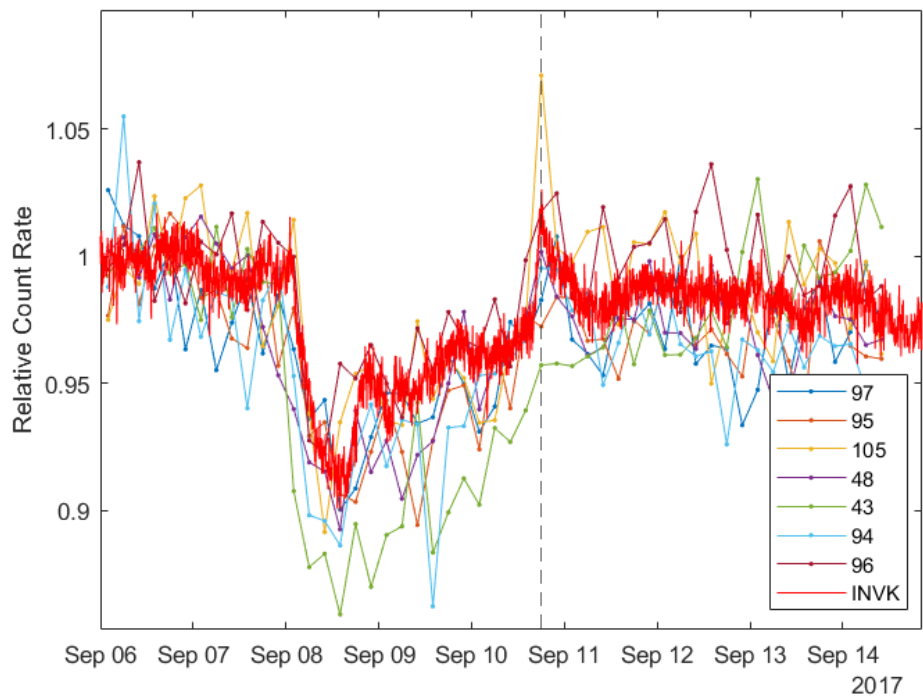


Figure 27: Renormalised COSMOS data from seven stations during GLE72 in September 2017 (dotted lines). Equivalent renormalised count rates from the Inuvik (INVK) neutron monitor station are also plotted (red line). GLE72 is represented by a dashed vertical black line.



Figure 28: Map showing the relative locations of some of the low rigidity COSMOS stations and the Inuvik (INVK) neutron monitor station.

The magnitude of the increase at Inuvik is $\sim 6\%$ relative to the period immediately prior to the event (though this level is depressed due to the ongoing Forbush decrease and is reduced to $\sim 4\%$ if an equivalent 4-hr averaging scheme is used). Renormalised count rates for the four COSMOS stations in close proximity to Inuvik show fluctuations that are of the same order of magnitude as the increase at Inuvik but are also clearly consistent with simple statistical variance. By contrast the peak at Barrow is approximately twice the size implied by neutron monitor data. Although the distance between Barrow and Inuvik is nearly 1000 km, this excess is not necessarily caused by longitudinal anisotropy in the GLE as several other neutron monitors spanning a wide longitudinal range (Thule, Peawanuck and Nain) all show increases in the 4 – 6 % range.

Another factor that may play a role in the prominence of the peak at Barrow is the local soil moisture conditions at the time of GLE72. Figure 29 shows again the 4-hr binned count rate at Barrow, with ERA5-Land hourly rainfall data plotted below on the same time axis. The rainfall data are based on a remodelled gridded dataset with 9 km spatial resolution rather than rainfall gauges co-located with the COSMOS detector. The data from the Barrow region indicate that rainfall did occur in the area prior to the event and coincident with the early stages of the Forbush decrease. Hence it is possible that there is an underlying gradual increase in count rate caused by the drying of local soil. However, as with the recovery of the count rate following the Forbush decrease, this is unlikely to be on a short enough timescale to significantly affect the prominence of the peak coincident with GLE72. Also, as shown in Figure 31, similar levels of rainfall were recorded in the vicinity of most of the other COSMOS stations, without this leading to a spike in the count rate coincident with GLE72.

One further consideration when considering the value of sigma in the Barrow data at GLE72 ($\sigma = 6.9$) is the systematic uncertainty in the data caused, primarily, by soil moisture effects. We have defined significance ('sigma') using Poisson statistics based on the count rate over the previous 24 hours (where $\bar{\sigma}_p$ in Equation 1 is used as an estimator of the underlying population standard deviation). Figure 31 shows the histogram of sigma values for the Barrow site (equivalent to Figure 23 for Park Falls) with two Gaussian distributions overlaid. The blue curve is a Gaussian fit to the histogram, showing that the sigma distribution closely follows a normal curve. The standard deviation of this fit, $\sigma' = 1.14$ sigma, shows that the total variance is slightly larger than the ideal curve (shown in green) for which standard deviation is exactly 1 sigma. Hence it is reasonable to adjust the value of $\sigma = 6.9$ at GLE72 by this factor to get a better estimate of the true significance of this outlier. This adjusted value of $\sigma' = 6.0$ still suggests a high level of statistical significance, though, as discussed

above, the high prominence of the Barrow peak relative to Inuvik neutron monitor data suggests that to some degree that this is artificial. It is impossible to definitively determine how much, if any, of the excess counts in the Barrow data during GLE72 were a direct result of the event and how much are simply statistical fluctuation.

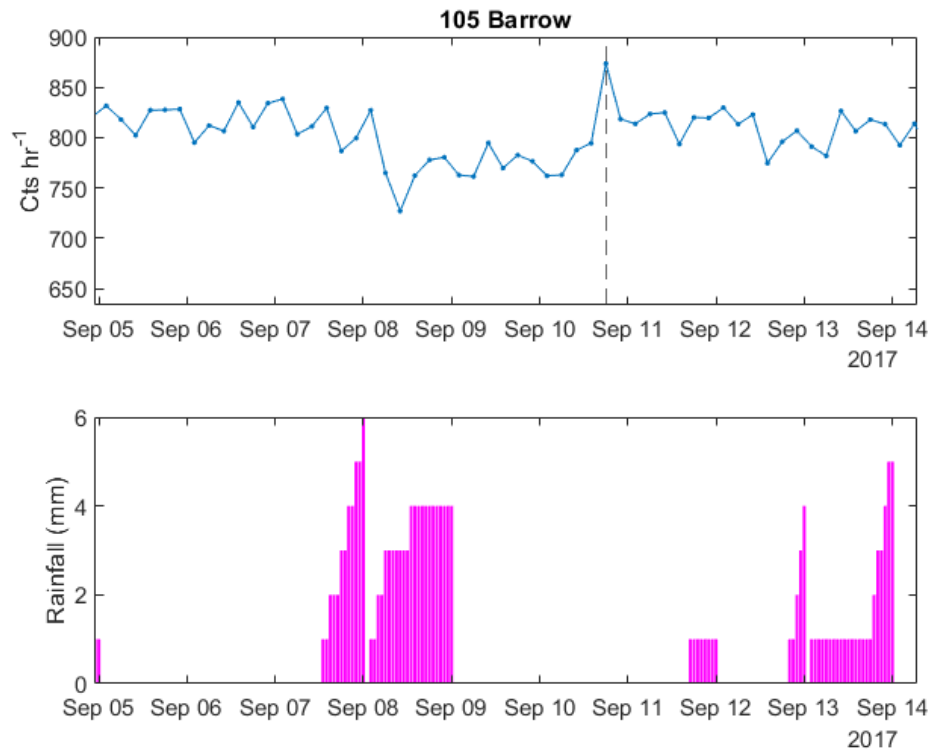


Figure 29: COSMOS Barrow count rate (upper panel) in 4-hr bins compared to ERA5-Land hourly rainfall data (lower panel) from a 9 km grid resolution. GLE72 is represented by a dashed vertical black line.

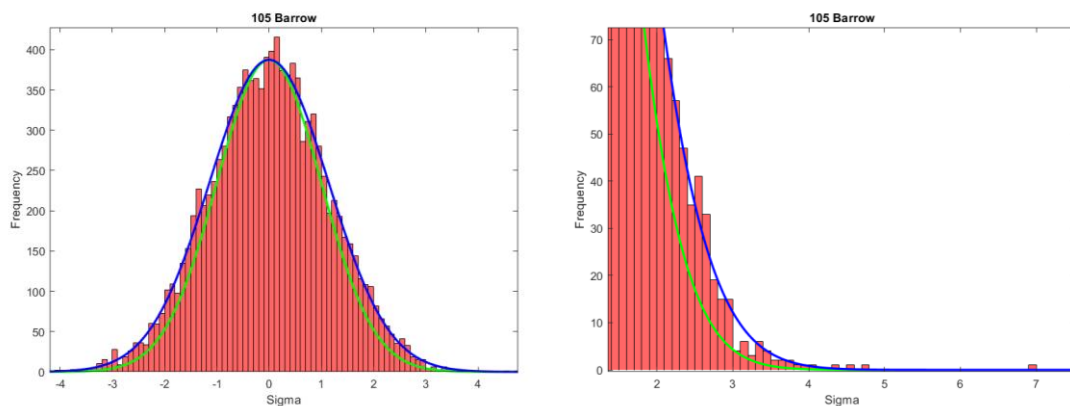


Figure 30: (LHS) Histogram of Barrow COSMOS sigma parameter. The green curve shows a Gaussian distribution with standard deviation $\sigma = 1$ sigma, the blue curve shows a Gaussian distribution fitted to the histogram ($\sigma' = 1.14$ sigma). (RHS) A close-up view of the same plot with the point coincident with GLE72 (sigma = 6.9) very clearly shown as an outlier in the distribution.

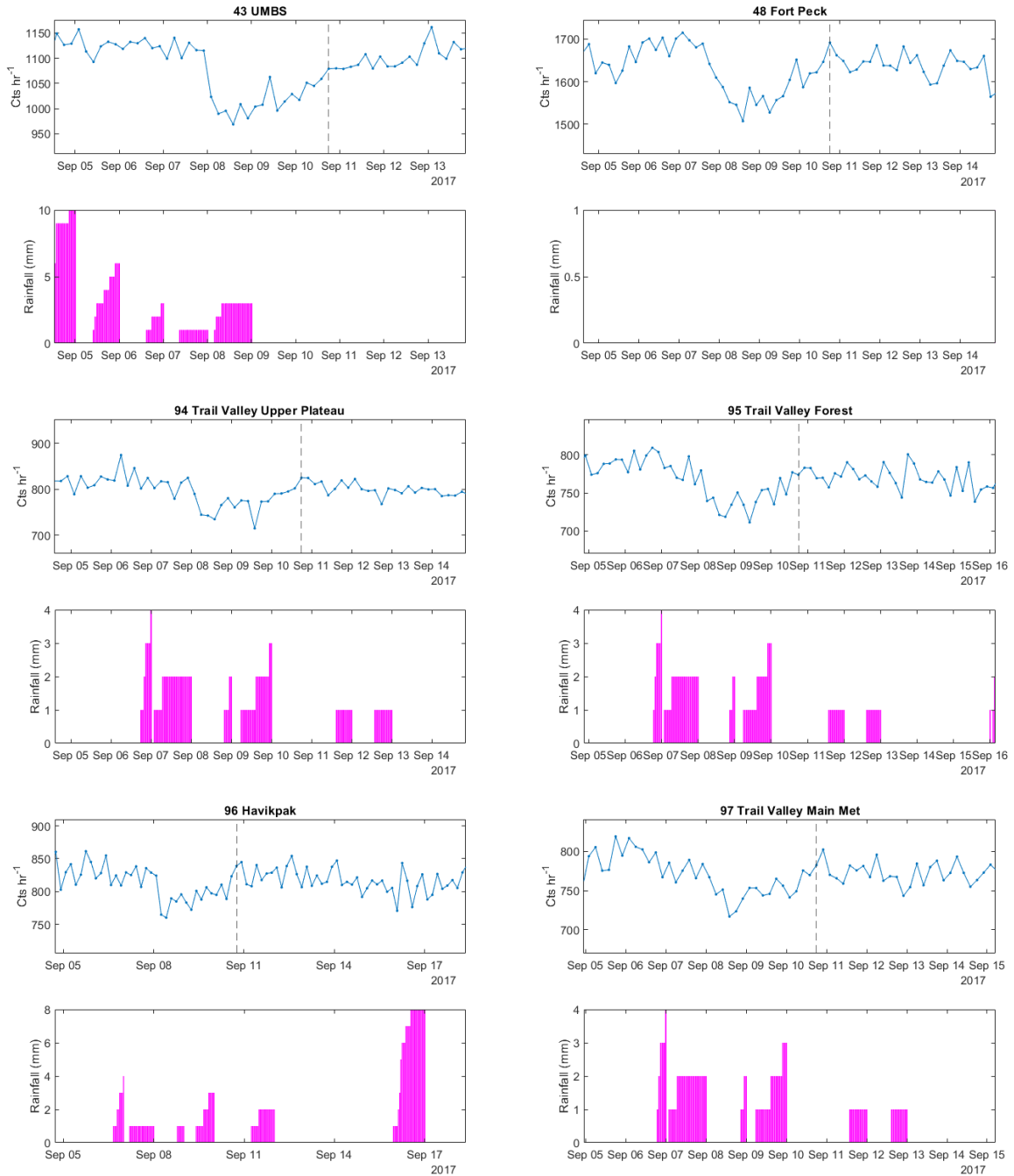


Figure 31: Count rates (upper panels) in 4-hr bins for six COSMOS stations compared to ERA5-Land hourly rainfall data (lower panels) from a 9 km grid resolution. GLE72 is represented by a dashed vertical black line in each case.

5 Theoretical Sensitivity to historic and future events

5.1 Atmospheric environment simulations

5.1.1 Primary GLE Spectra

The starting point for simulating COSMOS detector count rates during potential ground level enhancement events is to define the primary proton spectra (defined as solar proton spectra incident at Earth before magnetospheric or atmospheric attenuation) for the hypothetical events of interest. Here we use both primary spectra derived from recent or prominent historical events, and also contrived spectra based on a parameterised spectral shape. The historical events we consider are listed in Table 8. Figure 32 shows primary (peak flux) spectra for the historical GLEs compared to a GCR background spectrum. Four of the spectra are derived from the work of Allan Tylka [25] and are embedded in the MAIRE model [26], the remaining two are based on fits of the GLE71 and GLE72 by Mishev et al. [21, 23]. In all cases the GLE spectra are far softer than the GCR spectrum, though there is considerable variation in spectral shape between the GLEs.

Table 8: List of historical GLEs used in this analysis.

Reference	Date
GLE05	23 rd February 1956
GLE42	29 th September 1989
GLE59	14 th July 2000
GLE60	15 th April 2001
GLE71	17 th May 2012
GLE72	10 th September 2017

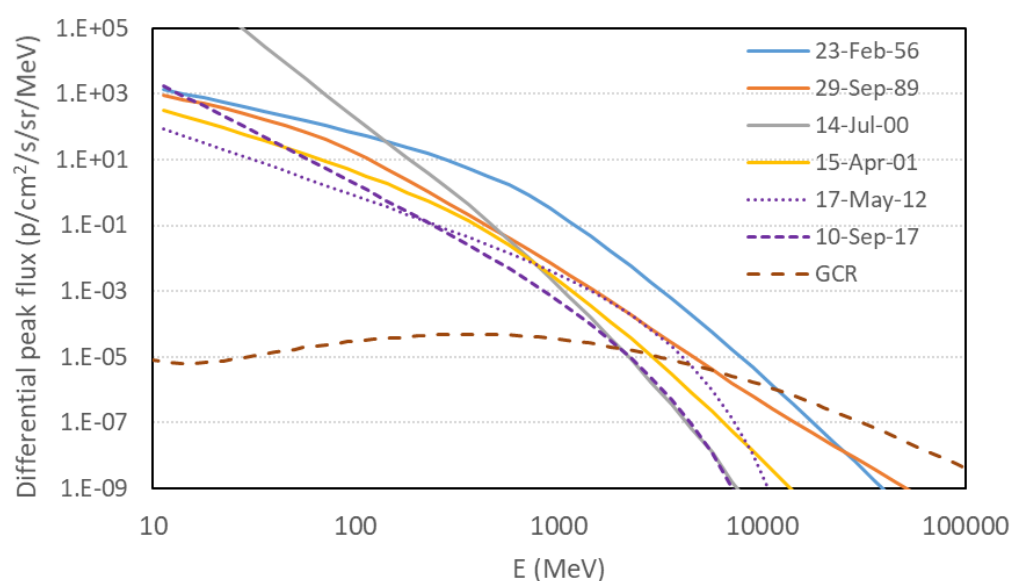


Figure 32: Peak flux energy spectra for six historical GLEs. The background galactic cosmic ray spectrum is also shown for comparison.

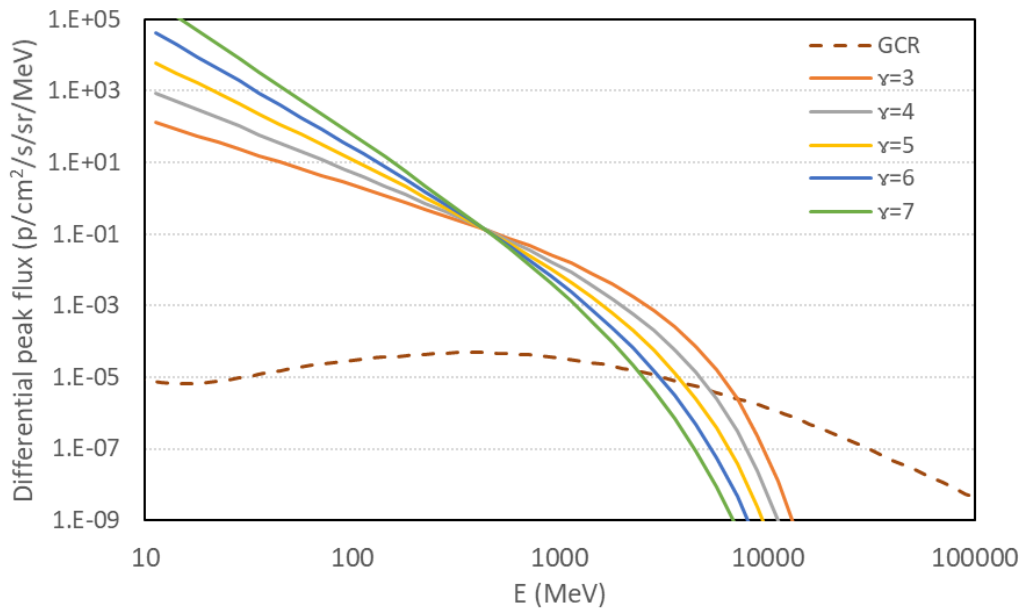


Figure 33: Peak flux energy spectra for five GLEs with different spectral indices. The background galactic cosmic ray spectrum is also shown for comparison.

To test the impact of spectral shape in a more controlled way, we also use contrived primary proton spectra using a simplified version of the power law in rigidity used by Mishev:

$$J(P) = J_0 P^{-(\gamma + 0.3 \times (P-1))}$$

Equation 2

Where P is the rigidity, γ is the spectral index and J_0 is a normalisation factor for omnidirectional intensity, arbitrarily set at 100 protons/cm²/s/sr/GV. This value is unimportant as our interpretations of these spectra are based on *relative* impacts at different rigidities or altitudes, rather than absolute fluxes or count rates. Figure 33 shows five such spectra (converted to be functions of energy) with γ ranging from 3 to 7, alongside a background GCR spectrum.

All spectra plotted in Figure 32 and Figure 33 were used as inputs to the Model for Atmospheric Ionising Radiation Effects (MAIRE), which uses Monte Carlo radiation transport simulations to calculate the atmospheric radiation environment at all geographic coordinates and altitudes up to 20 km [26]. MAIRE is capable of calculating differential and integral spectra for all major particle species, however for this task we only require neutron flux. Figure 34 shows a typical summary output page for a single position neutron flux calculation (using a UK location with geomagnetic cut-off rigidity of 2.6 GV). For a particular input primary spectrum, the two key determinants of the neutron spectrum are altitude and cut-off rigidity, and MAIRE further splits the output into upward and downward directions. Figure 35 shows downward differential neutron spectra at ground level and zero cut-off rigidity for each historical event shown in Figure 32.

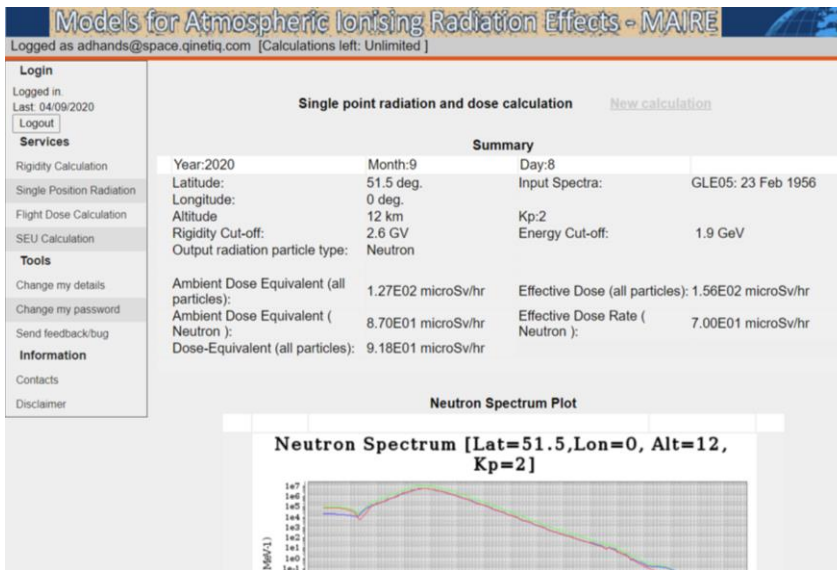


Figure 34: Example of MAIRE output for a single position neutron flux calculation. The example shown is for a UK location with geomagnetic cut-off rigidity of 2.6 GV.

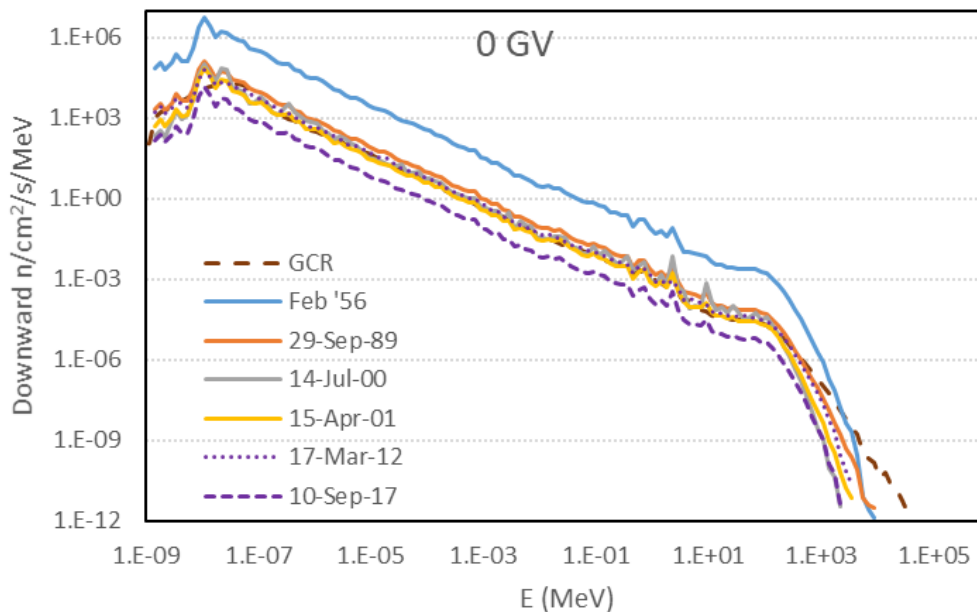


Figure 35: Ground level neutron spectra at zero cut-off rigidity for historical GLEs and the GCR background. The y axis is differential neutron flux in the downward direction.

The neutron spectra in Figure 35 show that the intensity of several of the historical events are comparable to the GCR background across a wide energy range. GLE72 (10-Sep-17) and GLE05 (23-Feb-56) are notable as respectively being significantly less or more intense than the other events and the GCR background. The event which occurred on 23-Feb-56 (GLE05), is the largest event ever directly measured [27-29]. The GCR background spectrum exceeds all GLE events at the highest neutron energies ($>10^4$ MeV) because of the much harder primary proton spectrum.

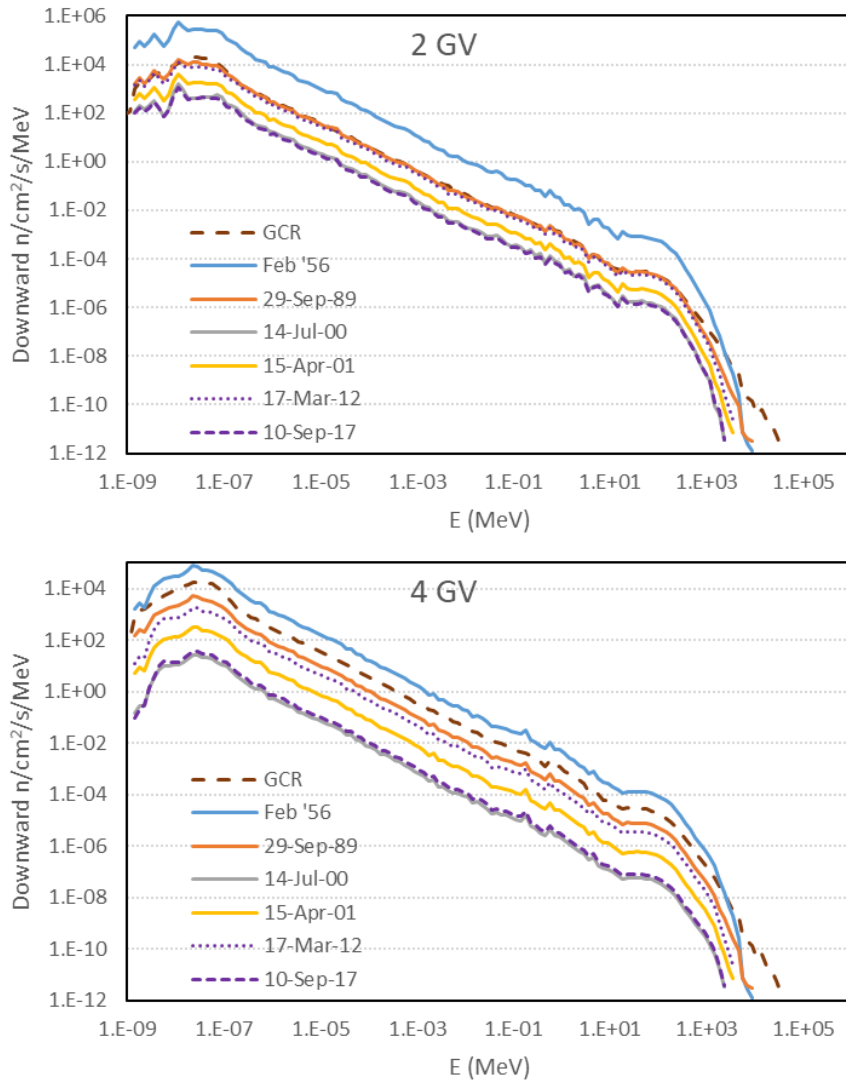


Figure 36: Ground level neutron spectra at R=2 (top) and R=4 (bottom) for historical GLEs and the GCR background.

Equivalent spectra at two higher rigidities (R=2 GV and R=4 GV) are shown in Figure 36. The higher rigidity causes the ground level neutron spectra to separate from each other due to the divergence of primary proton spectra at higher energies. The relative intensity of the GCR background also increases at higher rigidity as the relatively large number of soft (lower energy) protons in the GLE spectra are prevented from reaching the upper atmosphere by the magnetic field.

Figure 37 shows downward neutron spectra at ground level for the five contrived GLE spectra at the same three cut-off rigidities as above (R=0, R=2 and R=4 GV). As the normalisation of these primary input spectra is arbitrary the relative intensity between the events of different spectral index and compared to the GCR background is unimportant. However, the effect of rigidity on the relative intensity is very clear, as is the apparent similarity between the shapes of the ground-level neutron spectra, regardless of primary spectral index and cut-off rigidity. As will be demonstrated later, this latter observation greatly simplifies the interpretation of the effect of shape of the primary spectra on COSMOS detector count rates.

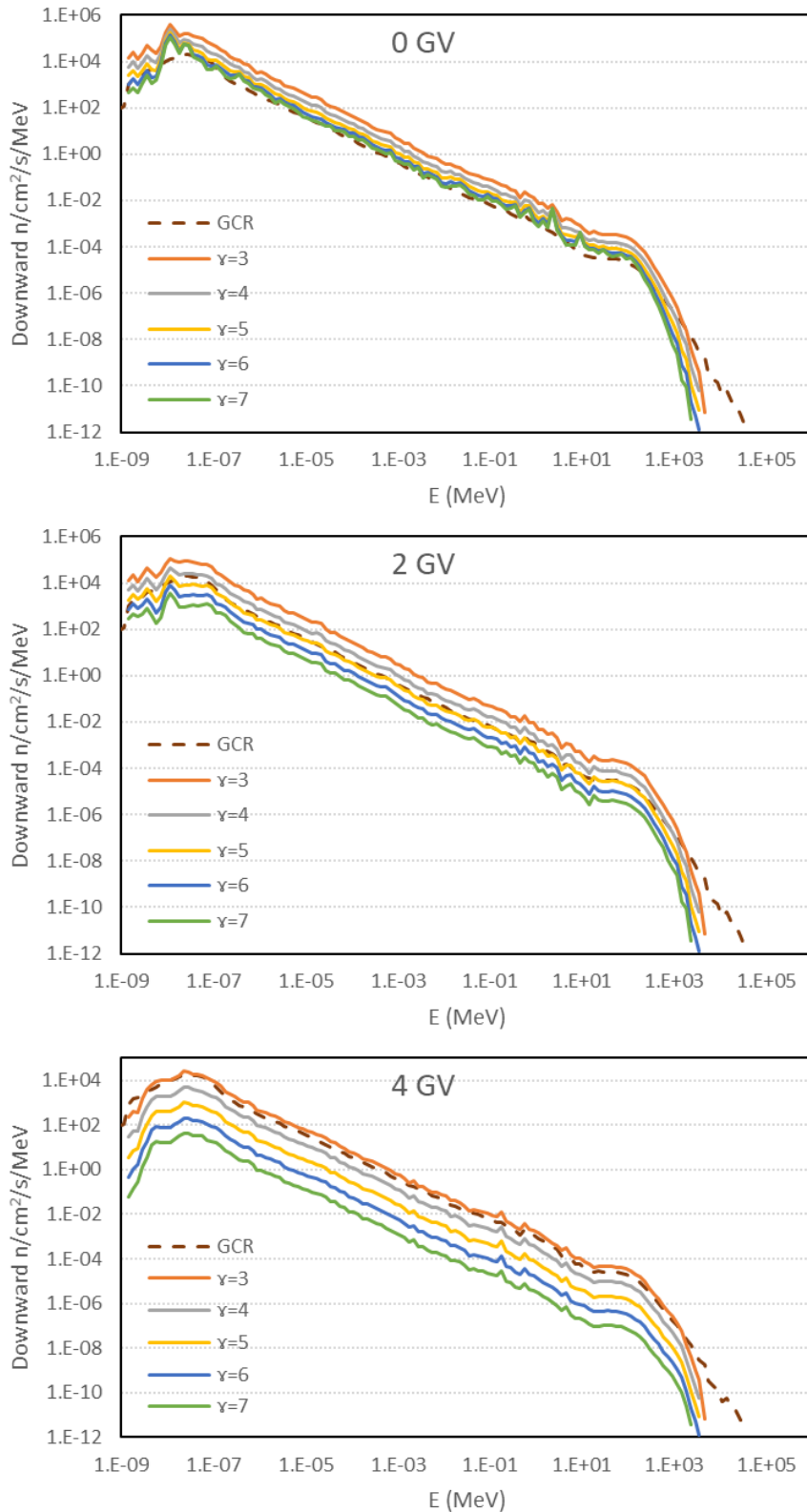


Figure 37: Ground level neutron spectra at $R=0$ (top), $R=2$ (middle) and $R=4$ (bottom) for contrived GLE spectra as a function of spectral index and the GCR background.

A common way of comparing atmospheric neutron spectra is to plot the flux per lethargy (the natural logarithm of the energy) against energy on linear-log axes, such that equal areas under the curve represent equal neutron flux. Figure 38 shows two examples of historical events compared to the GCR

background in flux per lethargy format. GLE59 (July 2000) has a much softer primary spectrum than GLE05 (February 1956), however this has a negligible effect on the shape of the secondary neutron spectra. The main difference between these spectra and the GCR background is seen at very high energies where the ratio between GCR and GLE flux increases substantially. However, as the fraction of neutrons in this part of the spectrum is small even for GCR, the impact is limited.

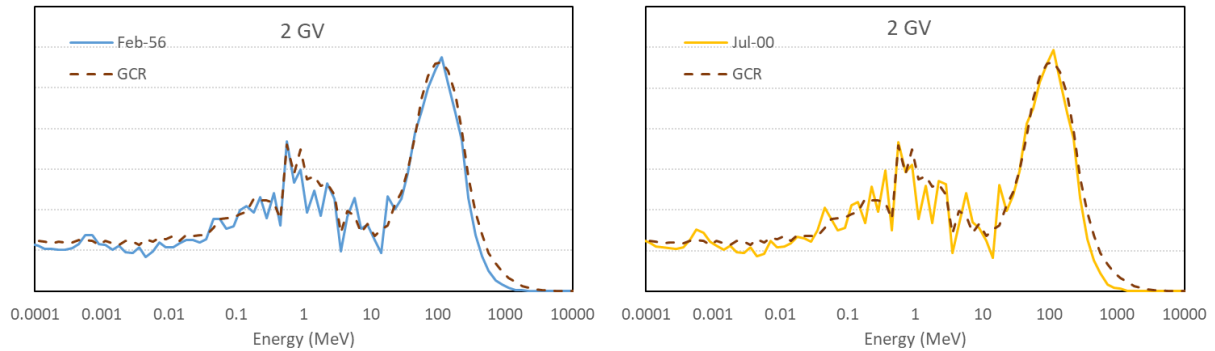


Figure 38: Flux per lethargy comparison of ground level GCR neutron spectrum at 2 GV with GLE05 (LHS) and GLE59 (RHS). The y axes have been renormalised to compare the shapes of each curve and the units are arbitrary.

5.1.2 URANOS Simulations

The URANOS Monte Carlo code [30] is designed to allow the rapid modelling of neutrons in the ground and lower atmosphere in order to address questions in environmental science. The representation of the soil in this model allows soil moisture to be easily changed. For typical applications, neutrons are injected into URANOS at very low altitudes (50m-80m) using an input spectrum designed to reproduce measured/simulated ground-level spectra after the neutron collisions simulated within URANOS itself have been accounted for. Here, we use URANOS to simulate the ground and lower atmosphere up to a height of 500m, while MAIRE is used to simulate the propagation of neutrons in the upper atmosphere down to a height of 500m. URANOS simulations are performed for both the historical and contrived ground level enhancement events with different rigidities and with several levels of soil moisture.

MAIRE downward neutron spectra at ground level and at 500 metres altitude are shown in Figure 39. At 500 metres the effect of ground interactions, which are built into MAIRE, is negligible. The difference in the shape of the two spectra is most visible in the thermal neutron regime ($\sim 10^{-8}$ MeV) but there is also a significant difference in the epithermal energy range up to ~ 0.01 MeV. Because of this all thermal neutrons and a significant fraction of epithermal neutrons in the resulting ground level spectra local to COSMOS detectors will be produced in the URANOS simulations rather than by MAIRE. A suitable input spectrum for URANOS is obtained by selecting the downwards moving neutrons from the MAIRE spectra at 500m, while the atmosphere within URANOS is terminated above 500m. Because of this any neutron that leaves the URANOS simulation domain (scatters above 500m) will be removed. This prevents the double counting of neutrons (already simulated by MAIRE) that would occur if such neutrons were allowed to scatter back into the simulation domain. Figure 40 shows input spectra for URANOS (MAIRE downward spectra at 500m) for GLE05 at R=0, 2 and 4 GV. Spectra are plotted as flux per lethargy and, although the shapes are again similar, and the y-axis units are

arbitrary, the relative flux between the spectra at the three different rigidities reflects the real impact of rigidity for this event.

Each MAIRE input spectrum is used by URANOS to simulate interactions with the ground and calculate ground level neutron spectra as a function of rigidity and soil moisture. The five combinations of volumetric water content (VWC) and cut-off rigidity are summarised in Table 9. Three values of VWC at a common rigidity (2 GV) allows us to explore the effect of that parameter in isolation, and similarly three values of rigidity at a common VWC value (25%).

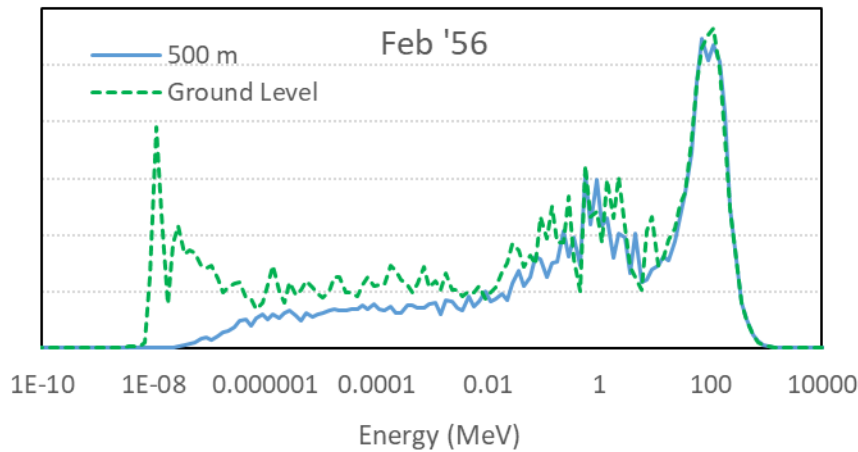


Figure 39: Downward flux per lethargy comparison of neutron spectrum for GLE05 (Feb '56) at ground level and 500 m altitude. The y axes have been renormalised to compare the shapes of each curve and the units are arbitrary.

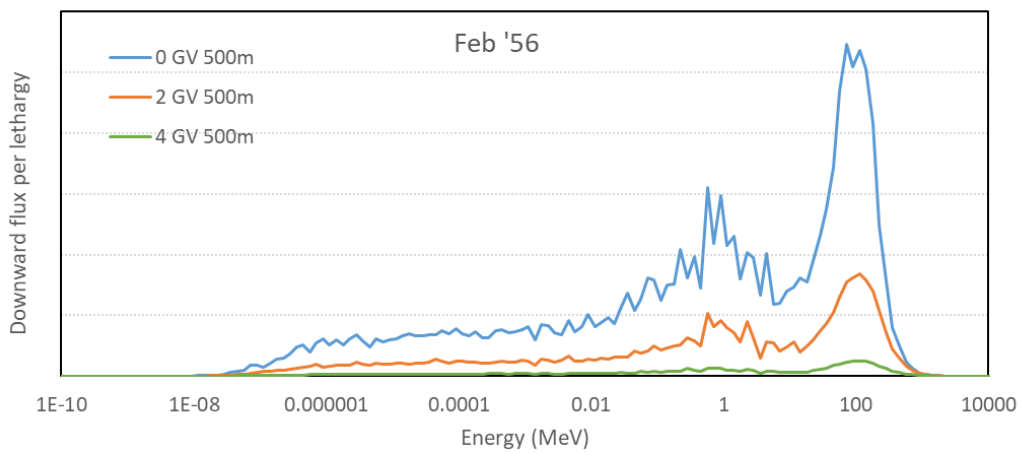


Figure 40: Downward flux per lethargy neutron spectra at 500 m altitude and three cut-off rigidities.

Table 9: Combinations of soil moisture and rigidity selected for evaluating URANOS ground level neutron spectra.

Rigidity (GV)	Volumetric Water Content (VWC)		
	5%	25%	45%
0		✓	
2	✓	✓	✓
4		✓	

Omnidirectional ground level neutron spectra have been calculated by URANOS in the energy range $10^{-8} - 2 \times 10^4$ MeV for the parametric combinations given in Table 9. Results for the background galactic cosmic ray environment were calculated using an input date of May 2016, which means solar modulation of the GCR environment is at a mid-level in between solar maximum and solar minimum. URANOS spectra for these input conditions are shown as flux per lethargy in Figure 41.

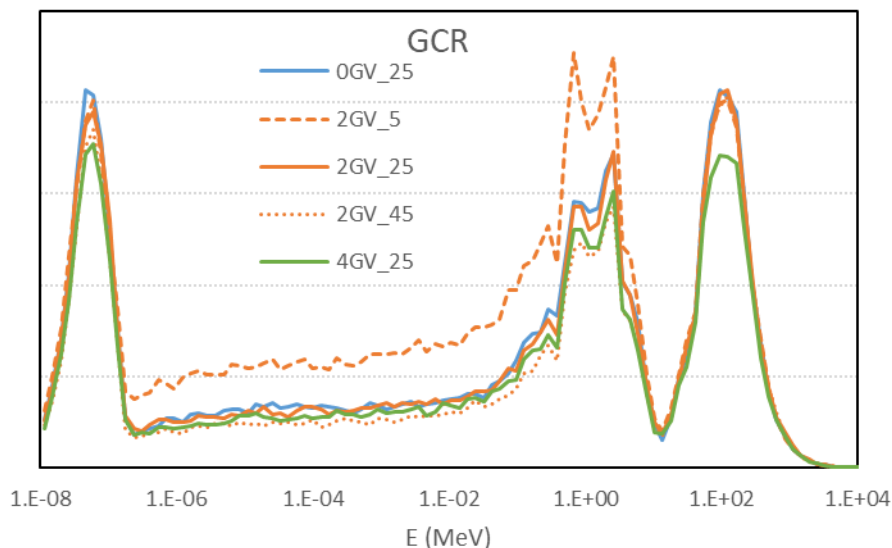


Figure 41: Ground level neutron spectra calculated by URANOS for GCR conditions, plotted as flux per lethargy with arbitrary y axis units. Blue, orange and green colours show rigidity variation from 0 – 4 GV; dashed, solid and dotted lines show volumetric water content (VWC) variation from 5% to 45%.

For a GCR spectrum the effect of cut-off rigidity on the ground level neutron spectrum is small. A much more significant VWC effect is visible, especially at the lowest value (5%) where the dryer conditions lead to less absorption and more reflection of the incident neutron spectrum by the ground layer. This is the well-known effect by which principle CRNS detectors are designed to operate.

Figure 42 shows equivalent ground level spectra for the six historical GLEs. Although the cut-off rigidity influences the different events to different degrees, the effect is found to be much larger than for the GCR spectra (Figure 41), and also larger than the influence of soil moisture in all cases. This is due to the softer primary input spectra for GLEs, which leads to significant variation in the downward neutron spectrum at 500 metres (see Figure 40) that serves as input to URANOS. Soil moisture influences the neutron spectra for energies approximately in the range 1 eV to 1 MeV. Proportionally, this influence has very little dependence on the historical event considered and is also proportionally the same as that seen for the GCR. The flux either increases by approximately 50%, or decreases by $\sim 20\%$, as VWC is changed to 5% or 45% respectively from a baseline of 25%. The same proportional change is expected regardless of the rigidity, and arises due to the similarity in the shapes of the secondary neutron flux (as noted, e.g., for Figure 37, and is clear in Figure 42 itself). The effect of the cut-off rigidity is illustrated even more clearly in Figure 43, which shows ground level neutron spectra for the contrived GLEs defined by spectral index parameter γ . As expected, the influence of the cut-off rigidity is strong for all events, but is considerably stronger for the softest event ($\gamma=7$) compared to the hardest ($\gamma=3$). The proportional effect of changing VWC is the same as for the historical events. As

discussed below, a Ground Level Neutron Monitor (GLNM) is most sensitive to the highest energy neutrons that display very little sensitivity to VWC. In contrast, COSMOS detectors are, by design, particularly sensitive to the neutron energies most influenced by VWC.

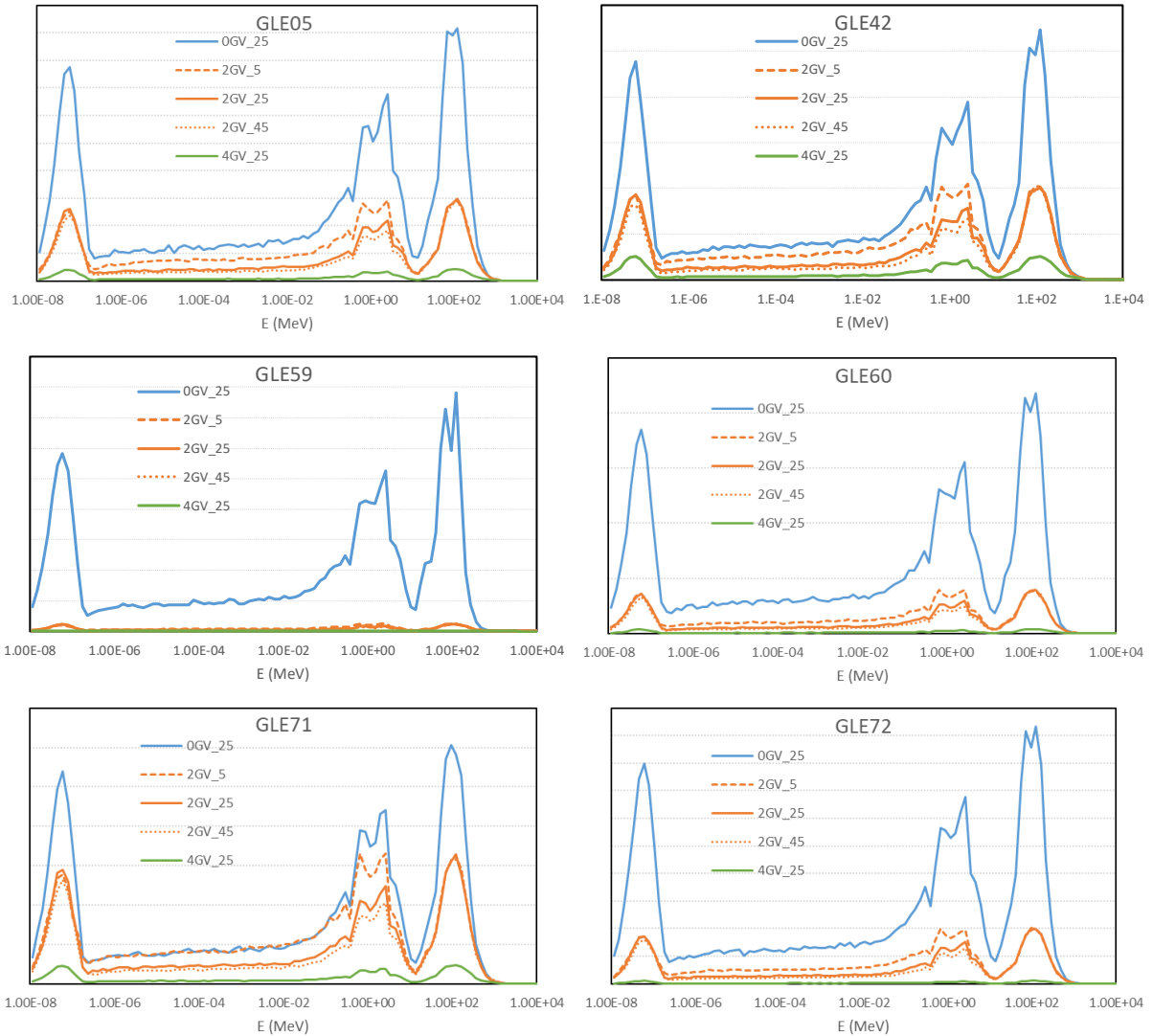


Figure 42: Ground level neutron spectra calculated by URANOS for historical GLEs, plotted as flux per lethargy with arbitrary y-axis units (not consistent between plots). Blue, orange and green colours show rigidity variation from 0 – 4 GV; dashed, solid and dotted lines show volumetric water content (VWC) variation from 5% to 45%.

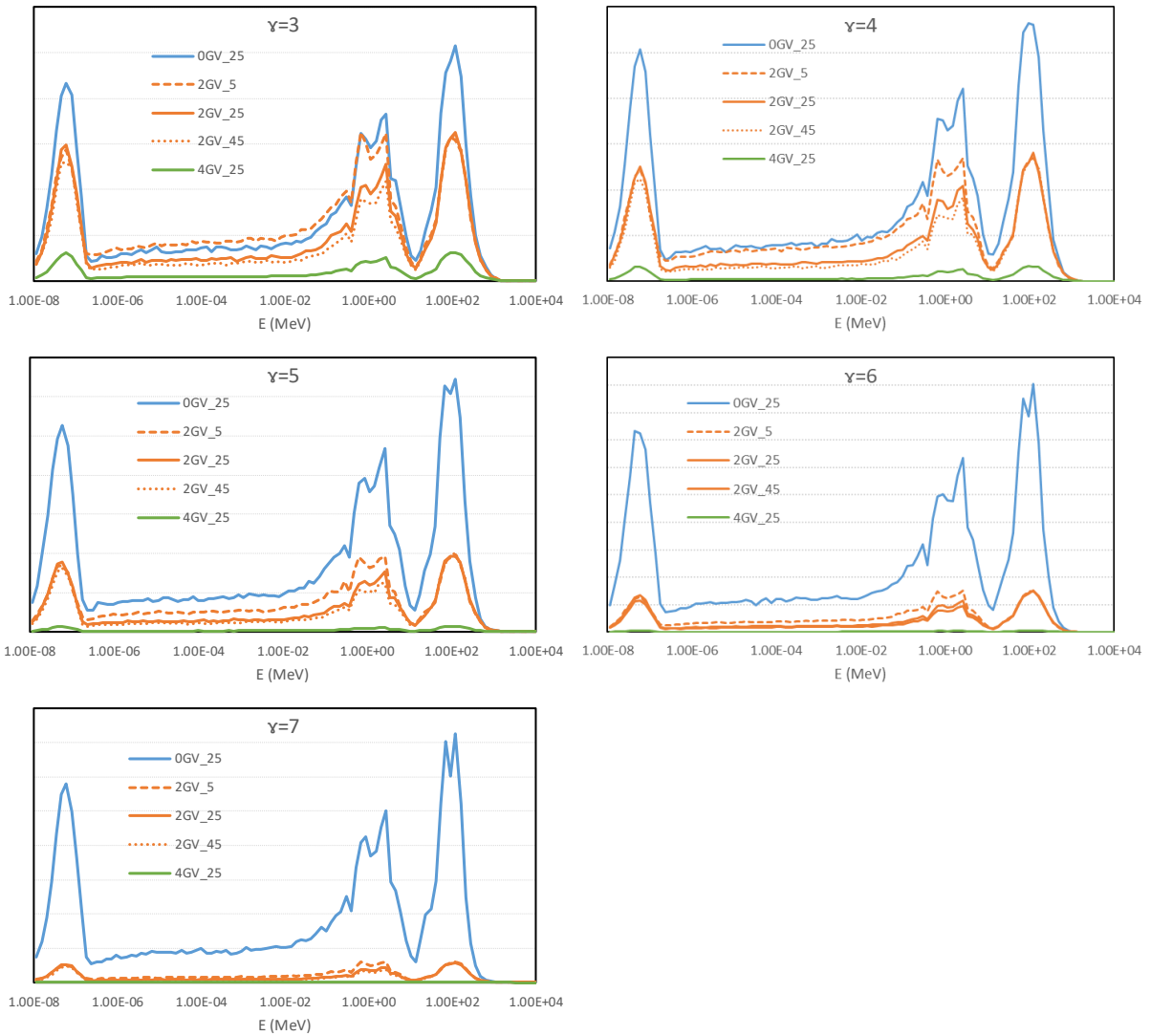


Figure 43: Ground level neutron spectra calculated by URANOS for contrived GLEs of different spectral index (γ), plotted as flux per lethargy with arbitrary y-axis units (not consistent between plots). Blue, orange and green colours show rigidity variation from 0 – 4 GV; dashed, solid and dotted lines show volumetric water content (VWC) variation from 5% to 45%.

The ground level neutron spectra calculated by URANOS can be used to estimate GLNM and CRNS (COSMOS) detector count rates by multiplication with appropriate detector response functions. Figure 44 compares response functions for the two detector types in units of counting efficiency (counts per incident neutron). The COSMOS detector response function is based on a CRS1000/B type [31] and the neutron monitor response function is based on a standard 6-NM64 design [32]. The dramatic difference in instrument response is clearly visible. The GLNM response is dominated by the high energy part of the energy spectrum, where the detector “efficiency” exceeds 1 because the neutron monitor design includes a lead producer that increases the number of local evaporation neutrons by more than an order of magnitude over the number of incident neutrons. These neutrons are then thermalised through scattering by a moderator before being counted by a ^3He or ^{10}B thermal neutron detector. By contrast, the CRNS response is much more evenly distributed from the thermal to fast energy regimes, peaking at around 1 eV (10^{-6} MeV). It is lower energy neutrons (<10 MeV) that are most affected by scattering due to water molecules, which demonstrates why COSMOS detectors are sensitive to local soil moisture conditions, whereas neutron monitors are not.

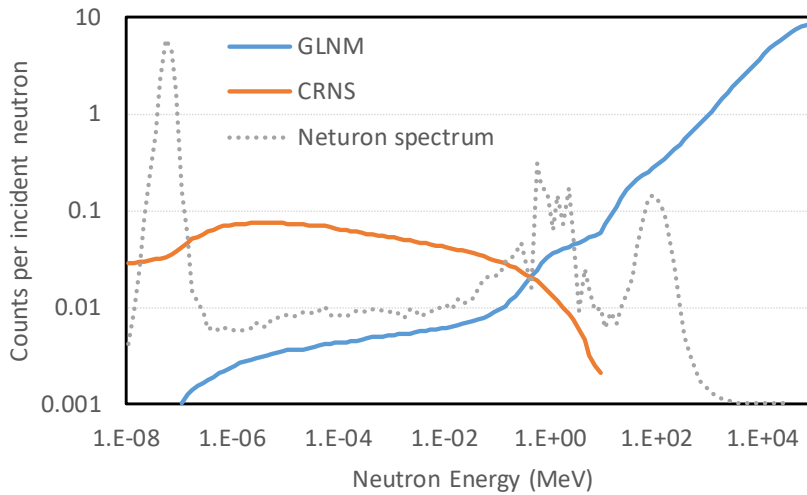


Figure 44: Detector efficiency comparison between a ground level neutron monitor (GLNM) and COSMOS CRS1000/B detector. Counts per incident neutron are shown on a logarithmic left-hand axis; a representative flux per lethargy ground level neutron spectrum is shown on a linear scale (unlabelled right-hand linear axis, arbitrary scale) to illustrate relative flux in different energy ranges.

5.1.3 COSMOS Count Rates

Estimates of absolute count rate are made for GCR conditions and historical GLEs. There is no relevance to this calculation for the contrived GLE events based on spectral index as the normalisation is arbitrary, however relative count rates are examined in a later section. Figure 45 shows an estimate of GLNM count rate as a function of cut-off rigidity. The range of 85 – 95 count per second compares well with an observed rate of ~70 counts per second for a 6-NM64 design at high latitude, given the significant uncertainty of incident spectrum attenuation by local building materials (for example incident neutron flux would be reduced by ~30% by only 20 cm of material at the density of concrete). Figure 46 shows equivalent count rate estimates for the six historical GLEs. These are not expected to be in exact agreement with measured increases in GLNM count rate due to large geographical anisotropies in the primary spectra, however the predicted count rates relative to GCR background are generally consistent with observations.

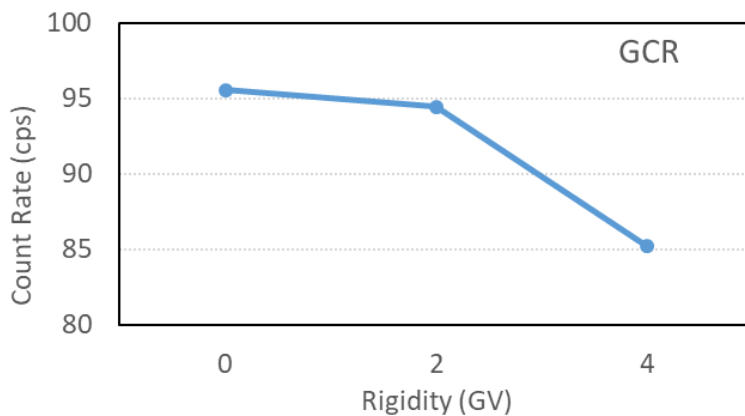


Figure 45: Estimate of neutron monitor count rate as a function of cut-off rigidity for GCR conditions.

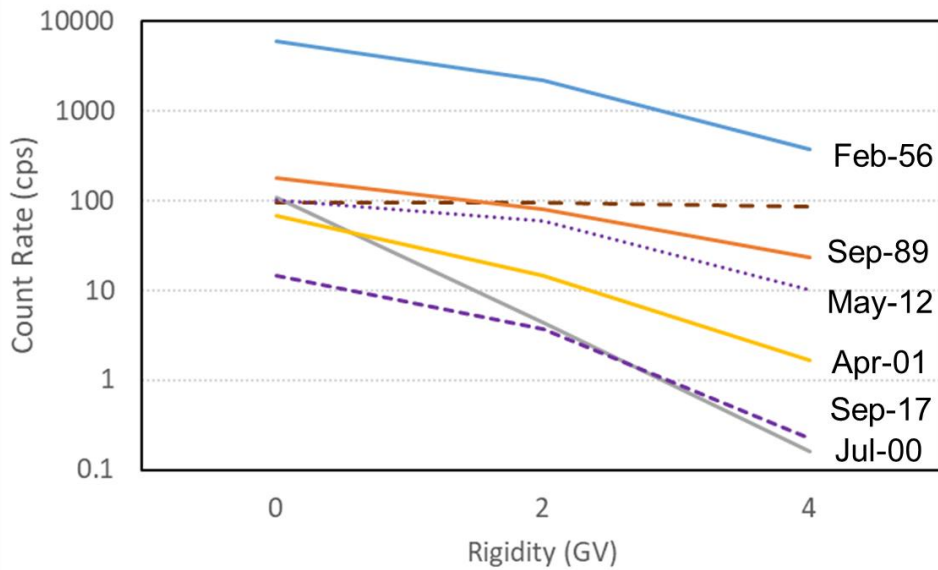


Figure 46: Estimate of neutron monitor count rate as a function of cut-off rigidity for six historical GLEs. The GCR estimate from Figure 45 is shown as a brown dashed line for comparison.

Absolute GLNM count rate estimates do not depend on local soil moisture conditions, however for CRNS detectors this must be taken into account. Figure 47 shows the estimated count rates for the GCR background spectra (at different cut-off rigidity and VWC combinations) and Figure 48 shows the equivalent count rate estimates for six historical GLEs (not inclusive of the GCR background). In all cases the effect of VWC is stable, i.e. the ratio between count rates at 5%, 25% and 45% VWC is independent of event spectrum.

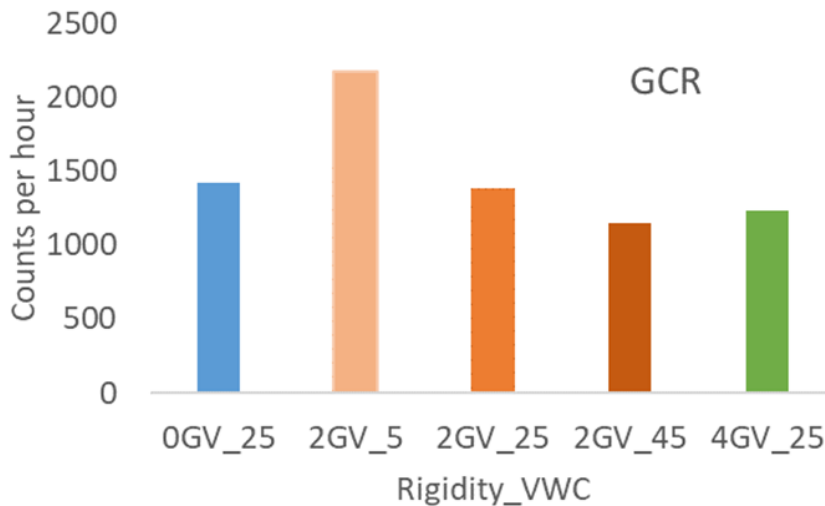


Figure 47: Estimates of CRNS count rate for GCR conditions at different cut-off rigidity (#GV) and volumetric water content (_#%). Blue, orange and green colours show rigidity variation and shades of orange show VWC variation.

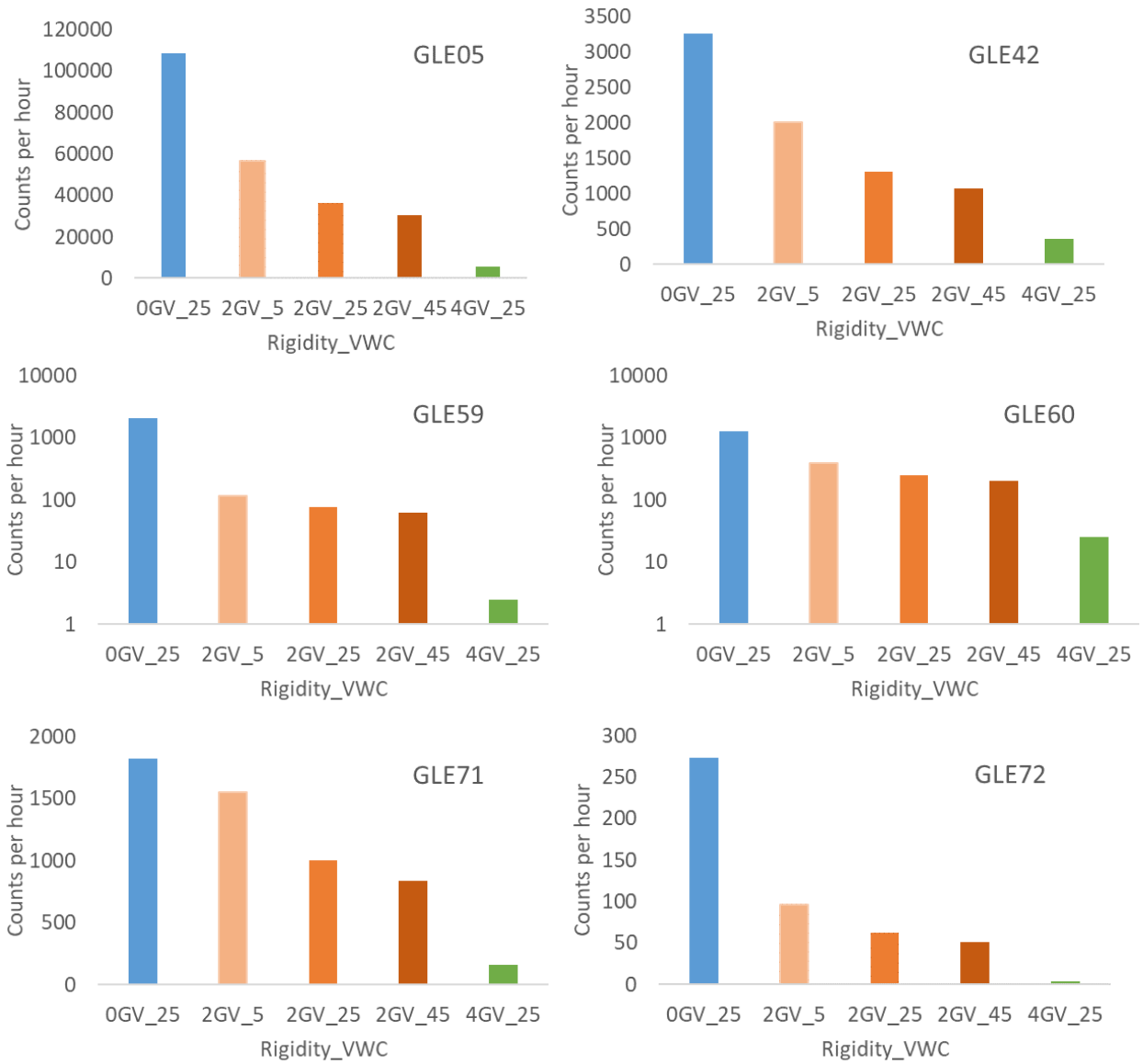


Figure 48: Estimates of CRNS count rate for six historical GLEs at different cut-off rigidity (#GV) and volumetric water content (#%). These are estimates of additional count rates above the GCR background rates shown in Figure 47. GLE59 and GLE60 are shown on a logarithmic scale, all others on a linear scale. Blue, orange and green colours show rigidity variation and shades of orange show VWC variation.

These count rate estimates show both the enormous variation in impact between GLE events and the relative impact of rigidity compared to VWC. For a hypothetical GLE alert system it is also of interest to compare the relative increases of GLNM and CRNS type detectors. Figure 49 shows predicted percentage increases during GLE05 (Feb '56) for a GLNM detector, a CRNS detector and the >10 MeV neutron flux. The energy threshold is largely arbitrary due to the relative insensitivity of the shape of ground neutron spectra to primary proton spectra. As this is a relative calculation (comparing to GCR background), even the CRNS increases are independent of VWC. Both >10 MeV flux and predicted CRNS count rate increase exceed the predicted count rate increase for GLNMs. This is entirely because the GLNM response function is so heavily skewed towards high energy neutrons. The apparently small difference in the high energy tail of the neutron spectra shown in Figure 38 is sufficient to mean that when the total neutron flux during a GLE increases by a factor, f , the increase in GLNM count rate is $< f$. However, the effect is small and, as can be seen in Figure 49, less significant

at higher rigidities where the influence of softer protons in the primary GLE spectrum is reduced. In terms of statistical significance, the much higher baseline count rate of GLNMs (hundreds of times greater than a COSMOS detector) more than compensates for a slightly lower percentage increase. In the next section we explore how the statistical significance of hypothetical GLEs can be improved by increasing the baseline count rate of COSMOS detectors.

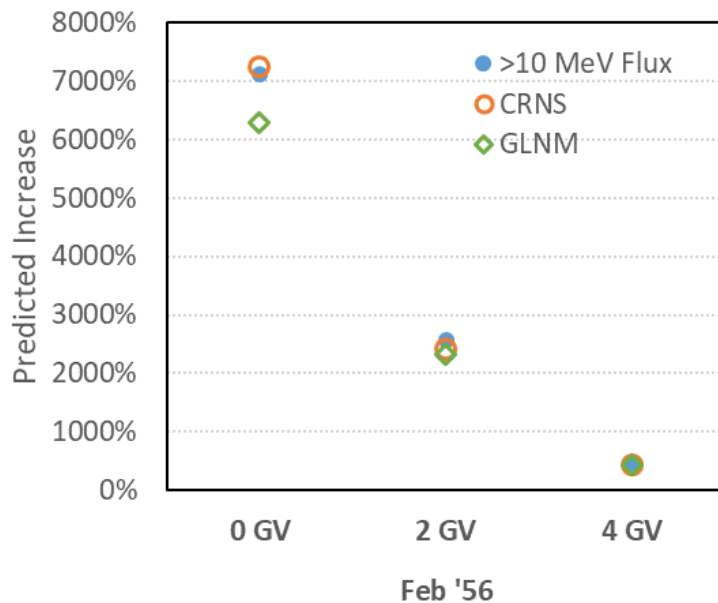


Figure 49: Predicted increase of GLNM count rate, CRNS count rate and >10 MeV neutron flux during GLE05.

5.2 Theoretical sensitivity to future events

The utility of a hypothetical COSMOS-based GLE alert system depends on its capacity to detect increases in the ground level neutron flux. This, in turn, depends on the statistical significance of increases in count rate relative to a baseline GCR rate. In this section we explore how statistical significance relates to the following event and detector parameters:

1. Event magnitude: increase in count rate relative to baseline during peak of event
2. Event time profile: the evolution of the intensity of the event with time
3. Event spectrum: primary spectral index and impact on count rate at different cut-off rigidities
4. Detector number: grouping many COSMOS detectors at a single site or aggregating data from individual detectors across many sites
5. Detector time resolution: cadence of recording/transmitting counts from each detector
6. VWC: soil moisture content of local environment

To simplify this analysis, we assume a baseline count rate of 1500 counts per hour for a single COSMOS detector during background conditions and a 25% VWC value. We also assume that the effect of different VWC values is fixed and consistent with the ratios in Figure 48, which means baseline count rates of 2325 and 1245 counts per hour for 5% and 45% VWC respectively. Unless otherwise stated all plots assume 25% VWC as default.

5.2.1 Event Time profile

The time profile of GLE events varies greatly not just from event to event but also between locations for a particular event. However, it is often possible to group events into two broad categories: impulsive events and gradual events (though in practice most events have elements of both). Impulsive events have a fast initial rise in ground level neutron flux, followed by a slower (but still relatively rapid) decline. These events are associated with active regions near the western solar limb, which are magnetically well-connected to the Earth. Gradual events are associated with more central origins in terms of solar longitude, resulting in significantly longer rise and fall times. Figure 50 shows some examples of increases in ground level neutron monitor data for several events (including, but not limited to, the six historical events we have considered) where these two broad categories are identifiable by early and late peaks in relative magnitude for impulsive and gradual events respectively. The specific station of origin for the neutron monitor data in each case is unimportant as this figure is illustrative only.

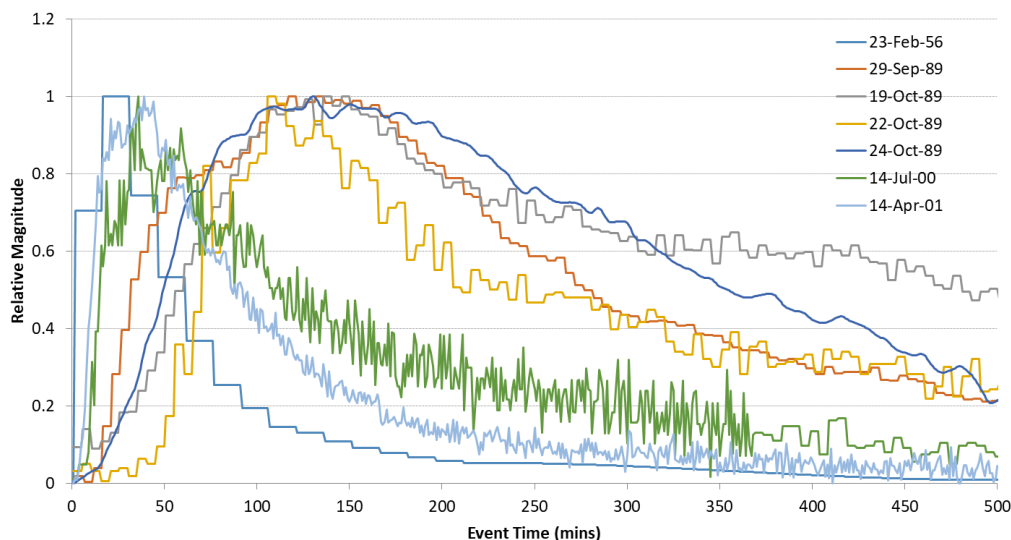


Figure 50: Examples of GLE time profiles based on neutron monitor data.

To recreate artificial time series of detector count rates we use contrived time profiles based on the exponential rise and fall times given in Table 10. The rise and fall times for an impulsive event are 2 minutes and 30 minutes respectively (this is a very fast rise time but even faster have been reported [33]). The rise and fall times for a gradual event are significantly longer at 120 minutes and 180 minutes respectively. The time profiles that result from these parameters are plotted in Figure 51.

Table 10: Rise and fall times (in minutes) of artificial time profiles for impulsive and gradual events.

	Rise time	Fall time
Impulsive	2	30
Gradual	120	180

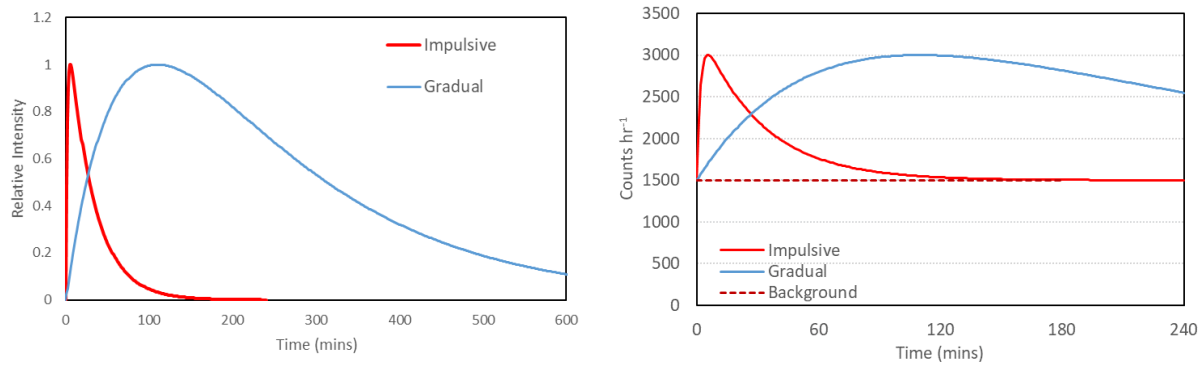


Figure 51: (LHS) Impulsive and gradual GLE time profiles based on exponential rise and fall times. (RHS) Example of artificial count rate time series using these time profiles with a GLE resulting in a 100% increase at peak and a baseline count rate of 1500 counts per hour.

The artificial count rates in Figure 51 (RHS) are based on a GLE with a peak magnitude at ground level that is equal to the cosmic ray background (thus a 100% increase and total count rate of 3000 counts per hour). For this time series, and others to follow, the primary GLE spectrum does not need to be specified as we are defining the event magnitude relative to the baseline, regardless of location. This is a simplification because the primary spectrum is likely to change during the course of an event, although this is in part taken into account as the artificial time profiles are based on real events which themselves have time-dependent spectra.

5.2.2 Detector time resolution

Typical COSMOS time resolution currently stands at 60 minutes for the North American network and 30 minutes for the UK network. This compares unfavourably to neutron monitors where the resolution is as fine as 1 minute. Although a basic trade-off exists in theory between statistical significance and time resolution – higher accumulation time results in more counts per bin and thus lower statistical error – in practice there is little disadvantage in improving the time resolution capability of operational detectors, as data can always be re-binned after they are accumulated.

The impact of time resolution on the measured profile of different types of GLE can be seen in Figure 52. For a gradual event profile, even a 60-minute counts-binning scheme is sufficient to resolve the profile of the event. By contrast, for an impulsive event such a coarse resolution results in the peak magnitude of the event being underestimated by nearly a factor of two. 15-minute resolution results in a smaller underestimate of ~13% but the profile of the rise time is missed entirely. This principle applies to all examples of count rate time series and statistical significance that follow.

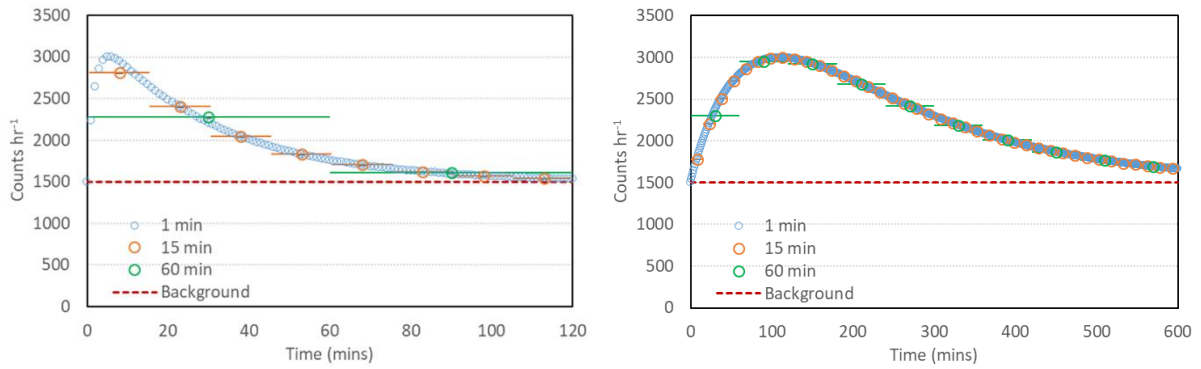


Figure 52: Artificial count rates at different time resolutions for an impulsive GLE (LHS) and a gradual GLE (RHS) that result in a 100% increase at peak. 1-minute, 15-minute and 60-minute resolution are represented by blue, orange and green circles respectively.

5.2.3 Statistical significance

In our examination of existing COSMOS data during recent GLEs we applied a simple test based on Poisson statistics to evaluate the significance of any observed data spikes. We apply the same basic principle here to test the significance of hypothetical count rate increases during possible future events. We define one standard deviation, σ , as the square root (Poisson error) of counts in a single time bin during the quiescent (baseline) period prior to the event (e.g. $\sigma = \sqrt{1500} = 38.7$ for 60-minute resolution and 25% VWC). In all examples that follow, significance ($\# \sigma$) is applicable to each individual time bin relative to baseline, rather than a post-event analysis of the overall significance of a well-resolved complete event profile. Also, given the many possible combinations of event magnitude, event time profile, detector time resolution, detector number and VWC, we present the following three examples based on impulsive and gradual GLEs each with a 10% increase at peak:

1. Single COSMOS detector, 25% VWC, variable time resolution (1 – 60 mins)
2. 15-minute resolution, 25% VWC, variable #detectors with aggregated counts (1 – 100)
3. Single COSMOS detector, 60-minute resolution, variable VWC (5% - 45%)

Figure 53, Figure 54 and Figure 55 show impulsive and gradual event time profiles of the value of significance for these three examples. For events of greater magnitude, the values can simply be scaled linearly (i.e. for an event with 100% increase at peak, all plotted significance values would be ten times higher). Peak significance as a function of time resolution scales as the square root of bin size (with the caveat that the peak of impulsive events is blurred at coarse resolution and the significance reduces accordingly), as does peak significance as a function of detector number. This is intuitive in both cases as increasing bin size or detector number increases accumulated counts for both baseline GCR and GLE. The effect of VWC is subtler as dryer conditions lead to small increases in both baseline count rate and GLE count rate, leading to an even smaller effect on significance. However, these examples clearly show how the significance of a GLE at its peak is highly dependent on a number of independent factors.

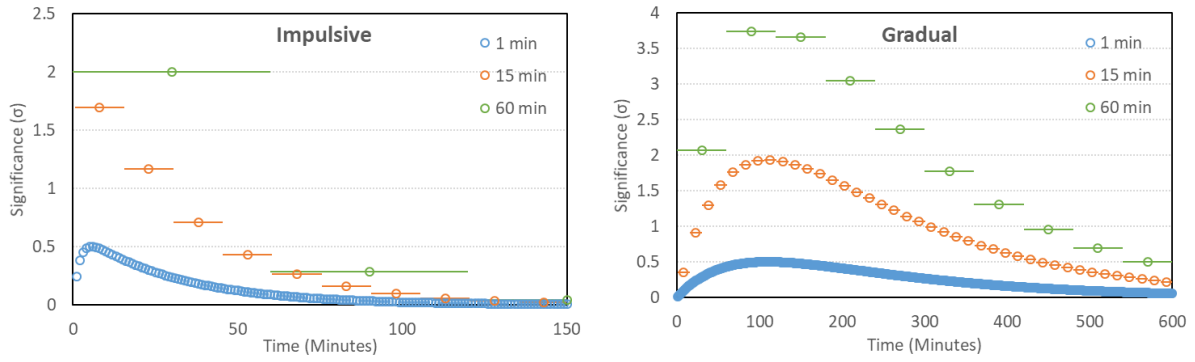


Figure 53: (Example 1) Time profile of statistical significance (per time bin) of a GLE with 10% peak magnitude relative to GCR, for a single COSMOS detector and 25% VWC.

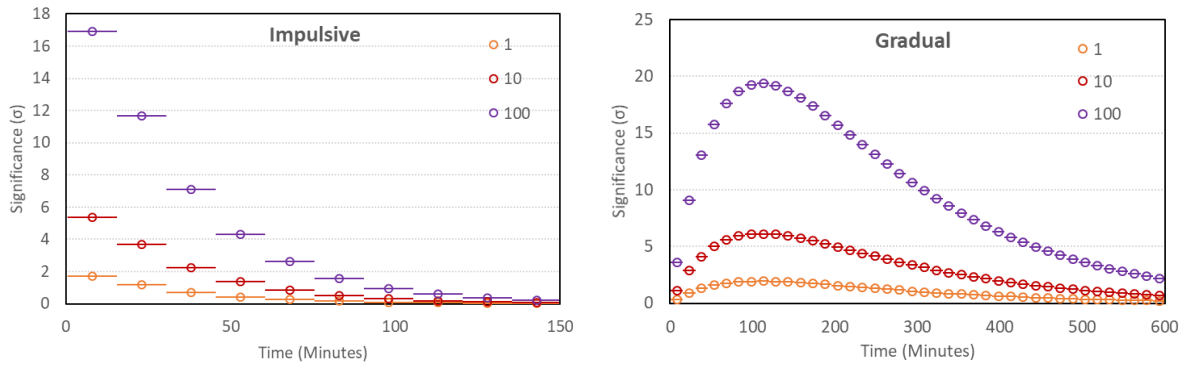


Figure 54: (Example 2) Time profile of statistical significance (per time bin) of a GLE with 10% peak magnitude relative to GCR, for a number of COSMOS detectors in aggregate (1 – 100), 25% VWC and 15-minute time resolution.

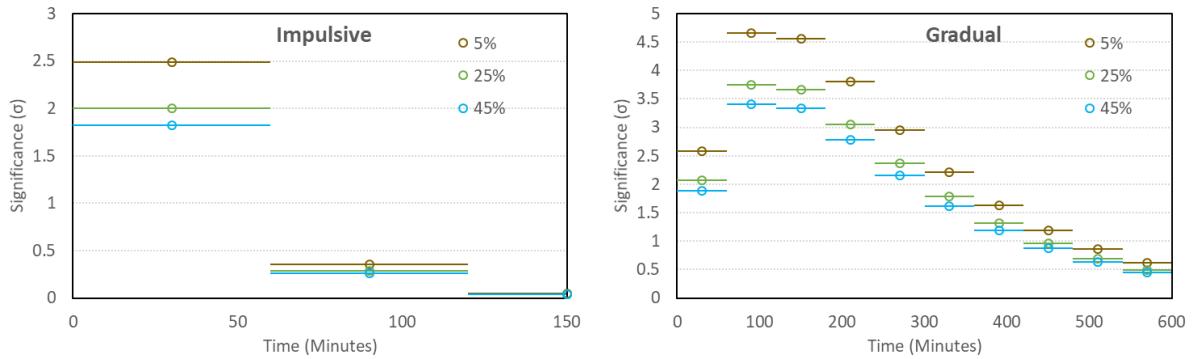


Figure 55: (Example 3) Time profile of statistical significance (per time bin) of a GLE with 10% peak magnitude relative to GCR, for a single COSMOS detector with 60-minute resolution and VWC from 5% to 45%.

5.2.4 Detection Threshold

As shown in Figure 54, achieving high statistical significance during a GLE is aided greatly by aggregating the data from a number of COSMOS detectors. Whether these detectors should be co-located is a separate consideration and depends to some extent on the impact of rigidity variation, as discussed in the next section. To consider how many detectors should be considered for aggregation it is helpful to quantify the effect this has on the capability for event detection as a function of event magnitude. For a very large event a small number of detectors, or even a single detector would be

sufficient, however our analysis of real COSMOS data has shown that this is not the case for smaller events.

Figure 56 shows the relationship between event magnitude (at peak) and the number of detectors required to record a 5σ significance detection at a particular time resolution. Figure 57 shows the equivalent plots for 3σ significance. For example, with our baseline assumptions a single detector is sufficient to measure a GLE peak of 100% magnitude with 1-minute time resolution. However, for an event that produces only a 17% increase at its peak (like GLE71 at the Apatity neutron monitor), data from more than 30 detectors would need to be aggregated for the increase to reach 5σ significance. This number decreases to only 2 detectors with 60-minute binning, and for a gradual event even just a single detector would be sufficient at this resolution.

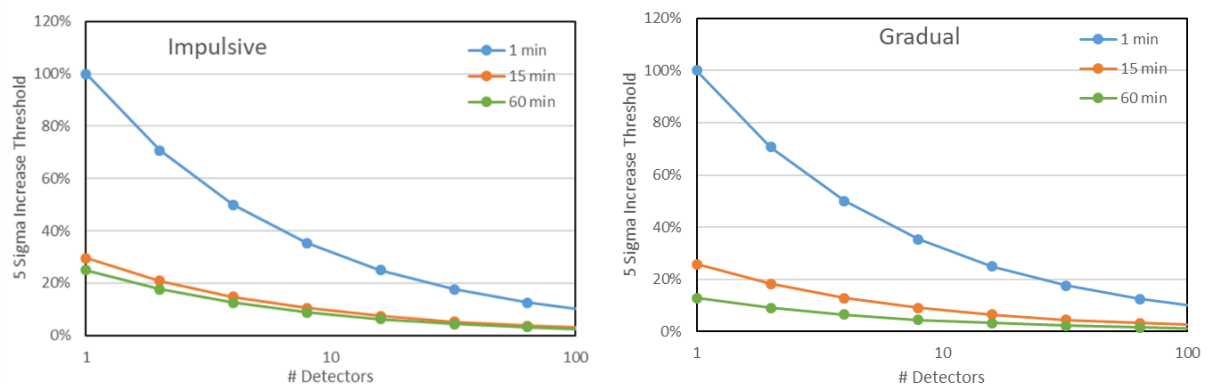


Figure 56: Peak event magnitude 5σ detection threshold as a function of the number of aggregated COSMOS detectors for impulsive event (LHS) and gradual event (RHS).

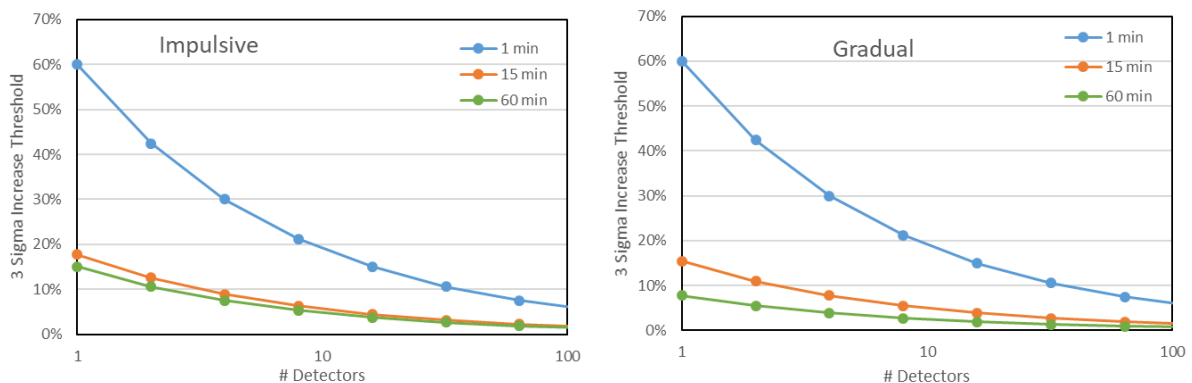


Figure 57: Peak event magnitude 3σ detection threshold as a function of the number of aggregated COSMOS detectors for impulsive event (LHS) and gradual event (RHS).

5.2.5 Rigidity and Spectral Index

If we assume that the baseline case of 1500 counts per hour during GCR conditions applies to a rigidity of 2 GV and VWC of 25% (which is consistent with the estimate plotted in Figure 47), we can use spectral index to explore the relative effect of GLEs at different rigidities. For example, an event that causes a 10% increase in the ground level count rate at high rigidity would be expected to cause a significantly larger increase at low rigidity, and the margin of difference must depend on the primary

GLE proton spectrum. Figure 58 shows expected increase in count rate as a function of spectral index for R=0 GV and R=4 GV, during an event that caused a peak increase of 10% at R=2. This relative comparison removes the arbitrary normalisation applied to our contrived GLE spectra in Figure 33.

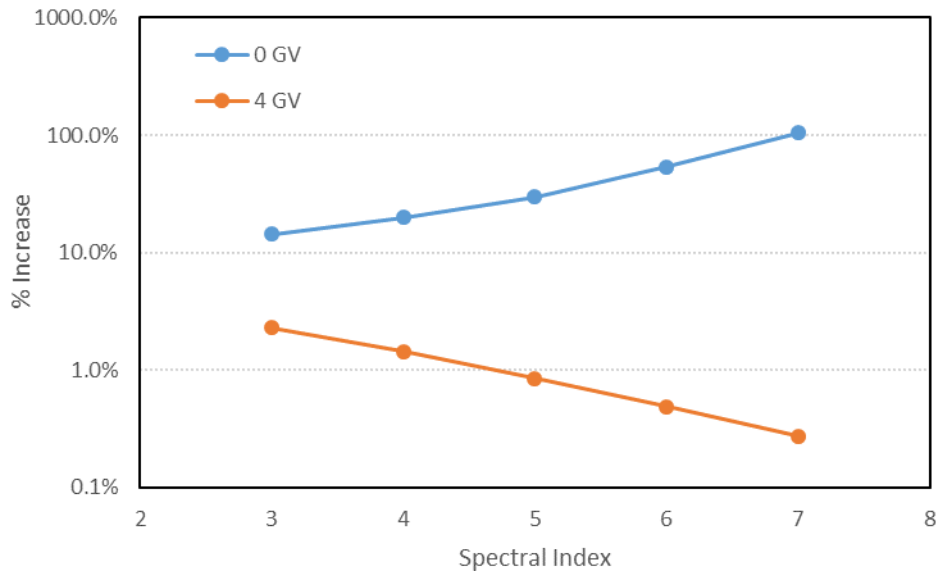


Figure 58: Expected % increase in COSMOS detector count rate as a function of spectral index for an event causing a 10% increase at 2 GV. Blue and orange curves show increases at 0 GV and 4 GV respectively.

Using this relationship, it is theoretically possible to use data from two stations at different rigidities to infer the spectral index of the primary GLE spectrum that is the common cause of increases at both locations. For example, Figure 59 shows two examples of the ratio of count rate increase as a function of spectral increase. For example, if an increase in count rate at a location corresponding to R=2 GV were ten times lower than a coincident increase at a higher latitude location with R=0 GV, this would imply a spectral index of $\gamma=7$. This is, of course, a simplification as there are several factors that complicate this relationship: spectral shape, longitudinal anisotropy, local soil moisture conditions, changes to cut-off rigidity during a geomagnetic storm etc. Nonetheless, the principle of using rigidity to infer spectral information during a GLE is well established by neutron monitors, and, as shown in Figure 13 (RHS), the UK spans a suitable rigidity range for a pair (or more) of detectors to be used for this purpose.

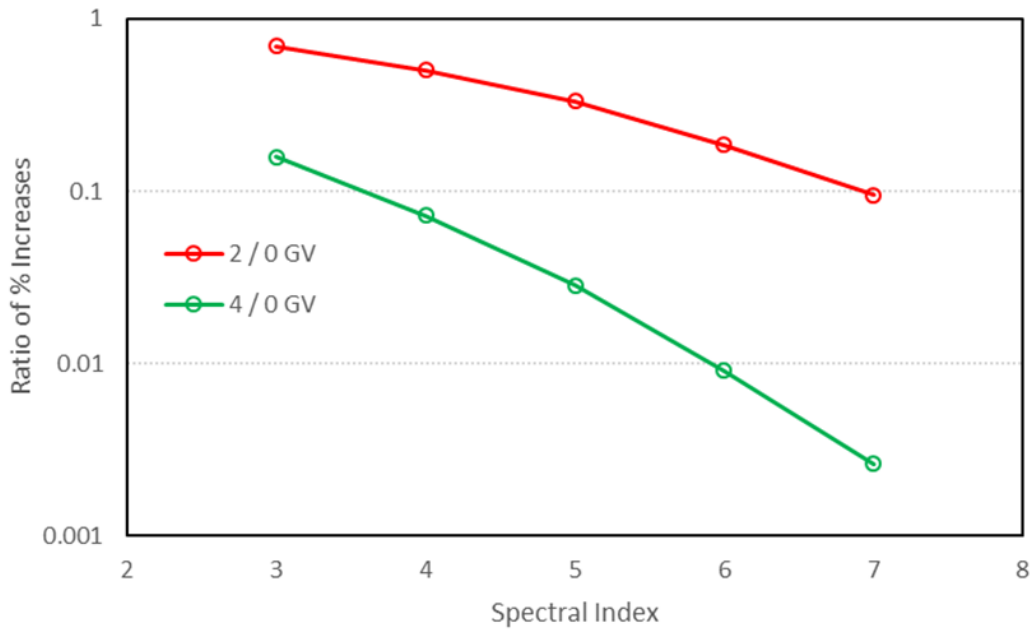


Figure 59: Hypothetical ratios of count rate increase for separate detectors at two rigidities. The red line shows the ratio for one detector at 2 GV and the other at 0 GV; the green line shows the ratio for one detector at 4 GV and the other at 0 GV.

5.2.6 Terrestrial Gamma-Ray Flashes

Elevated atmospheric neutron fluxes from non-cosmic sources have also been theorised and observed. Terrestrial gamma ray flashes (TGFs) in storm clouds can occur when electrons are excited to extremely high energies, leading to very short bursts of bremsstrahlung radiation with photon energies extending up to 10s of MeV [34]. It is postulated that this primary gamma spectrum can result in significant photonuclear production, leading to short bursts of neutron fluence that are detectable at ground level. Observational evidence is plentiful for the gamma ray signatures of TGFs, especially from satellite-based instruments [35]. Evidence for neutron fluences is far more limited, in part due to the highly localised nature of ground level neutrons from low altitude TGFs [36], but also due to the extremely rapid nature of the events. The timescale of particle acceleration in TGFs is of the order of 1 millisecond or below [37], which means a large but very brief increase in the ambient neutron flux would not necessarily be seen by a detector with a significantly larger integration time. TGF neutrons should be distinguished from elevated neutron flux from so-called ‘gamma glow’ events, which extend over much longer periods of time (seconds to minutes). For example, in September 2009 the Aragats neutron monitor in Armenia observed a ~3% increase in count rate that was sustained for several minutes and coincident with increased electron and gamma radiation seen in detectors on the same site during a thunderstorm [38]. Although this event cannot have been due to a TGF, recent observations and simulations have shown that TGFs and gamma ray glows may be directly related [39].

An example of a possible direct measurement of TGF-induced neutrons at ground level can be found in Martin and Alves (2010). During a lightning storm in January 2009 in Sao Jose dos Campos, Brazil, a thermal neutron detector recorded a ~900 fold increase in count rate [40]. However, as the time resolution of the detector was 1-minute, this increase was recorded as 690 counts in a single bin (compared to a mean rate of ~0.7 counts per minute). By estimating detector-to-source distance as

less than 500 metres based on the time between the observation of the lightning flash and hearing of the thunder, the authors estimate that $10^{12} - 10^{13}$ neutrons were produced by the lightning discharge. While this is consistent with, or even lower than, other estimates of TGF neutron production, the authors do not attempt to take into account the relationship between the source neutron spectrum, the modified spectrum at the detector location and the detector response function. Neutron spectra modelled by Carlson et al. [36] reveal that both the source neutron spectrum and modified ground neutron spectrum (in this case after passage through 2.5 km of atmosphere) have mean energies in the MeV range (see Figure 60). The thermal neutron detector located at Sao Jose dos Campos has a negligible response to the such neutrons, which means that a significant amount of thermalisation is implicitly assumed for the additional counts to be consistent with TGF origin. As the neutron spectra modelled in [36] extend down to only 1 keV, this analysis does not provide a thermal to fast neutron flux ratio. However, we can use the Carlson ground level spectrum to make order-of-magnitude count rate estimates for both ground level neutron monitors and COSMOS detectors.

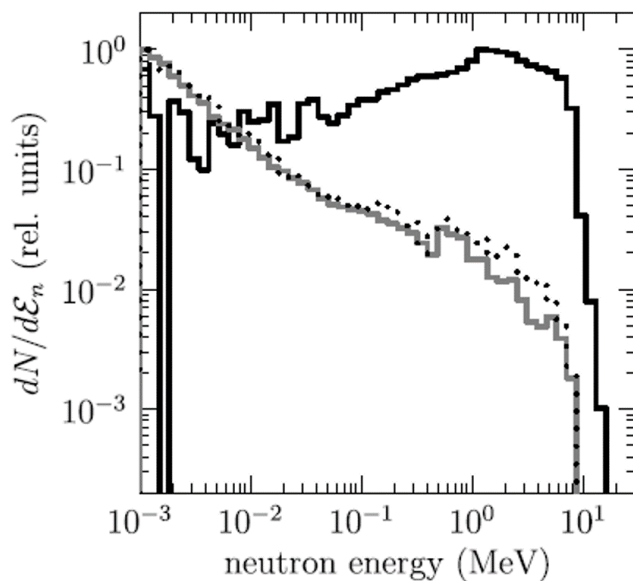


Figure 60: Simulated spectra for TGF source neutrons (black line), upper atmosphere escape neutrons (grey line) and ground level neutrons (dots) in relative units (reproduced from [36]).

A neutron monitor of 6-NM64 design records 2000 – 3000 counts per n/cm^2 in the neutron energy range 1-10 MeV [32]. Carlson et al. predict $1 \text{ n}/\text{cm}^2$ at ground level for a TGF at 2.5 km altitude (NB in their simulations the neutron flux at ground level is negligible for a TGF altitude above 5 km). We estimate two thirds of neutrons in their spectrum to be $>1 \text{ MeV}$, which implies up to 2000 additional counts from a low-altitude TGF. This compares to a typical count rate for this type of monitor at an equatorial location of ~ 50 counts per second. So, a TGF might be equivalent to 40 seconds worth of additional counts, or a 67% increase at 1-minute resolution. This would certainly be statistically significant, however, as the additional counts would all feature in a single counting bin, it such a signal could easily be dismissed as erroneous (and we are not accounting for possible detector saturation at such a high neutron flux). This increase is substantially lower than the 900-fold (90,000%) increase observed by Martin & Alves, in part due to the very different detector response functions, but also due to the shorter assumed detector-to-source distance of $<500 \text{ m}$.

COSMOS detectors have a very different response function, with a falling rather than rising response above 1 MeV. We estimate the net detection efficiency when combined with the Carlson ground level

spectrum to be of the order of 1%. For a neutron fluence of 1 n/cm^2 , we estimate an additional 12 counts would be recorded during a low-altitude TGF. For a background count rate of ~ 1500 counts per hour for an equatorial detector this corresponds to a $\sim 50\%$ increase in count rate in 1-minute bins, not dissimilar to the GLNM prediction. The similarity occurs because both detector types have relatively poor counting efficiency at $\sim \text{MeV}$ energies compared to other parts of the neutron spectrum (lower energies for COSMOS, higher energies for GLNM). At current COSMOS time resolutions of 30 mins to 1 hour, this would represent an increase of $<1\%$, which would not be visible in the count rate series.

Such modest increases are unlikely to pose a threat to ground level infrastructure. However, the threat to aviation could be more considerable as the distance between target and source could be very short. An attempt to quantify this threat was made by Tavani et al., by parameterising various radiation quantities and damage effects (including neutron fluence and single event effect rate) in terms of particle production number and cylindrical beam radius [41]. As these parameters each have potential ranges extending over orders of magnitude, this leads to an extremely wide range for the neutron fluence induced by a TGF. Neutron production in their analysis is due to interactions between gamma rays and an aircraft hull, rather than with atmospheric molecules.

Using a standard SEU upset cross section, the authors claim a critical threshold for neutron fluence of 10^6 n/cm^2 , with a potential maximum fluence of 10^9 n/cm^2 . The neutron spectrum they derive is similar to the source spectrum in [36]. However, the authors take no account of the how the SEU cross section varies as a function of neutron energy. This is known to rise steeply from 1 to 10 MeV [42], leading to considerable uncertainty in the prediction of SEU from neutrons in this range [43, 44]. The authors also seem to assume that a single SEU in a standard size SRAM represents a significant problem, whereas this is extremely unlikely to be the case. Nonetheless, even though a fluence of 10^6 n/cm^2 (predominantly $<10 \text{ MeV}$) may not represent a critical threat to avionics in terms of SEUs, the probability of single event latch-up (SEL), single event burnout (SEB) and other potentially destructive phenomena could be high in this environment [45]. However, these cross sections are also more significant at neutron energies above 10 MeV, and we estimate that only $\sim 4\%$ of neutrons in the Tavani spectrum are this energetic. The large uncertainty in the fluence of fast neutrons is problematic in terms of using this parametrised model to gauge risk to avionics. However, even at the lower end of fluence for the parameter range specified (10^3 n/cm^2) the average neutron flux over a one second timescale is orders of magnitude greater than both the background level at altitude, and the ground level environment predicted for TGFs elsewhere. There is clearly potential for single event effects to occur in any susceptible microelectronic component that finds itself in close proximity to a TGF, but there remains a large degree of uncertainty in quantifying this threat. An aircraft radiation detector capable of millisecond resolution, would be invaluable in potentially capturing empirical evidence of this phenomenon and gauging the scale of its effect on the local aircraft radiation environment.

6 Scope for enhancing the existing network

6.1 Time resolution and data transmission

At present, the COSMOS-UK network is configured to log neutron counts from the CRS2000/B every 30 minutes; this is the highest time resolution of counts recorded. For space weather events, there can be a need to detect events with very fast rise times of seconds, and to report or send alerts for such events as soon as they are detected. This places a requirement on the network to

- a) log neutron counts at much faster rates than the current configuration and
- b) instantaneously send alerts to the relevant space weather data centres when certain events are detected.

In this feasibility study, both aspects were investigated, and tested under laboratory conditions. For this trial, the data logger (model CR3000, Campbell Scientific Ltd., Shepshed, Leicestershire, UK) was programmed to request the accumulated neutron counts every 10 seconds, from the NPM-2000 module within the CRS2000/B. These values of counts per 10 seconds were logged in a data table (with air pressure, temperature and relative humidity) on the data logger and transmitted to the UKCEH data server. This trial was conducted using a wireless router/modem (cellular gateway), transmitting data over a mobile phone network, necessitating the modem to be always on, ready to transmit data. During the test, all of the other sensors were also interrogated, and data logged normally to ensure that the data logger has sufficient processing time to maintain normal network data acquisition, as well as the additional new load of the 10 second neutron count logging.

There are rare drop-outs, where no data from the NPM-2000 were received by the logger. These missed values (only 0.1% of all counts logged) are so rare that they are unlikely to have any impact on a space weather application. The impact, if any, would be limited to a 10 second delay in detecting an event at a single station (and the probability that more than one station would be affected in this way, in the same 10 second interval is very low). A sample of the successfully acquired and telemetered data is shown in Figure 61. This trial was run over a two-week period, and a histogram (Figure 62) shows the distribution all of the pressure-corrected counts for the whole period.

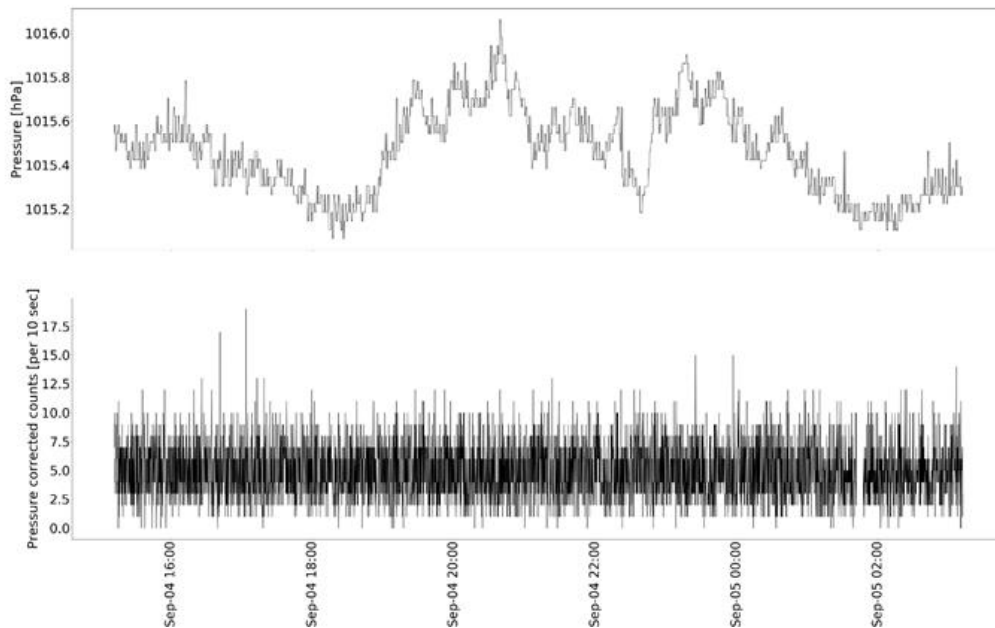


Figure 61: Sample of logged 10 second neutron count data.

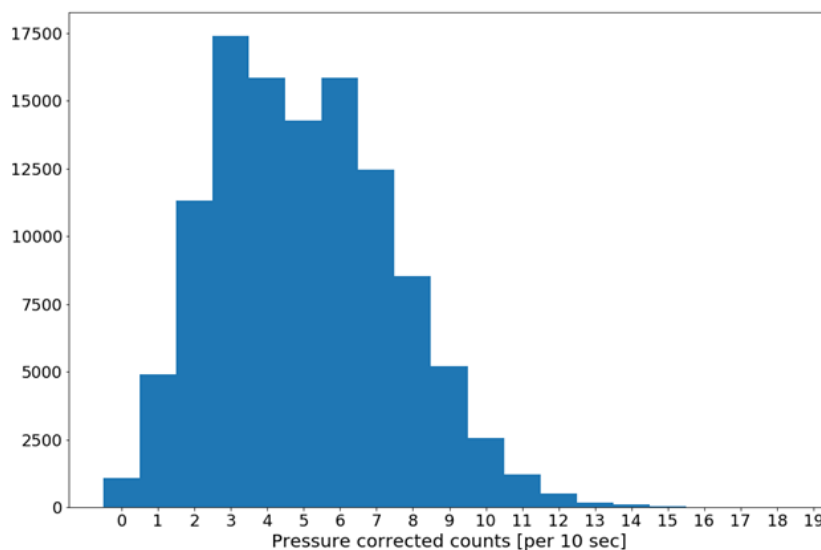


Figure 62: Histogram of All Counts Over Two Weeks

In summary:

1. We have shown that it is feasible to record and transmit counts from the CRS2000/B with a 10 second time resolution.
2. We can transmit the 10 s count data in near real-time, with minimal lag (probably only a few seconds after the 10 s data was acquired by the logger.)
3. The new 10 s data table on the logger could follow, in principle, a different transmission route to the current COSMOS-UK data tables – so we can minimise changes to our current data system and may have the opportunity to directly transmit that data to alternative servers e.g. at UKMO, for example.

4. For an always-on modem setup, there would need to be around a +50% power system upgrade at field sites, with a rough cost of around £1000 per site (total cost £49k).
5. We may also consider upgrading the router/modem to support text message (SMS) alerts if that was considered to improve resilience of alerts in case of mobile networks being impacted by space weather (see cost below).
6. We may reduce or eliminate the very few data dropouts that we see, by changing to an RS232 interface (instead of SDI-12) to connect to the CRS2000/B (not costed).

6.2 Cybersecurity Considerations

UKCEH is compliant with the Government's Cyber Essentials certification. Amongst other measures in place, all staff receive annual training in cyber security. This, in turn, raises staff awareness and instils best practice on risk areas such as social engineering attacks and poor password practices. It is acknowledged that human vulnerability is a high-risk area, and such training of staff and enforcement of best practice is vital to control these threats. Phishing attacks can be mitigated by training staff on how to recognise and thwart them, although they are becoming more sophisticated and may appear to come from colleagues within our own organisation. Some typical threats and control measures are outlined below, but this is not intended as an inclusive list, and further information is available from the National Cyber Security Centre.

Control measures are in place to prevent or reduce the risk of the diverse attacks that may affect the network. Many of these measures use a combination of basic security features such as firewalls and encryption as well as encouraging good practice amongst staff and physically securing network assets. The risk of unauthorised network access is reduced by the use of strong passwords. The use of non-alpha numeric characters as well as letters and digits increases the strength of the password. Passwords can be further hardened using two factor authentication. Keys and passwords should be protected from theft by storing them in a trusted key store such as KeePass - staff using encrypted password stores are much more likely to use strong and varied passwords.

Malware can also be avoided by raising staff awareness on when to avoid installing software or opening suspicious attachments. System administrators enforce this through a "whitelist" of approved apps that are allowed to be installed. If the user attempts to install an app that is not on the whitelist, the installation process is blocked.

Man-in-the-middle attacks can be prevented by keeping gateways physically locked away and by configuring them to restrict network access to authenticated accounts.

Distributed Denial of Service attacks (DDoS) attacks can be avoided by enabling functions in the firewall which identify and block them. Designated staff should be allocated to monitor internet activity and intervene when a DDoS attack occurs.

Exploits can be prevented by regularly updating applications and operating systems when vulnerabilities have been discovered. Regular updates need to occur across the entire network and are from a central server. Updates should be rolled out using keys which validate the update and/or the source of the update. If there is no key infrastructure available for updates, then the update file should at least be verified with a digital digest such as SHA-256. Applying this practice to field station equipment, such as cellular gateways and data loggers, can be more challenging, as it may not be practical to roll these out remotely, and therefore updates may only occur during a site visit (which may only be annually).

Intrusions into the network can be mitigated further by using the principle of least privilege. The principle of least privilege restricts a device's and user's capabilities to only those which are needed. This reduces the complexity of the network as a whole and lessens the chance of a user or device gaining access to unauthorised resources. Firewalls are often used to enforce this principle by restricting the types of transactions that occur across the network.

For the UKCEH COSMOS-UK environmental monitoring network, there is no physical (hard-wired) connection to the rest of the internet at the field stations. The gateway at the installation must reach the internet using wireless communications over a cellular or satellite network. The cellular/satellite network converts the wirelessly transmitted data into internet packets which it forwards to the internet. The internet packets it receives are forwarded wirelessly back to the remote gateway. Figure 63 depicts a COSMOS-UK style installation using the cellular network for internet communications.

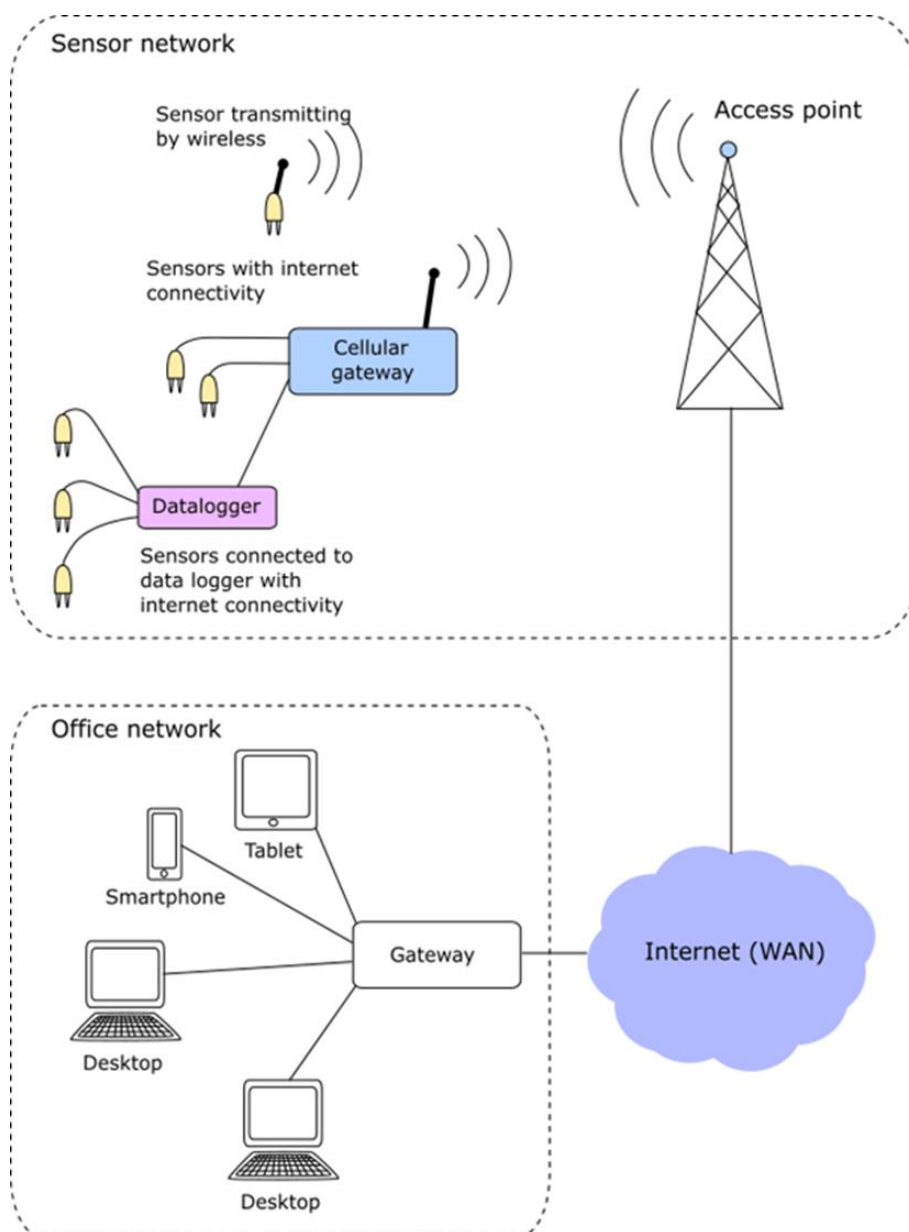


Figure 63: Schematic showing the use of the cellular network for internet communications from a COSMOS-UK field site to an office network, or telemetry data server.

The COSMOS-UK network faces the same threats as those listed above for more general (office) computer networks. However, some threats are more likely due to the kinds of devices used in COSMOS-UK. Default configurations for remote gateways and internet-ready devices often use easily guessed logins and passwords (these are replaced with strong passwords, which are also changed at regular intervals). They can come with many different communication protocols enabled by default. This can expose them to brute force attacks. Less robustly engineered devices can be more “buggy”. Support and documentation for these components can be minimal or non-existent. This offers a bad actor greater potential for exploits. Lack of human presence at the site allows greater possibility of theft, tampering or damage and potentially physical access to the site's cellular gateway.

Conversely, the specialised nature of the COSMOS-UK networks also makes it slightly less vulnerable to certain attacks. Specialised components of a network are inherently protected to a degree by their obscurity. Data loggers may use proprietary communication protocols and communications software which an attacker may not be familiar with. The data assets of the sensor network may also be less appealing to attackers. The environmental science sector targets offer less financial gain to attackers compared to those of the financial sector. However, there is a chance that environmental data could be stolen for military or political purposes, and there have been reports of such incidents.

Dual purposing the COSMOS-UK network for Space Weather alerts would change both the potential cyber security threats and threat level, as well as increasing the requirement for very robust and secure (safety critical) communications. This would be risk assessed with collaborators specialising in the most secure systems for national security. For example, consideration would be taken of the following:

1. COSMOS-UK becoming a high impact cyber-attack target, because of its importance as a space weather alert system. If being specifically targeted, an actor could easily obtain publicly available information on the devices deployed and the communication protocols used - therefore any benefits (aforementioned) of obscurity of devices would not hold for a targeted attack.
2. Efficacy of data could be affected, if not secure, e.g. a malicious actor could spoof data to trigger an alert.
3. These data would be delivered to other agencies in near real time, increasing the connectedness of systems, and system complexity, requiring careful design and maintenance of cyber security.

Again, this is not a comprehensive list, and further development of this alert system would require a revised cyber security risk analysis by an appropriate consultant, and implementation of the recommendations. It is likely, for example, that the COSMOS-UK network would be reconfigured to only operate over private or Virtual Private Networks (VPN), to eliminate any exposure to the public internet. The consultant's time and subsequent reconfiguration would require funding:

1. Certified cyber security consultancy fee, estimated £18,000.
2. UKCEH staff time for network reconfiguration to use VPN, updating all system documentation, writing implementation procedures, managing and implementing changes, estimated £9,500.
3. VPN implementation 3rd party licence fees etc. for first 3 years £4,500.
4. Depending on other requirements, it may be necessary or highly recommended to upgrade the cellular gateway at all 49 sites, at an estimated hardware cost of £39,000.

5. Depending on how the VPN and/or gateways are rolled out: if this work can be included in annual site planned preventative maintenance visits, then additional labour, travel and subsistence costs are minimised; otherwise, if additional site visits are required for reconfiguration and/or installation of new gateways, this would cost additionally around £34,000. It is recommended to include this cost, as based on experience, there will be (in either case) further reactive maintenance site visits required, to address snagging - therefore budgeting to pay for one site visit per site for this activity is reasonable.

Hence, the estimated total reasonable cost of this work to further tighten cyber security and provide additional functionality and security of the cellular gateway, would be around £105k (inclusive of VAT, where applicable) or £154k, including the required power upgrade (above) for the cellular gateway to be always-on.

6.3 Potential for creating multiple-detector hubs in strategic locations

The uncertainty in the neutron counting rate measured by the cosmic-ray neutron sensors follows Poisson statistics. In other words, the standard deviation of the signal is defined as $\sqrt{N_{raw}}$, and consequently the coefficient of variation defined as $(N_{raw})^{-0.5}$; with N_{raw} being the raw neutron counting rates measured by the sensor and typically recorded in counts per hour. The higher the number of counts measured over a pre-defined period, the lower is the uncertainty. Counting rates can be increased in two ways with cosmic-ray sensors: (1) by increasing the time integration window; or (2) by increasing the surface area of contact with fast neutrons within the sensor footprint. For space weather events, a longer integration period, such as 3-hour, 6-hour, or even daily; can mask out some of the signals, hence limiting its primary application (note that for typical applications of the sensor in hydrology and environmental monitoring that longer integration is used quite commonly).

The alternative is to increase the surface area interacting with neutron counts. This can be done, for example, by manufacturing bigger/longer tubes. Despite being an alternative, the non-standardized aspects for tube size and additional requirement for shielding and installation logistics and costs, can pose some practical limitations in this case. However, increase in surface area can also be achieved by employing multiple standard tubes simultaneously while covering a relatively small area. The multiple tube aspects allow for simplified deployment, a fail-safe aspect in case of single tube failure and can be additionally beneficial for assessing the heterogeneity of environmental factors for hydrology and environmental applications.

The MOSAIC team has identified at least one potentially feasible location in the UK where a 'super-site' of multiple cosmic-ray neutron sensors has been operating for many years. Each station is located approximately less than 1 km from each other in the Sheepdrove Organic Farm, near Lambourn (see Figure 64). The sensors are maintained individually by the University of Bristol (Rosolem) and CEH (COSMOS-UK), respectively. In order to illustrate the benefits of this 'super-site' arrangement, we compare the signal-to-noise characteristics from the measured raw neutron counts obtained from a single tube located in one of the sites with those obtained under the 'super-site' 4-tube configuration (Figure 65). The results indicate that the typical error associated with the signal (related to the coefficient of variation) is significantly reduced from about 2.5% to less than 1.5% on average (bottom panel in Figure 65).

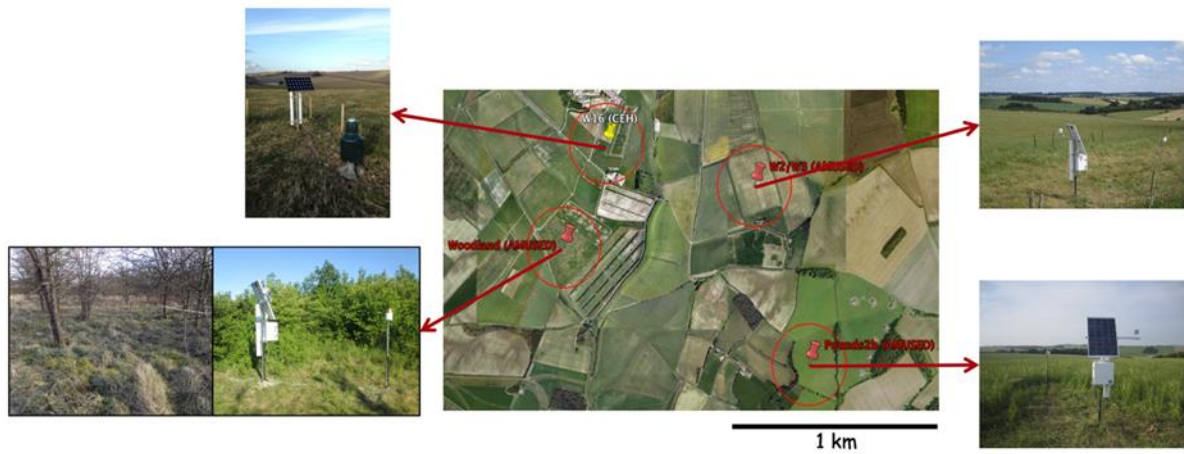


Figure 64: Distribution of cosmic-ray neutron stations at the Sheepdrove Organic Farm, near Lambourn. Stations highlighted as red markers are maintained by the University of Bristol while the yellow marker corresponds to the COSMOS-UK station.

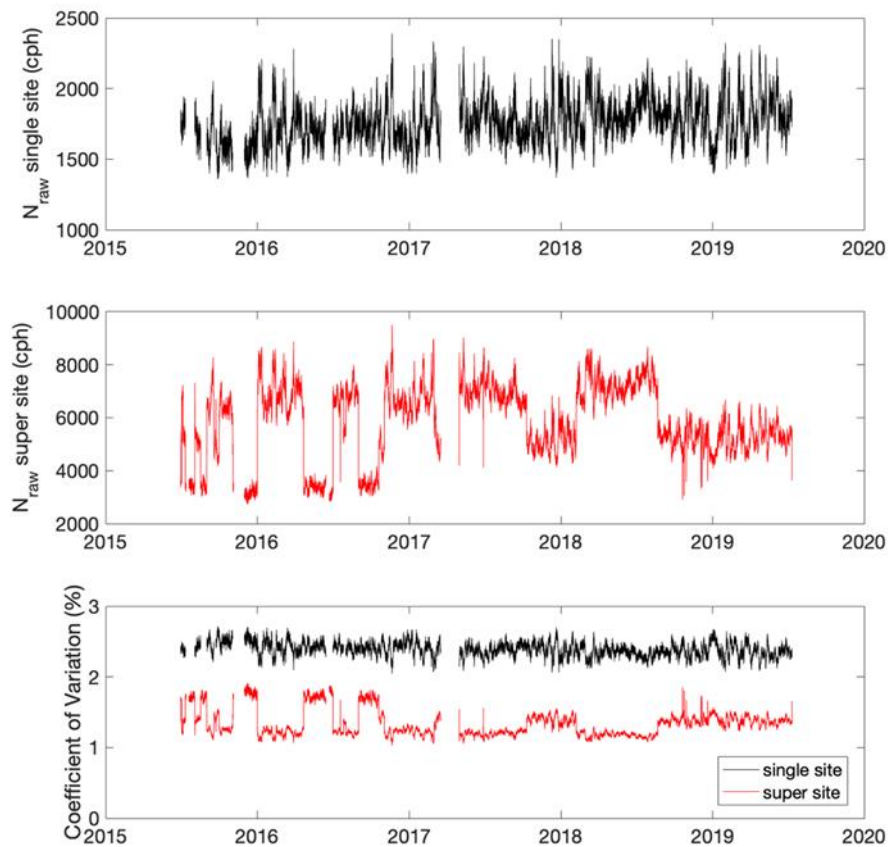


Figure 65: Top. Hourly raw neutron counts (cph) measured from a single site at Sheepdrove farm. Middle. Hourly raw neutron counts (cph) measured from the multi-sensor super site at Sheepdrove farm. Bottom: Impact of multi-sensor integration from the super site (red) on the coefficient of variation (%) compared to a single site (black).

6.4 Independent soil moisture adjustment

The ultimate objective of MOSAIC is to determine the value of using raw neutron counts from cosmic-ray neutron sensors. Unlike the traditional use of CRS for hydrological applications, MOSAIC focuses on exploiting the nature of CRS technology for space weather events. Raw neutron counting rates are readily available from cosmic-ray sensors as a direct measurement. However, a nation-wide system for neutron counts monitoring/prediction is still difficult because of the low-density characteristic of cosmic-ray networks compared to the country's spatial extent.

A full spatial analysis at the UK-scale is beyond the nature of the MOSAIC project (see recommendations below); however, we carried out initial analysis in order to test the ability of using independent environmental measurements already available in the UK to potentially deliver a spatially distributed product of neutron count. We tested this approach at the same locations where cosmic-ray sensors are deployed. This was done because at these locations we access to actual measured raw neutron counts can readily be used for validation. Originally, to derive soil moisture estimates from neutron counts, we refer to the following equation which is an updated version from [46].

$$\theta_{VOL} = \left[\frac{a_0}{\frac{N_{raw} \cdot (f_p \cdot f_i \cdot f_h \cdot f_v)}{N_0} - a_1} - a_2 - LW - SOC \right] \rho_{bd}$$

Equation 3

Where θ_{VOL} is the cosmic-ray derived volumetric soil moisture (m^3m^{-3}), ρ_{bd} is the dry soil bulk density (g cm^{-3}), LW (g g^{-1}) is the chemically-bounded lattice water content, and SOC (g g^{-1}) is the soil organic carbon. The N_0 corresponds to a site-specific calibration parameter that defines a theoretical neutron counting rate in a hypothetical dry environment (counts per hour; cph), and the individual corrections for changes in atmospheric pressure (f_p), water vapour (f_h), solar intensity (f_i) and aboveground biomass (f_v) are applied to the measured raw neutron count, N_{raw} (cph). Finally, $a_0 = 0.0808$, $a_1 = 0.372$, and $a_2 = 0.115$ are fixed constants.

We rearranged the terms in Equation 3 to calculate raw neutron counts as a function of all other variables [Equation 4]. In this case, notice that the volumetric soil moisture (θ_{VOL}) is the key variable that needs to be provided independently. Alternative sources for this variable are discussed in the recommendations but for this initial analysis we used soil moisture measurements from point-scale soil moisture reflectometry sensors co-located with the cosmic-ray sensors.

$$N_{raw} = N_0 \frac{\left[\frac{a_0}{\frac{\theta_{VOL}}{\rho_{bd}} + a_2 + LW + SOC} + a_1 \right]}{f_p \cdot f_i \cdot f_h \cdot f_v}$$

Equation 4

Our initial test was done at one of the University of Bristol sites located in the Sheepdrove Organic Farm (site W2/W3). The site is characterized by a relatively homogeneous short vegetation (grass) cover which results in minimal influence of aboveground biomass on the neutron signal. This site also contains clayey soils with a hard-chalky layer observed below 30-40 cm depth. Notice that the independent soil moisture measurement used in our analysis has a much more localized spatial coverage compared to the typical footprint of the cosmic-ray sensor. However, because the UK weather is typically homogeneous at spatial scales of about a few hundreds of meters, the time-series of both measurement techniques are relatively comparable (Figure 66 top panel). We apply Equation 4 above using the information from the point-scale soil moisture to independently calculate the raw neutron counts obtained at the site and further compare with the observations (Figure 66 middle panel). The results suggest that the calculated raw neutron count using the independent point-scale soil moisture have very good agreement with the actual raw neutron counting rates measured by the cosmic-ray sensors. Our proposed approach tends to overpredict slightly the raw neutron counts when soil conditions are relatively dry (Figure 66 bottom panel), with average neutron count biases on the order of 100 cph for the soil moisture range between 0.15 and 0.25 $\text{m}^3 \text{m}^{-3}$, approximately, corresponding to about 5% of the actual raw neutron count measurements. For relatively wetter conditions, the overall bias is around zero with some deviations within the -100 to +100 cph range (i.e., -5% to +5% of the signal). The results are surprisingly optimistic given the relatively low error with the approach. The fact that relatively drier conditions result in small positive biases is expected due to the fact that heterogeneities in soil moisture spatial patterns at field scales begin to appear as soil moisture conditions get dry.

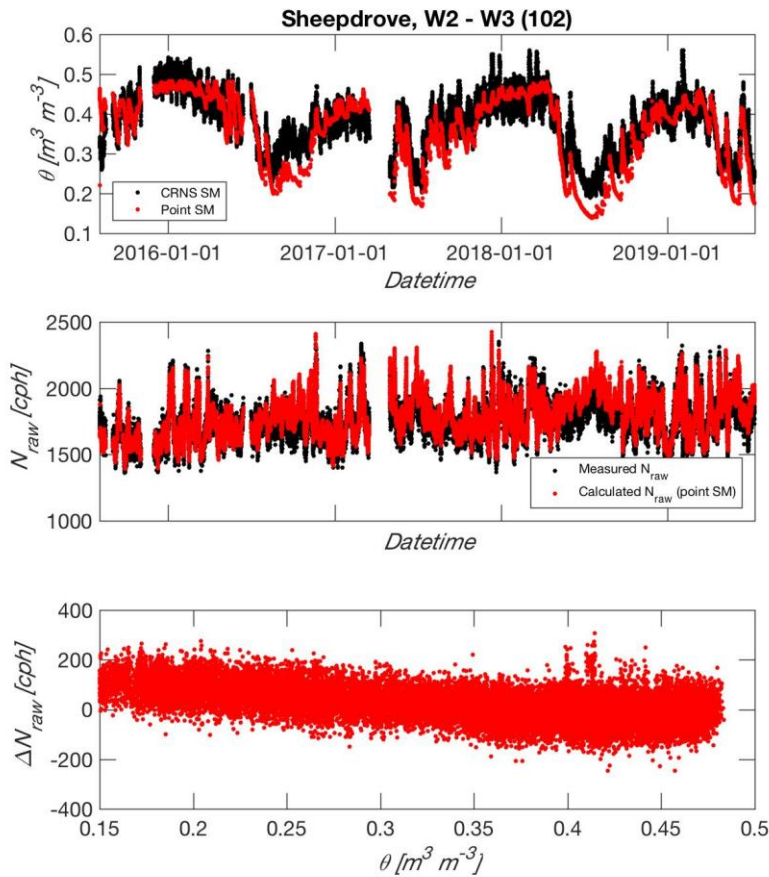


Figure 66: Top: Soil moisture ($m^3 m^{-3}$) time-series at the Sheepdrove Organic Farm from cosmic-ray sensor (black) and point-scale sensor (red). Middle: Raw neutron counting rates (cph) directly measured by the cosmic-ray sensor (black) and calculated indirectly from Equation 4 (red). Bottom: Difference between measured and calculated raw neutron counting rates (cph).

The results in Figure 66 are shown in detail for a single UK site. We therefore expanded this analysis across the entire COSMOS-UK network which allows us to obtain a broader perspective of the potential application of such approach in distinct regions of the UK. For that analysis, we included the dataset from COSMOS-UK provided by [47], in addition to the three sites located in the Sheepdrove Farm, making a total of 49 sites analysed. For each site, we compare the calculated raw neutron counting rates against the directly measured quantity by the cosmic-ray sensor. Figure 67 shows the overall results for the relative error (i.e., the percent different between the calculated and measured raw neutron counting rate normalized by the measured raw neutron counting rates). The results suggest that most of the relative error magnitude observed falls within the -5% to +5% range, similar to what was observed specifically at the Sheepdrove Farm site (Figure 66). There are very few sites where the relative error exceeds +5% magnitude. The average relative error observed across all 49 sites is $2.8 \pm 5.0\%$. Given the inherent uncertainty of the cosmic-ray sensors the observed relative error distribution suggests the approach to be potentially promising and feasible in the UK domain.

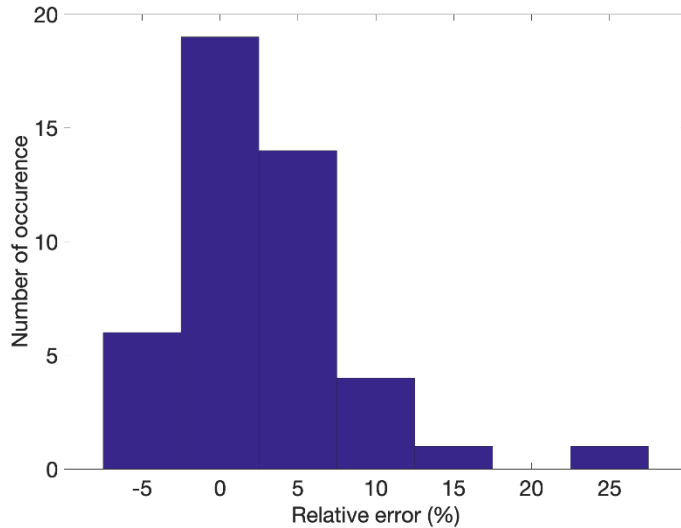


Figure 67: Histogram of relative error (%) for all 49 sites located within the UK domain. The relative error is computed as the percent different between the calculated and measured raw neutron counting rate normalized by the measured raw neutron counting rates.

Overall, our preliminary feasibility study shows a promising potential to develop the capability for neutron counting rates monitoring at high-resolution and at national scale. The work within the MOSAIC objectives was limited to test the value and possible limitations associated with the use of an independent soil moisture estimate to indirectly calculate raw neutron counts used for space weather applications. The steps needed to introduce a nationwide monitoring system are beyond the scope of the MOSAIC feasibility study but are highlighted below for future reference. Our key findings and recommendations regarding this sub-section are listed as follows:

1. There is a clear potential for using ground-based network of cosmic-ray neutron sensors beyond hydrological applications and encompassing space weather applications to derive raw neutron counting rates
2. For the nationwide product, other spatially distributed gridded datasets should be used. There are a few potential sources of grid-based products that can be evaluated in the future: (i) satellite remote sensing products such as the Soil Moisture Active Passive (SMAP) mission (<https://smap.jpl.nasa.gov/>) or the Sentinel 1 (<https://land.copernicus.eu/global/products/ssm>); or (ii) model-derived soil moisture fields from the Joint UK Land Environment Simulator (JULES) [48, 49] (see initial comparison in [50]) or from reanalysis product such as the new ERA5-Land (<https://cds.climate.copernicus.eu/cdsapp#!/dataset/reanalysis-era5-land?tab=overview>).
3. The adoption of any grid-based dataset should be accompanied by a careful evaluation and appropriate correction for any systematic biases on the soil moisture signal. The use of biased soil moisture estimates can significantly affect the quality of the derived raw neutron counting rates, affecting the operational and reliability of the monitoring system at regional to national scales. Notice that regional bias correction techniques can make use of the already established COSMOS-UK network soil moisture data.
4. There are still some additional challenges regarding the development of a high-resolution national map for supporting information for lattice water, soil organic carbon, and biomass. Most importantly, the definition of a national map for the N_0 parameter is critical for the success of any future development of a high-resolution neutron counting rate product for the UK. The parameter N_0 can be influenced by local characteristics associated with elevation, atmospheric pressure, and fluctuations in solar intensity; all factors relating to the global

patterns for cut-off rigidity (Darin Desilets – Hydroinnova and MOSAIC project partner, pers. comm.). As an initial step, we recommend empirical multi-variate relationships to be established to determine the spatial interpolation of NO across the UK domain. The crspy tool has been developed with that in mind and collects a large number of meta-data from different global and local sources to allow for future multi-variate and meta-data analysis.

6.5 Use of Artificial Intelligence in data processing

Machine Learning (ML) techniques may be applied to automate detection of certain types of SW events. In this particular application, we can benefit from the catalogues of known SW events, for ML training to identify these events in the historical COSMOS-UK data. This would be limited to events that have occurred during the lifetime of COSMOS-UK (since October 2013). As there have not been any large GLEs in this time frame, this likely limits any ML training (using real data) to Forbush decreases. In some senses this is fortuitous, since GLEs should be detectable with standard test algorithms (based on the rate of increase and absolute increase in counts etc.), whereas arguably, a Forbush decrease may be partially concealed by, or interpreted as, a sudden increase in soil moisture (e.g. due to intense rainfall). Such confounding factors can make detection of count decreases more complicated and thus ML may provide reliable automated detection in these challenging circumstances. Note that very rapid increases in neutron count rates (GLEs), can be easily distinguished from soil moisture changes, as the soil cannot dry out so rapidly as to be confused with a GLE.

ML approaches, readily combine correlated data, such that the co-located sensor information (e.g. precipitation measurements), will aid the interpretation of neutron counts – if there is no rainfall, we do not expect an increase in soil moisture, and hence no decrease in corrected neutron counts. If a significant decrease is observed without rainfall, then it is likely to be related to a change in the incoming cosmic-ray neutron flux. Ultimately, any events detected by the COSMOS-UK network (whether or not identified by ML) would be combined with other SW information. To combine information, and make appropriate decisions, will require uncertainty estimates for event detection. The required decision support system may well lend itself to a Bayesian network analysis, to efficiently determine the overall likelihood of a given event, considering all of the available information.

6.6 Use of complementary data sources to enhance potential alert system

6.6.1 Neutron Monitor Data

Neutron monitors have been discussed earlier in the report. Regardless of any potential future exploitation of COSMOS network data for space weather applications, neutron monitors will remain an indispensable source of data during ground level enhancements. The utility of neutron monitor

data for a COSMOS-based GLE alert system is likely to be based around benchmarking due to the much higher count rate compared to individual COSMOS detectors. For example, were a sudden sharp increase in count rate to occur in a selection of COSMOS detectors, but not in a neutron monitor of reasonably close proximity, then it is highly unlikely that the COSMOS-detected rise is linked to space weather. The key factor in this example is the distance between COSMOS detectors and the reference neutron monitor. Anisotropy in ground level enhancements is a well-known feature, especially early on in the event. However, this effect applies over international distances of the order of thousands of miles – for example the large difference in GLE05 (Feb-56) between the increase recorded at Leeds, UK, compared to increases at North American stations at similar or even lower cut-off rigidities (Figure 5). Taking this anisotropy into account can increase the calculated primary spectrum [2].

Ideally a UK COSMOS network would be accompanied by a UK-based neutron monitor station for local cross-referencing of count rate data. Even with a fully-operational UK neutron monitor, data provided by COSMOS would still be useful due to the rigidity range it covers and thus, as described earlier, the information on the primary GLE spectrum this would provide. In the absence of a UK-based neutron monitor, the existing monitors located at Dourbes in Belgium or Kiel in Germany are likely to be the nearest sources for benchmarking. However, while these may be suitable for cross-referencing data from the southern England, they are not necessarily adequate for comparing COSMOS detectors based in Scotland. Figure 68 shows the relative count rate for the Kiel and Oulu neutron monitors during GLE71. Although there is no significant increase in the Kiel count rate, at a cut-off rigidity of $R=2.36$ GV – similar to southern England, there is a significant increase at Oulu, where the cut-off rigidity of 0.81 GV is only slightly lower than in northern Scotland. Therefore, a lack of increase at Kiel should not be used to nullify a measured increase in a COSMOS detector in the north of the UK.

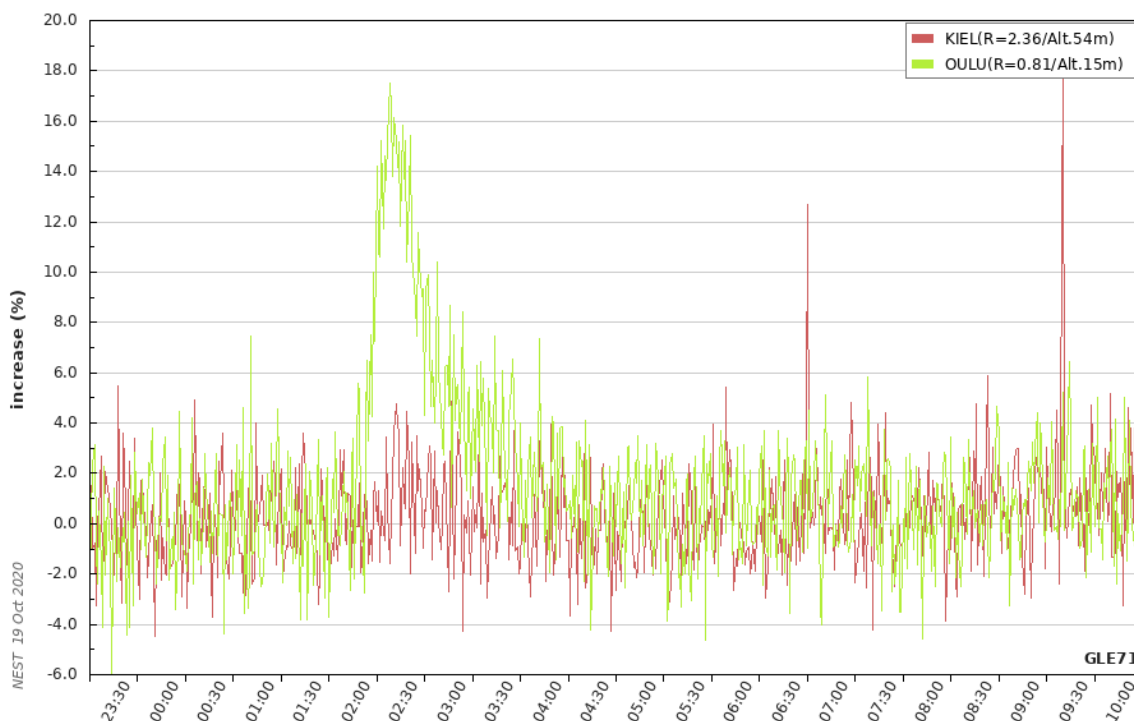


Figure 68: Normalised neutron monitor data from Oulu and Kiel stations during GLE71 on 17th May 2012.

This is just one example of how care would need to be taken when using neutron monitor data to sanity check observed increases in a UK COSMOS detector network. In practice, any measured increase in COSMOS count rate should be observable in at least one northern European neutron monitor for it to be attributable to space weather. Once authenticated in this way, the additional spatial and spectral information provided by a distributed network of COSMOS detectors could be exploited with higher confidence.

Another consideration is the availability of neutron monitor data. Figure 69 shows that, although over seventy neutron monitors are currently maintained in the global network, only a fraction of these may provide real-time data (listed as “online” by nmdb.eu) at any one time. Hence a resilient alert system using cross-comparisons to neutron monitor data would have to allow for the possibility that the desired data may not be available and enable a backup station to be used instead.

47.	Neumayer 3	NEU3	Offline	Offline	Offline
48.	Newark	NEWK	Online	Online	Offline
49.	Norilsk	NRLK	Offline	Offline	Offline
50.	Novosibirsk	NVBK	Offline	Offline	Offline
51.	Ny Alesund	NYAA	Offline	Offline	Offline
52.	Livingston Island	ORCA	Offline	Offline	Offline
53.	Livingston Island, bare	ORCB	Offline	Offline	Offline
54.	Oulu	OULU	Online	Online	Offline
55.	Polarstern	POLI	Offline	Offline	Offline
56.	Doi Inthanon	PSNM	Offline	Offline	Offline
57.	Potchefstroom	PTFM	Offline	Offline	Offline
58.	Peawanuk	PWNK	Online	Online	Offline
59.	Rome	ROME	Online	Offline	Offline
60.	Sanae, bare	SANB	Offline	Offline	Offline
61.	Sanae	SAEA	Offline	Offline	Offline
62.	South Pole, bare	SOPB	Online	Online	Offline
63.	South Pole	SOPO	Online	Online	Offline
64.	Terre Adelie	TERA	Online	Offline	Offline
65.	Thule	THUL	Online	Offline	Offline
66.	Tibet	TIBT	Offline	Offline	Offline
67.	Tsumeb	TSMB	Offline	Offline	Offline
68.	Tixie Bay	TXBY	Online	Offline	Offline
69.	Zugspitze, bonner sphere	UFSZ	Offline	Offline	Offline
70.	Yakutsk	YKTK	Online	Offline	Offline
71.	Zugspitze	ZUGS	Offline	Offline	Offline
			Online: 25 Offline: 46	Online: 15 Offline: 56	Online: 2 Offline: 69

Figure 69: Snapshot of neutron monitor real-time availability from nmdb.eu.

6.6.2 Aircraft Monitors

The industrial sector most at risk from elevated atmospheric neutron fluxes during ground level enhancements is the aviation sector [2, 45, 51, 52]. Increases at aircraft altitudes are significantly greater than increases measured on the ground [53, 54]. Therefore, the most useful location to measure the radiation environment is within aircraft. There are only a handful of examples of such in-flight measurements during a GLE [55-60], however this underestimates efforts in recent years to perform such measurements, which have been thwarted by the paucity of events in that time frame.

Various types of in-flight radiation monitor have been used to record increases in neutron flux, or other parts of the radiation environment. These range from single-channel dosimeters that primarily respond to directly ionising radiation, to tissue equivalent proportional counters that are calibrated to include radiobiological weighting factors for different types of radiation. For the purpose of using in-flight data in conjunction with ground level neutron monitors or COSMOS detectors, the most useful type of detector is one from which it is possible to infer neutron flux, rather than just a general increase in the level of ionisation. The calibration issues associated with this task are beyond the scope of this report, but the following analysis is based on having this information available from aircraft detectors.

The exploitation of in-flight data in conjunction with ground data can be thought of in a similar way as having two detectors at different cut-off rigidities (Figure 58). A detector at high altitude is responsive to a slightly different part of the primary GLE spectrum than one at ground level. This is particularly true when the high-altitude location is also at low cut-off rigidity. Figure 70 shows the expected increase in neutron flux at 12 km altitude as a function of GLE spectral index, for an event that causes a 10% increase in count rate in a ground level neutron monitor. For example, an increase of ~100% measured by an in-flight monitor at 12 km and R=0 GV implies a primary spectral of $\gamma=5$. Where both detectors are located at R=4 GV the slope of the relationship is much shallower, which makes the estimation of spectral index far more difficult.

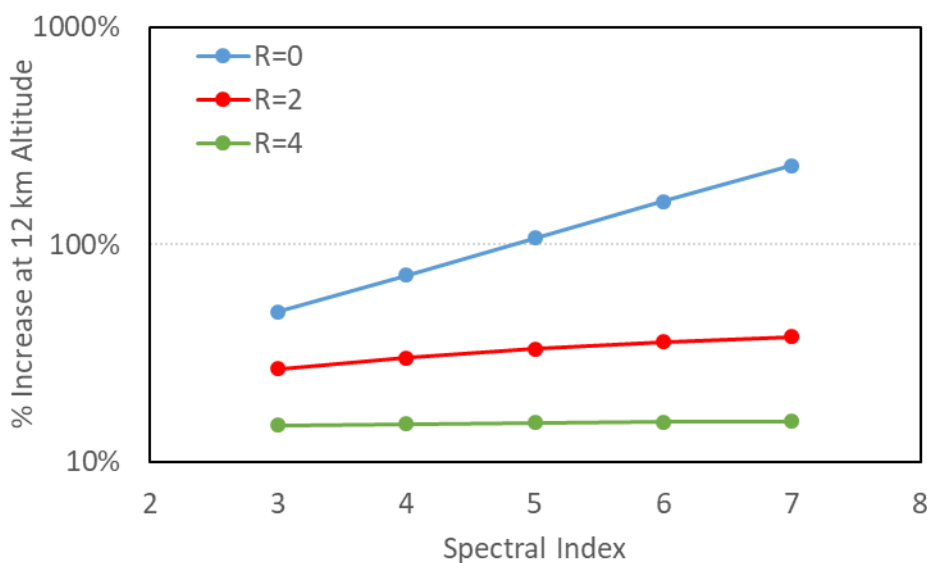


Figure 70: Predicted increase in high altitude neutron flux for an event leading to a 10% increase in GLNM count rate. Increases are shown for ground level and in-flight monitors located at the same rigidity (0, 2 or 4 GV) as a function of spectral index.

It is, of course, possible (if not very likely) that the in-flight detector and ground detector will not be located at the same cut-off rigidity. Figure 71 shows the ratio of flight increase (at 12 km) to ground increase for nine combinations of rigidity (0, 2 and 4 GV for each altitude) as a function of spectral index. Although the relationship on log-linear axes is exactly quite linear, it is clear that the slope of each combination line is related to the rigidity of each detector location. Figure 72 shows how this slope varies with different combinations of flight detector rigidity and ground detector rigidity. The combinations where the slope is close to zero (typically when the flight and ground detectors are at the same cut-off rigidity) are the ones where it is hardest to infer spectral index from the ratio of

percentage increase at the two altitude. Of course, the nature of these relationships also depends on the altitude at which the in-flight measurement is made, so Figure 73 shows the equivalent plots for an altitude of 9 km.

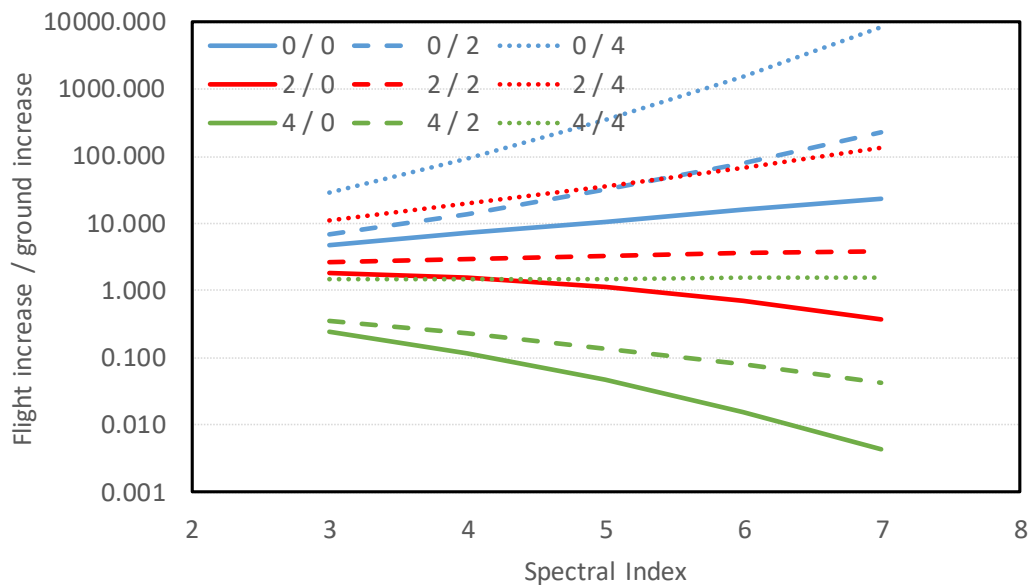


Figure 71: Predicted ratio of neutron flux increase at 12 km altitude to GLNM count rate as a function of spectral index. Flight detectors located at R=0, 2 & 4 GV are represented by blue, red and green lines respectively. Ground level monitors located at R=0, 2 & 4 GV are represented by solid, dashed and dotted lines respectively.

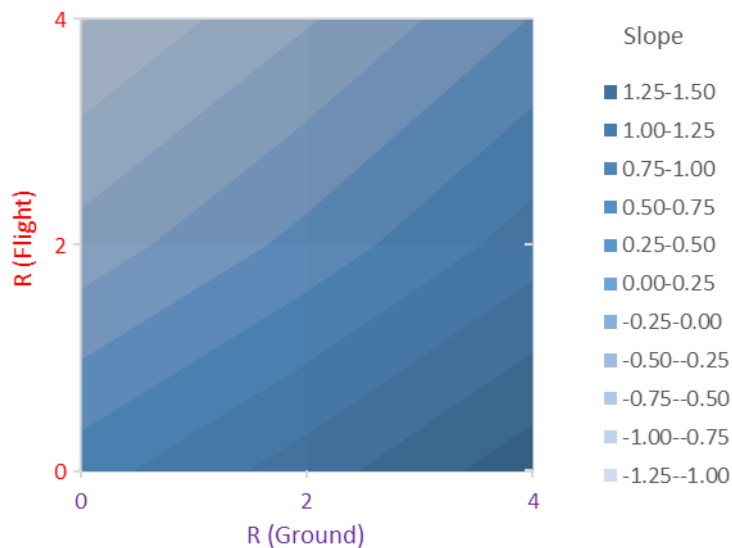


Figure 72: Illustration of the relationship between the rigidity of two detectors (Flight = 12 km) and the gradient of the slope relating the ratio of % increase to spectral index. The larger the modulus of the slope, the easier it is to infer spectral index.

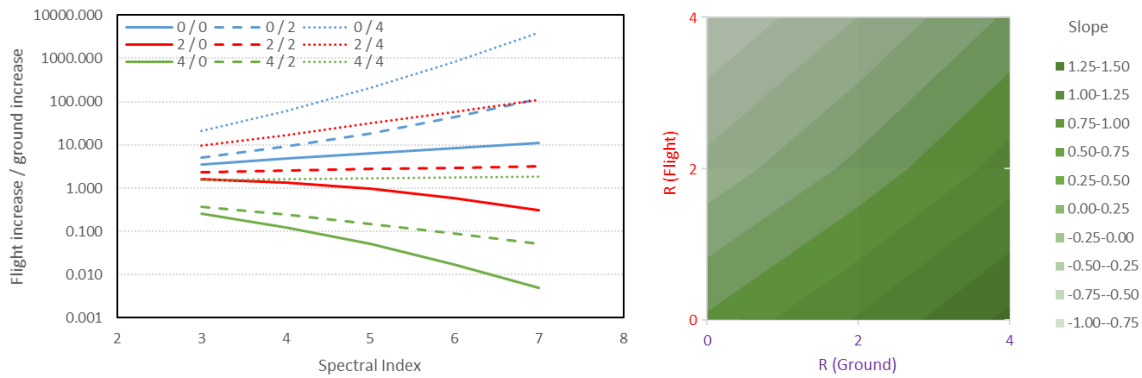


Figure 73: (LHS) Predicted ratio of neutron flux increase at 9 km altitude to GLNM count rate as a function of spectral index. Flight detectors located at R=0,2 & 4 GV are represented by blue, red and green lines respectively. Ground level monitors located at R=0, 2 & 4 GV are represented by solid, dashed and dotted lines respectively. (RHS) Illustration of the relationship between the rigidity of two detectors (Flight = 9 km) and the gradient of the slope relating the ratio of % increase to spectral index. The larger the modulus of the slope, the easier it is to infer spectral index.

Various caveats must be applied when considering this simple approach to inferring spectral information from only two measurements of neutron flux increase, as they must when using rigidity alone in the method described earlier. However, it is clear that in-flight measurements can provide more information on a GLE than simply the local radiation environment at the time of measurement (although that may nevertheless be the primary function of an in-flight detector).

6.6.3 ICAO Space Weather Thresholds

The International Civil Aviation Organization (ICAO) has summarised its guidance on space weather for aviation service providers in a manual of information in support of international air navigation. The manual defines thresholds for advisory notifications about space weather activity based on “moderate” and “severe” levels of a particular metric. For atmospheric radiation it defines these levels in terms of effective dose rather than neutron flux, with moderate and severe thresholds set at 30 and 80 micro Sieverts per hour respectively. As these thresholds apply up to an altitude of 46,000 feet (14 km), and are inclusive of the GCR background dose, the relationship between them and the increase at ground level depends on a number of factors including rigidity, GLE spectral index, solar cycle year and aircraft altitude.

For example, Figure 74 shows dose rate profiles for five different spectral indices as a function of altitude at zero rigidity, normalised to a 10% increase in dose rate at ground level (NB this is slightly different to a 10% increase in detector count rate, but the difference is unimportant on the scale shown). ICAO thresholds are shown at the levels they would be reached at an altitude of 12 km, corresponding to a ~300% and ~960% increase in background dose rate respectively. This shows that a 10% increase at ground level would not be expected to trigger an ICAO Severe alert with any GLE with a primary spectral index in this range, whereas a Moderate advisory threshold would be reached for a GLE with a spectral index above ~6.

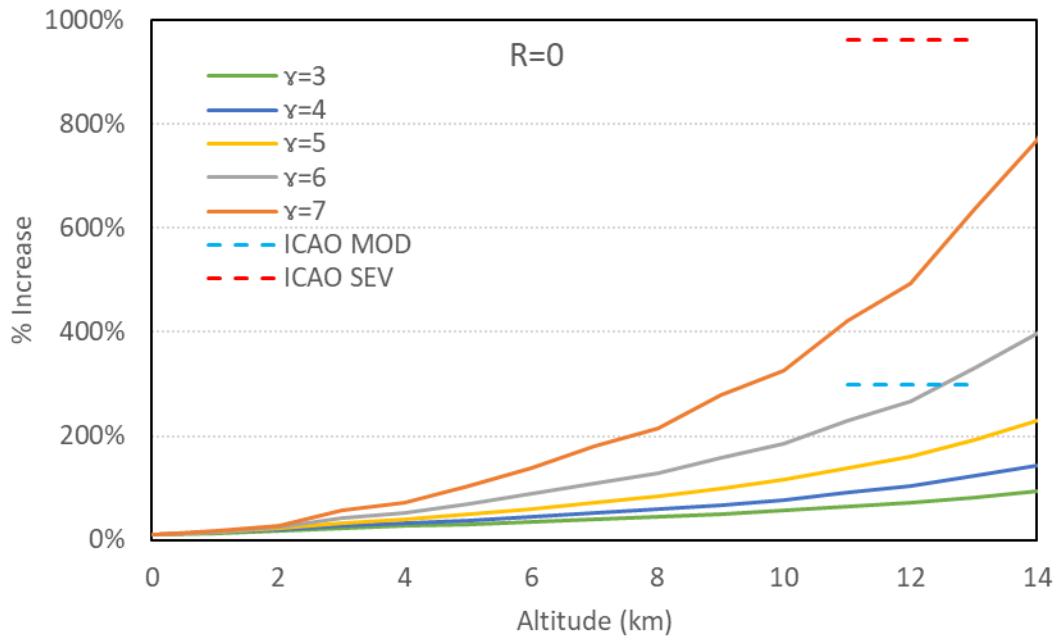


Figure 74: Increase in effective dose rate as a function of altitude at $R=0$ GV. Five curves, representing GLE spectral index from $\gamma=3$ to $\gamma=7$ are normalised to a 10% increase at ground level. “Moderate” and “Severe” ICAO thresholds are shown at the level at which they would be triggered at an altitude of 12 km.

The strong dependence of dose rate altitude profile on spectral index highlights the uncertainty involved when extrapolating from ground level data to the high-altitude environment. Nevertheless, we can use equivalent relationships between dose increase at altitude and neutron flux increase at ground level (as a function of spectral index) to invert this process and calculate the ground level flux increase that would be expected for each ICAO threshold. These predicted increases can subsequently be used to calculate the number of COSMOS detectors that would be required in aggregate to achieve a sufficient count rate for the peak of the event to be statistically significant. For example, as shown in Figure 56, if the moderate threshold ($30 \mu\text{Sv/h}$) were reached at 12 km, and the spectral index was estimated or calculated to be such that this corresponded to a 100% increase in neutron flux at ground level, this would mean that a single detector is sufficient for a 5σ detection of the increase in count rate. A higher spectral index (softer spectrum) would imply a smaller increase at ground level and thus a higher requirement for the number of COSMOS detectors needed to see the peak at 5σ . The steep dependence on spectral index, rigidity (of both flight detector triggering ICAO threshold and ground location), and, to a lesser extent, on COSMOS time resolution, leads to enormous variation in the number of detectors required to observe the event at 5σ significance. Several examples are given below, all assuming 1500 counts per hour baseline as before. Figure 75 and Figure 76 show the detector requirement Moderate and Severe ICAO thresholds respectively, both assuming 15-minute COSMOS detector resolution. Figure 77 and Figure 78 are the equivalent plots for 1-minute COSMOS detector resolution.

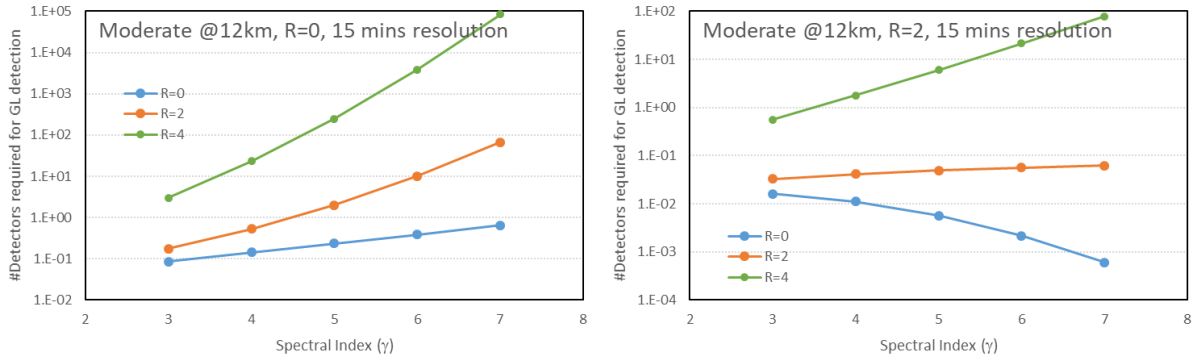


Figure 75: Number of COSMOS detectors required to observe a GLE triggering a Moderate ICAO advisory at 12 km and R=0 GV (LHS) or R=2 GV (RHS) rigidity. The number required for 5σ detection is shown as function of COSMOS detectors' location for R=0 GV (blue), R=2 GV (orange) and R=4 GV (green). COSMOS detector resolution is 15 minutes.

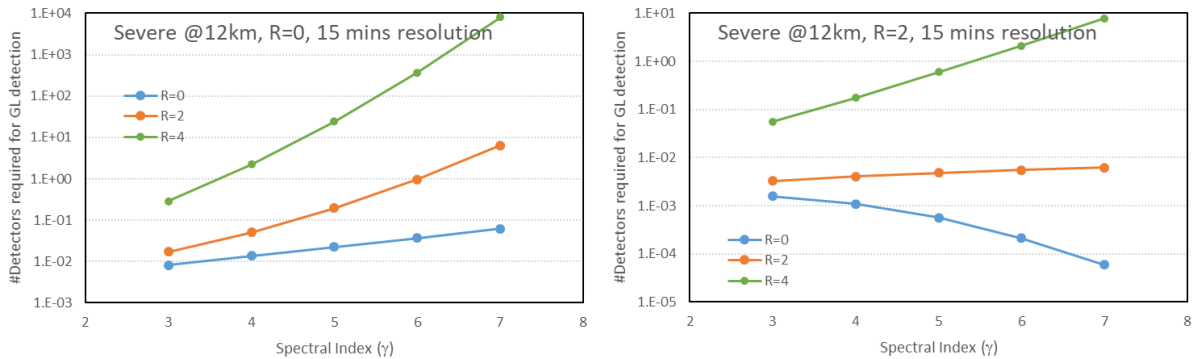


Figure 76: Number of COSMOS detectors required to observe a GLE triggering a Severe ICAO advisory at 12 km and R=0 GV (LHS) or R=2 GV (RHS) rigidity. The number required for 5σ detection is shown as function of COSMOS detectors' location for R=0 GV (blue), R=2 GV (orange) and R=4 GV (green). COSMOS detector resolution is 15 minutes.

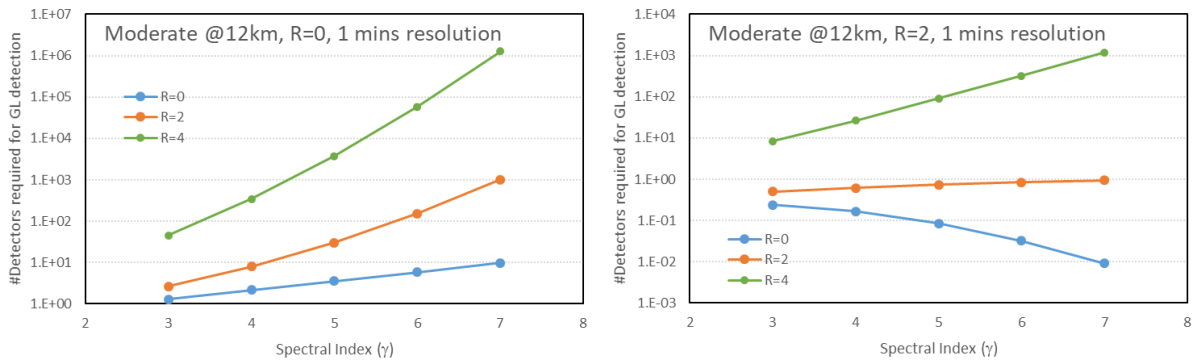


Figure 77: Number of COSMOS detectors required to observe a GLE triggering a Moderate ICAO advisory at 12 km and R=0 GV (LHS) or R=2 GV (RHS) rigidity. The number required for 5σ detection is shown as function of COSMOS detectors' location for R=0 GV (blue), R=2 GV (orange) and R=4 GV (green). COSMOS detector resolution is 1 minute.

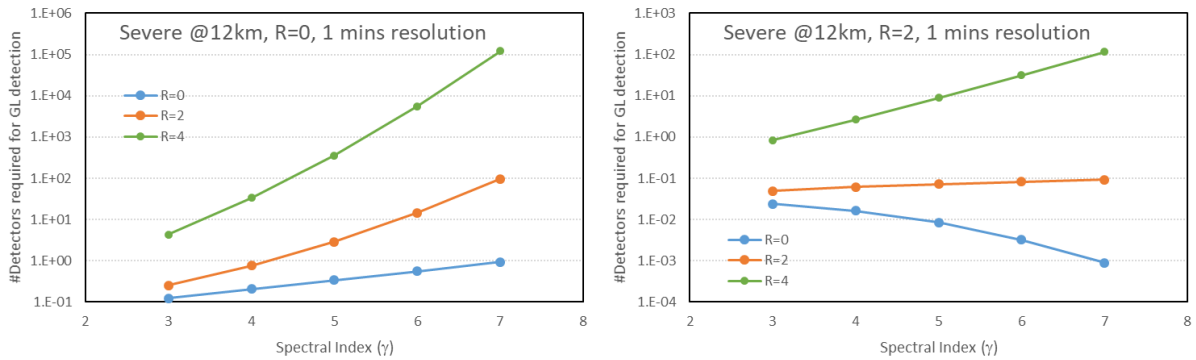


Figure 78: Number of COSMOS detectors required to observe a GLE triggering a Severe ICAO advisory at 12 km and R=0 GV (LHS) or R=2 GV (RHS) rigidity. The number required for 5σ detection is shown as function of COSMOS detectors' location for R=0 GV (blue), R=2 GV (orange) and R=4 GV (green). COSMOS detector resolution is 1 minute.

Notwithstanding the various assumptions and caveats that apply to these calculations, the plots above show that it is too simplistic to relate ICAO thresholds directly to the number of COSMOS detectors required to provide an alert to it. Even if only the R=2 GV curves are considered (orange in the plots, most relevant to the COSMOS-UK network), the variation is considerable – anything from a single detector being easily sufficient, to one thousand being only barely adequate. This range would expand further if GLE anisotropy and a broader altitude range were considered. Any COSMOS-based GLE alert system would need to be aware of this range when considering its use in conjunction with the ICAO space weather advisory thresholds as they are currently specified.

6.6.4 Other atmospheric measurements

Regular deployment of in-flight detectors, possibly carried by passengers or crew rather than incorporated as cabin equipment [61], is the optimum approach for measuring the high-altitude radiation environment. However, this could potentially be supplemented by stratospheric measurements from monitors deployed on high-altitude long-endurance unmanned aerial vehicles (UAVs) or rapid-launch balloon-borne payloads. Figure 79 shows count rate versus altitude for the solid-state Zenith radiation detector, which was deployed on a MET Office weather balloon in December 2016 [62]. The Pfofzter maximum [63] is visible in the data at around 18,000 feet, although this applies to the ionisation rate or absorbed dose profile and has been observed to not apply to effective dose due to the influence of heavy ions with high relative biological effectiveness in the upper atmosphere [53].

The principle of a rapid-launch balloon detector is straight forward. On receiving a notification of the onset of a GLE, a weather balloon with a radiation monitor payload is launched within minutes and measures the progress of all but the earliest stages of the event during its ascent. The utility of such a system depends primarily on two factors: the delay between the notification and launch and the time profile of the GLE. The former is largely dependent on the quality of the infrastructure for manual deployment of the weather balloon, i.e. whether or not it is practical to have a dedicated platform prepared for launch 24 hours a day. The latter is uncontrollable; however, it is obvious that such a system is more useful in the case of a gradual event than for an impulsive event that could have diminished substantially before launch. Zenith took 100 minutes to ascend to an altitude of 33.5 km

(~110,000 feet), thus even for a gradual event the first phase would be measured within the lower atmosphere. However, as some events can occur in sequences lasting over many hours, or even days, in the absence of local in-flight data such a system could provide invaluable data to inform civil aviation authorities on the safety of continued commercial air traffic.

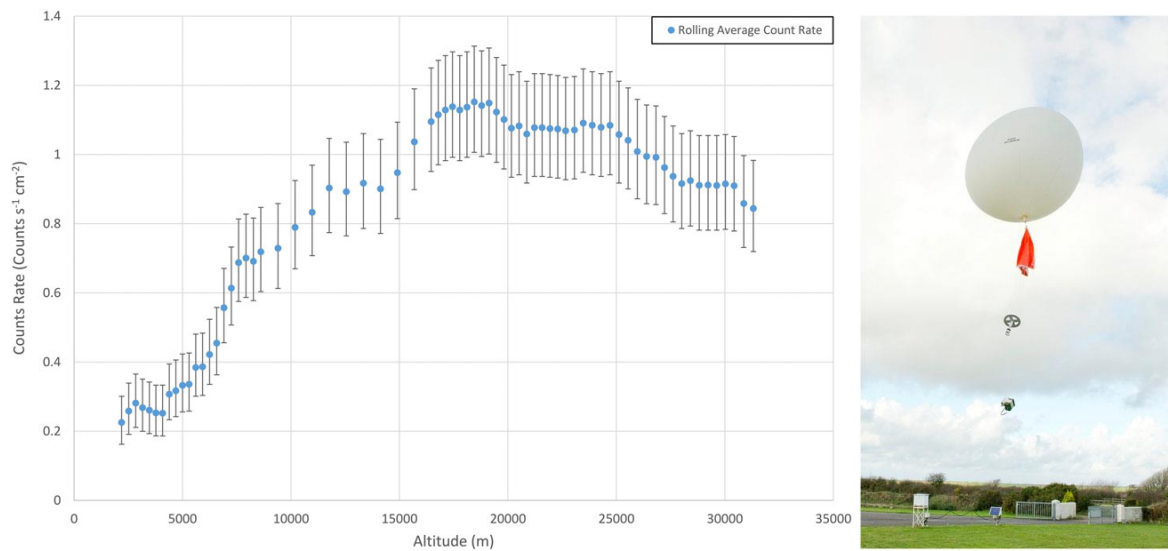


Figure 79: (LHS) Count rate as a function of altitude for the Zenith detector. (RHS) Photo of the launch of a weather balloon carrying Zenith in December 2016.

7 Feasibility Assessment Summary

The objective of this study is to evaluate whether the UK COSMOS soil moisture sensor network can be dual-purposed to be an effective alert system for space weather events that pose a hazard to ground level infrastructure and the aviation sector. We have shown through analysis of existing data and simulations of hypothetical events, that COSMOS detectors are sensitive to the changes in the ground level radiation environment that occur during such events, and upgrades to the network that would enable an effective GLE alert system are feasible. A summary of requirements and recommendations to implement such a system are outlined below.

1. Count Rate

A typical count rate for a single UK COSMOS detector is of the order of 1000 – 2000 counts per hour depending on local conditions. This is substantially lower than that of a standard design (6-NM64) ground level neutron monitor, which typically records ~70 counts per second (250,000 counts per hour) in a mid-latitude location. This is partly due to the deliberate amplification of neutron flux in the design of neutron monitors, which makes them especially sensitive to high energy neutrons. However, in spite of the substantial differences in response function between these detectors, our analysis shows that the expected percentage increases during a GLE event are similar. This means that, to a first approximation, recreating the count rate of a neutron monitor for both background and GLE conditions (if that were necessary) would simply be a matter of aggregating counts from a larger number of COSMOS detectors. This would imply ~150 sensors, considerably more than the entire UK network of ~50 stations. However, we have shown that sensitivity to even relatively small GLEs can be achieved with a much lower number of sensors (see Figure 56 for example). Indeed, even a single sensor would observe a statistically significant increase in a 1-minute averaged count rate for an event of moderate magnitude (>100% increase above background). Nevertheless, to improve the signal-to-noise ratio it would be advantageous to group COSMOS detectors together at selected strategic locations. This would also help to mitigate the impact of a potentially reduced count rate during wet conditions. Conversely, aggregating data from geographically separated stations would compensate for the effect of dynamic local moisture conditions, except during very widespread rainfall events.

The optimum approach is therefore to have the ability to aggregate data both locally and nationally. In order to achieve this, we recommend significantly expanding the number of COSMOS detectors in at least two strategic UK locations, ideally covering the maximum range in rigidity from northern Scotland to southern England. These detector hubs would act like mini neutron monitors, i.e. with total count rates in between a single COSMOS detector and a full neutron monitor. To resolve the peak of an impulsive event that leads to 25% increase in background count rate at 5σ significance with 1-minute time resolution, 16 co-located detectors are required. This is 100 times smaller than the Feb-56 GLE (ignoring anisotropy), and thus represents a very low detection threshold. Smaller or softer events may not be observed in a statistically significant way, but such events are very unlikely to pose a threat to microelectronics, even at high altitude and latitude.

2. Time resolution

Unlike improvements to count rate, which are useful, improvements to time resolution are essential for the COSMOS network to serve as an effective GLE alert system. The existing half-

hourly resolution of the UK network may just be sufficient to monitor the progress of a gradual GLE as it unfolds over many hours, but it is inadequate for an impulsive GLE with a rise-time potentially below one minute. 1-minute resolution is both an achievable and a desirable capability for an enhanced COSMOS network. Such an enhancement would make the time resolution comparable to the ground level neutron monitor network that is currently the basis of a number of GLE alert services. Defining the criteria for triggering a GLE alert based on COSMOS data is out of scope for this report and would depend heavily on the number of detectors aggregated in a collective count rate as well as other factors.

The volume of data that would be required to be collected and transmitted for a 1-minute resolution service is relatively small and, as we have demonstrated, achievable with only minor modifications to existing network infrastructure. The estimated cost for such an upgrade is £1000 per station, with additional costs of up to £150,000 for cybersecurity considerations, thus a total cost of the order of £200,000.

Ideally 1-minute data would be available in real time for all UK stations. However, in the near term it may be more feasible to roll out the capacity to a smaller number of stations, i.e. those selected as strategic hubs for placing multiple detector tubes together to increase overall count rate. Sub-minute time resolution may be achievable in a similar way, though it is questionable whether this would add anything practically to the observation of GLEs. Very fine time resolution would be useful for resolving other phenomena, such as TGFs. However, as these are expected primarily in tropical locations, this is not a high priority for the UK network.

3. Geographical distribution

The UK spans a geomagnetic cut-off rigidity range that potentially leads to dramatic differences in the impact of space weather. In quiescent conditions this range is approximately 0.8 – 3.0 GV (from the Shetlands to Cornwall), but the lower end of this range could drop to zero during the disturbed conditions of a geomagnetic storm. Regardless of the precise range, a ΔR of ~ 2 GV is very useful for inferring information on the primary proton spectrum of a GLE event, which is important for extrapolating from UK ground level measurements to other altitudes and latitudes. While there are several stations in south west England, the current northernmost UK COSMOS station is at Glensaugh in Aberdeenshire, with a latitude of 56.9° and a corresponding cut-off rigidity (quiet-time) of 1.5 GV. Although this is sufficiently different from the lower latitude stations to be useful, maximising capacity to infer spectral information by establishing COSMOS stations even further north would be sensible.

Examples of count rate ratios during a GLE are plotted in Figure 59. While these are heavily dependent on the spectral index of the GLE proton spectrum, it is clear that as broad a spread in rigidity range as possible would maximise the ratio and improve the fidelity of extracting information on spectral index. This is why we recommend that one of the proposed strategic detector hubs be located in as high a latitude as is practical, whether that be at Glensaugh or elsewhere. If higher latitude locations are not suitable for such a hub, it would still be useful to establish regular COSMOS stations at such locations in order to further exploit the rigidity range of the United Kingdom.

4. Adjustment for local conditions

The primary function of the COSMOS network will remain hydrological. Secular variations in count rate due to cosmic ray modulation are already accounted for in the derivation of soil moisture from COSMOS count rates. GLEs and Forbush decreases are relatively rare and will be considered as noise rather than signal in this context. However, rapid changes in local soil moisture conditions could affect the analysis of the same data in a space weather context, for example during gradual GLEs and Forbush decreases. Fortunately, the impact of such local environment effects would be far lower for GLEs of greater magnitude.

The ability to “correct” COSMOS count rates so as to remove the effect of local soil moisture (as well as pressure, humidity etc.) would nevertheless be advantageous. Although implementing such a correction is out of scope for the MOSAIC project, we have explored the feasibility of using independent data to accomplish this task, with promising initial results. We recommend that this work is continued so that eventually users of the COSMOS network have the option to view the data with this correction applied. This would make interpretation of the data very similar to that of neutron monitors, which is already familiar to many in the space weather community. It is not yet possible to say how reliable this will turn out to be, but it is a helpful objective to target in future work.

To summarize, our final recommendation based on the preliminary results from this feasibility study is that there is certainly potential for producing a UK-wide high spatial resolution product. However, a programme of dedicated testing and evaluation as well as the production of additional supporting information is required but falls beyond the nature of this initial MOSAIC feasibility study.

5. Complementary data sources

The UK COSMOS network has been identified as a novel source of space weather data with the potential to be a key national asset for the protection of infrastructure from future ground level enhancement events. However, it should not be regarded as a sufficient solution to address space weather impacts in isolation. We have reviewed various other existing and possible future sources of relevant space weather data, all of which would add value to the fidelity of any GLE alert service. The existing ground level neutron monitor network, although completely independent of the UK, currently holds the most important capability to monitor the global impact of GLEs and is likely to continue to do so for the foreseeable future. Wherever possible, the UK should support the maintenance of the GLNM network, both as a stakeholder in international station data and as a potential location for an addition to the network.

The most valuable source of data for the aviation sector is, of course, *in situ* data from in-flight monitors. The UK should invest in the development and routine deployment of calibrated monitors on regular high-latitude (most likely North Atlantic) routes to maximise the likelihood of capturing a GLE when one occurs. Ultimately these data should be fed into a real-time alert system that ingests multiple data sources. However, even before such a comprehensive service is developed, these data would be invaluable for retrospective calculation of GLE event characteristics and the dose received by passengers and crew. The viability of bespoke high-altitude measurement platforms for radiation monitoring, such as quick-launch weather balloons and UAVs, should also be fully explored in future UKRI research and development activities.

Civilian flight routes from the UK are particularly vulnerable to space weather impacts, but this situation can be significantly ameliorated through targeted monitoring and warning systems,

including both those based *in situ* and on the ground. The UK COSMOS network is well-placed to be an integral part of such future systems.

8 Conclusions

Data from the COSMOS world-wide network of soil moisture monitors over the last ten years have been examined for signatures of space weather events giving both Forbush decreases and sharp increases from ground level enhancements. While Fds are clearly seen, the two rather small GLEs in this period are only just discernible and the larger of the two occurred when there were no high latitude stations. However, simulations of detector response show that significant GLEs, such as have occurred historically, would be readily detected. The UK COSMOS network covers a wide range of geomagnetic latitude and this could be valuably extended by siting monitors in Shetland. Required improvements to time resolution and data transmission could be easily implemented, together with aggregating data from multiple detectors, to provide an effective UK space weather warning system for radiation hazards to aviation and ground level safety critical systems. This would complement other UK programmes to monitor radiation on aircraft and spacecraft. It is recommended that modifications and trials be initiated as soon as possible in order to detect events of the new solar cycle which is now steadily increasing.

References

- [1] P. Cannon *et al.*, *Extreme space weather: impacts on engineered systems and infrastructure*. Royal Academy of Engineering, 2013.
- [2] C. Dyer, A. Hands, K. Ryden, and F. Lei, "Extreme Atmospheric Radiation Environments and Single Event Effects," *IEEE Transactions on Nuclear Science*, vol. 65, no. 1, pp. 432-438, 2018, doi: 10.1109/TNS.2017.2761258.
- [3] "Process management for avionics - Atmospheric radiation effects - Part 6: Extreme Space Weather," IEC, 2017.
- [4] J. G. Evans *et al.*, "Soil water content in southern England derived from a cosmic-ray soil moisture observing system – COSMOS-UK," *Hydrological Processes*, vol. 30, no. 26, pp. 4987-4999, 2016, doi: 10.1002/hyp.10929.
- [5] H. M. Cooper *et al.*, "COSMOS-UK: National soil moisture and hydrometeorology data for empowering UK environmental science," *Earth System Science Data Discussions*, pp. 1-36, 2020.
- [6] M. Zreda *et al.*, "COSMOS: The cosmic-ray soil moisture observing system," *Hydrology and Earth System Sciences*, vol. 16, no. 11, pp. 4079-4099, 2012.
- [7] D. McJannet *et al.*, "Field testing of the universal calibration function for determination of soil moisture with cosmic-ray neutrons," *Water Resources Research*, vol. 50, no. 6, pp. 5235-5248, 2014.
- [8] S. Lindgren, "On the pressure dependence of the cosmic ray intensity recorded by the standard neutron monitor," *Tellus*, vol. 14, no. 1, pp. 44-48, 1962.
- [9] J. Simpson, "Cosmic-radiation neutron intensity monitor," *Annals of the IGY*, vol. 4, pp. 351-373, 1957.
- [10] A. Mishev and I. Usoskin, "Current status and possible extension of the global neutron monitor network," *Journal of Space Weather and Space Climate*, vol. 10, p. 17, 2020.
- [11] C. Hatton and H. Carimichael, "Experimental investigation of the NM-64 neutron monitor," *Canadian Journal of Physics*, vol. 42, no. 12, pp. 2443-2472, 1964.
- [12] A. Hawdon, D. McJannet, and J. Wallace, "Calibration and correction procedures for cosmic-ray neutron soil moisture probes located across Australia," *Water Resources Research*, vol. 50, no. 6, pp. 5029-5043, 2014.
- [13] R. Baatz, H. Bogena, H. J. Hendricks Franssen, J. Huisman, C. Montzka, and H. Vereecken, "An empirical vegetation correction for soil water content quantification using cosmic ray probes," *Water Resources Research*, vol. 51, no. 4, pp. 2030-2046, 2015.
- [14] R. Rosolem, W. J. Shuttleworth, M. Zreda, T. Franz, X. Zeng, and S. Kurc, "The effect of atmospheric water vapor on neutron count in the cosmic-ray soil moisture observing system," *Journal of Hydrometeorology*, vol. 14, no. 5, pp. 1659-1671, 2013.
- [15] M. Schrön *et al.*, "Improving calibration and validation of cosmic-ray neutron sensors in the light of spatial sensitivity," *Hydrology and Earth System Sciences*, vol. 21, no. 10, pp. 5009-5030, 2017.
- [16] D. Power, R. Rosolem, and M. A. Rico-Ramirez "The Cosmic-Ray Sensor PYthon tool (crspy)," 2020 (to be submitted).
- [17] A. Belov, "Forbush effects and their connection with solar, interplanetary and geomagnetic phenomena," *Proceedings of the International Astronomical Union*, vol. 4, no. S257, pp. 439-450, 2008.
- [18] H. V. Cane, "Coronal mass ejections and Forbush decreases," in *Cosmic Rays and Earth*: Springer, 2000, pp. 55-77.
- [19] J. A. Lockwood, "Forbush decreases in the cosmic radiation," *Space Science Reviews*, vol. 12, no. 5, pp. 658-715, 1971.
- [20] C. Light *et al.*, "Interplanetary Coronal Mass Ejection Associated Forbush Decreases in Neutron Monitors," *The Astrophysical Journal*, vol. 896, no. 2, p. 133, 2020.

- [21] A. Mishev, L. Kocharov, and I. Usoskin, "Analysis of the ground level enhancement on 17 May 2012 using data from the global neutron monitor network," *Journal of Geophysical Research: Space Physics*, vol. 119, no. 2, pp. 670-679, 2014.
- [22] P. Jiggins *et al.*, "In situ data and effect correlation during September 2017 solar particle event," *Space Weather*, vol. 17, no. 1, pp. 99-117, 2019.
- [23] A. Mishev and I. Usoskin, "Assessment of the radiation environment at commercial jet-flight altitudes during GLE 72 on 10 September 2017 using neutron monitor data," *Space Weather*, vol. 16, no. 12, pp. 1921-1929, 2018.
- [24] D. Smart and M. Shea, "A review of geomagnetic cutoff rigidities for earth-orbiting spacecraft," *Advances in Space Research*, vol. 36, no. 10, pp. 2012-2020, 2005.
- [25] A. J. Tylka, "Proton Spectra in Ground-Level Enhanced (GLE) Solar Particle Events," *cosp*, vol. 37, p. 3246, 2008.
- [26] A. Hands, F. Lei, K. Ryden, C. Dyer, C. Underwood, and C. Mertens, "New Data and Modelling for Single Event Effects in the Stratospheric Radiation Environment," *IEEE Transactions on Nuclear Science*, vol. 64, no. 1, pp. 587-595, 2017, doi: 10.1109/TNS.2016.2612000.
- [27] A. Belov, E. Eroshenko, H. Mavromichalaki, C. Plainaki, and V. Yanke, "Solar cosmic rays during the extremely high ground level enhancement on 23 February 1956," 2005.
- [28] K. Copeland and W. Atwell, "Flight safety implications of the extreme solar proton event of 23 February 1956," *Advances in Space Research*, vol. 63, no. 1, pp. 665-671, 2019.
- [29] J. R. Winckler, "Cosmic-ray increase at high altitude on February 23, 1956," *Physical Review*, vol. 104, no. 1, p. 220, 1956.
- [30] M. Köhli, M. Schrön, M. Zreda, U. Schmidt, P. Dietrich, and S. Zacharias, "Footprint characteristics revised for field-scale soil moisture monitoring with cosmic-ray neutrons," *Water Resources Research*, vol. 51, no. 7, pp. 5772-5790, 2015.
- [31] M. Köhli, M. Schrön, and U. Schmidt, "Response functions for detectors in cosmic ray neutron sensing," *Nuclear Instruments and Methods in Physics Research Section A: Accelerators, Spectrometers, Detectors and Associated Equipment*, vol. 902, pp. 184-189, 2018.
- [32] J. M. Clem and L. I. Dorman, "Neutron monitor response functions," in *Cosmic Rays and Earth*: Springer, 2000, pp. 335-359.
- [33] K. McCracken, M. A. Shea, and D. Smart, "The short-lived (< 2 minutes) acceleration of protons to > 13 GeV in association with solar flares," *EGUGA*, pp. EPSC2016-9634, 2016.
- [34] J. R. Dwyer, D. M. Smith, and S. A. Cummer, "High-energy atmospheric physics: Terrestrial gamma-ray flashes and related phenomena," *Space Science Reviews*, vol. 173, no. 1-4, pp. 133-196, 2012.
- [35] J. Dwyer *et al.*, "Estimation of the fluence of high-energy electron bursts produced by thunderclouds and the resulting radiation doses received in aircraft," *Journal of Geophysical Research: Atmospheres*, vol. 115, no. D9, 2010.
- [36] B. Carlson, N. G. Lehtinen, and U. S. Inan, "Neutron production in terrestrial gamma ray flashes," *Journal of Geophysical Research: Space Physics*, vol. 115, no. A4, 2010.
- [37] L. Babich, A. Y. Kudryavtsev, M. Kudryavtseva, and I. Kutsyk, "Atmospheric gamma-ray and neutron flashes," *Journal of Experimental and Theoretical Physics*, vol. 106, no. 1, pp. 65-76, 2008.
- [38] A. Chilingarian *et al.*, "Ground-based observations of thunderstorm-correlated fluxes of high-energy electrons, gamma rays, and neutrons," *Physical Review D*, vol. 82, no. 4, p. 043009, 2010.
- [39] Y. Wada *et al.*, "Gamma-ray glow preceding downward terrestrial gamma-ray flash," *Communications Physics*, vol. 2, no. 1, pp. 1-9, 2019.
- [40] I. M. Martin and M. A. Alves, "Observation of a possible neutron burst associated with a lightning discharge?," *Journal of Geophysical Research: Space Physics*, vol. 115, no. A2, 2010.
- [41] M. Tavani *et al.*, "Possible effects on avionics induced by terrestrial gamma-ray flashes," *Natural Hazards and Earth System Sciences*, vol. 13, no. 4, pp. 1127-1133, 2013.

- [42] C. Dyer, A. Hands, K. Ford, A. Frydland, and P. Truscott, "Neutron-induced single event effects testing across a wide range of energies and facilities and implications for standards," *IEEE transactions on nuclear science*, vol. 53, no. 6, pp. 3596-3601, 2006.
- [43] A. Hands, C. S. Dyer, and F. Lei, "SEU Rates in Atmospheric Environments: Variations Due to Cross-Section Fits and Environment Models," *IEEE Transactions on Nuclear Science*, vol. 56, no. 4, pp. 2026-2034, 2009, doi: 10.1109/TNS.2009.2013466.
- [44] H. Quinn, A. Watkins, L. Dominik, and C. Slayman, "The Effect of 1–10-MeV Neutrons on the JESD89 Test Standard," *IEEE Transactions on Nuclear Science*, vol. 66, no. 1, pp. 140-147, 2018.
- [45] A. Hands *et al.*, "Single Event Effects in Power MOSFETs Due to Atmospheric and Thermal Neutrons," *IEEE Transactions on Nuclear Science*, vol. 58, no. 6, pp. 2687-2694, 2011, doi: 10.1109/TNS.2011.2168540.
- [46] D. Desilets, M. Zreda, and T. P. Ferré, "Nature's neutron probe: Land surface hydrology at an elusive scale with cosmic rays," *Water Resources Research*, vol. 46, no. 11, 2010.
- [47] S. Stanley *et al.*, "Daily and sub-daily hydrometeorological and soil data (2013-2017)[COSMOS-UK]."
- [48] M. Best *et al.*, "The Joint UK Land Environment Simulator (JULES), model description—Part 1: energy and water fluxes," *Geoscientific Model Development*, vol. 4, no. 1, pp. 677-699, 2011.
- [49] D. Clark *et al.*, "The Joint UK Land Environment Simulator (JULES), model description—part 2: carbon fluxes and vegetation," *Geosci. Model Dev. Discuss*, vol. 4, pp. 641-688, 2011.
- [50] M. D'Alessio *et al.*, "SRAMs SEL and SEU in-flight data from PROBA-II spacecraft," in *2013 14th European Conference on Radiation and Its Effects on Components and Systems (RADECS)*, 2013, pp. 1-8.
- [51] F. Lei, A. Hands, S. Clucas, C. Dyer, and P. Truscott, "Improvements to and validations of the QinetiQ Atmospheric Radiation Model (QARM)," in *2005 8th European Conference on Radiation and Its Effects on Components and Systems*, 2005: IEEE, pp. D3-1-D3-8.
- [52] C. Dyer *et al.*, "Advances in Measuring and Modeling the Atmospheric Radiation Environment," *IEEE Transactions on Nuclear Science*, vol. 56, no. 6, pp. 3415-3422, 2009, doi: 10.1109/TNS.2009.2032185.
- [53] A. D. P. Hands, K. A. Ryden, and C. J. Mertens, "The disappearance of the pfozter-regener maximum in dose equivalent measurements in the stratosphere," *Space Weather*, vol. 14, no. 10, pp. 776-785, 2016, doi: 10.1002/2016sw001402.
- [54] C. J. Mertens, "Overview of the radiation dosimetry experiment (RaD-X) flight mission," *Space Weather*, vol. 14, no. 11, pp. 921-934, 2016.
- [55] P. Lantos and N. Fuller, "History of the solar particle event radiation doses on-board aeroplanes using a semi-empirical model and Concorde measurements," *Radiation Protection Dosimetry*, vol. 104, no. 3, pp. 199-210, 2003.
- [56] I. L. Getley, M. Duldig, D. Smart, and M. Shea, "Radiation dose along North American transcontinental flight paths during quiescent and disturbed geomagnetic conditions," *Space Weather*, vol. 3, no. 1, 2005.
- [57] P. Beck *et al.*, "Validation of modelling the radiation exposure due to solar particle events at aircraft altitudes," *Radiation protection dosimetry*, vol. 131, no. 1, pp. 51-58, 2008.
- [58] P. Beck *et al.*, "Overview of on-board measurements during solar storm periods," *Radiation protection dosimetry*, vol. 136, no. 4, pp. 297-303, 2009.
- [59] P. Beck, M. Latocha, S. Rollet, and G. Stehno, "TEPC reference measurements at aircraft altitudes during a solar storm," *Advances in Space Research*, vol. 36, no. 9, pp. 1627-1633, 2005.
- [60] C. Dyer, A. Sims, J. Farren, and J. Stephen, "Measurements of solar flare enhancements to the single event upset environment in the upper atmosphere (avionics)," *IEEE Transactions on Nuclear Science*, vol. 37, no. 6, pp. 1929-1937, 1990.
- [61] B. Clewer, K. Ryden, A. Dyer, A. Hands, and D. Jackson, "A citizen science network for measurements of atmospheric ionizing radiation levels," *Space Weather*, vol. 17, no. 6, pp. 877-893, 2019.

- [62] A. Dyer, K. Ryden, A. Hands, C. Dyer, C. Burnett, and M. Gibbs, "Zenith: A radiosonde detector for rapid-response ionizing atmospheric radiation measurements during solar particle events," *Space Weather*, vol. 16, no. 3, pp. 261-272, 2018.
- [63] E. Regener and G. Pfozter, "Vertical intensity of cosmic rays by threefold coincidences in the stratosphere," *Nature*, vol. 136, no. 3444, pp. 718-719, 1935.